QUANTUM COMPUTATION AND MULTI-PARTICLE ENTANGLEMENT WITH TRAPPED ATOMS AND IONS

Ph.D. Thesis

Anders Søndberg Sørensen

Institute of Physics and Astronomy
University of Aarhus

July 2001

Preface

This thesis is presented for the Faculty of Science at the University of Aarhus, Denmark in order to fulfill the requirements for the Ph.D. degree in Physics. The work has mostly been carried out at the Institute of Physics and Astronomy, University of Aarhus under the supervision of Klaus Mølmer. Most of the material presented in this thesis has been published elsewhere [1–15].

In this thesis I shall use the words "we" and "our" rather than "I" and "mine". This is not because I prefer to refer to myself in plural. The purpose is mainly to reflect the fact that the work has not been carried out by me alone but in close collaboration with my colleagues.

During my studies I have had the pleasure of working with a number of people. I thank all my friends and colleagues at the institute who have made my Ph.D. studies a pleasant experience. I can not list them all here and I shall only mention a few.

First of all I would like to thank my supervisor Klaus Mølmer. Klaus suggested this project to me and he has continued to be a source of inspiration. I am especially grateful that he has always encouraged me to come up with my own ideas and he has always had something nice to say about my ideas even when they were not so good.

In the spring 2000 I had the pleasure of visiting the University of Innsbruck. I am grateful to Ignacio Cirac and Peter Zoller for letting me visit their group. My stay in Innsbruck was very fruitful scientifically and I learned a lot by being there. I thank all my friends in Austria for the good times we spent together.

Thanks to Sune Jespersen and Gregers Neergaard who have been good company in the office and to my family for their support and interest in my work. I also wish to thank all my friends outside the physics community who have had to listen to me talking about the physics of quantum information and the difference between quantum and classical logic for several hours.

Last but not least, I thank my wife Anne Mette for her love and understanding. Anne Mette has always supported me and kept up my spirit when things didn't work out the way I wanted them, and she has shared my joy when things did work out.

Anders Søndberg Sørensen
July 2001

Contents

Part I

Introduction

Chapter 1

Introduction to the thesis

Quantum computation and entanglement merges two of the major scientific developments in the 20th century, information theory and quantum mechanics. Since the birth of quantum mechanics, several strange effects and paradoxes have altered our perception of fundamental physical principles. Entanglement arose in the philosophical discussions between Bohr, Einstein, and others about the implication of quantum mechanics for our understanding of Nature. In contrast to what one would naively think, entanglement apparently enables particles to exhibit instantaneous non-local correlations even though they are very far from each other. Bell's inequalities prove that any description of these correlations assuming locality and realism are at variance with the prediction of quantum mechanics; by performing experiments on entangled particles there are measurable differences between a local realism description and the prediction of quantum mechanics [16], and this has made an important contribution to our understanding of the physical reality.

For the founders of quantum mechanics, these discussions were pure speculations. Today, however, experiments have been pushed to a stage where we are able to control and observe individual quantum systems, and we are thereby testing many of the peculiar predictions of quantum mechanics in the laboratory. The experimental violation of Bell's inequalities in Aspect's experiment [17] has dramatically changed our understanding of the physical reality and it proves that there is fundamental difference between quantum and classical logic. Initially these investigations of entanglement were mainly motivated by our desire to understand quantum mechanics, but recently it has been discovered that entanglement and the paradoxical effects of quantum mechanics have a number of practical computer science applications in the fields of quantum computation and quantum communication. Today, quantum computation begin to come into reality with the realization of the first quantum computers using NMR in molecules [18–20].

Despite the achievements of NMR quantum computers, the quantum computer has not yet found its final form. The current NMR technique is very difficult to scale beyond, say, 10 qubits [21], and it is difficult to predict in which direction the field will evolve in the future. Indeed, it is far from certain that we will ever construct a large scale quantum computer. There are a large number of proposals for the construction of a quantum computer, but most of these proposals are far from being realizable with current technology. Coming from a background in atomic physics and quantum optics, we have tried to suggest implementations involving lasers and trapped atoms and ions, and we have focussed on proposals which are experimentally feasible in the near future. In the following chapters we shall present these proposals.

Thesis outline

This thesis is divided into four parts. In this part (part I) we give an introduction to the thesis. Chapter 1 is almost finished so we will not say more about it (since the reader has presumably read it). In chapter 2 we give a brief introduction to quantum computation and the experimental requirement for building such a computer.

In part II we describe our work with trapped ions. Chapter 3 contains an introduction to the physics of trapped ions and their application in quantum computation. We have developed an implementation of a quantum computer in an ion trap by using bichromatic light. This proposal is described in chapter 4. In chapter 5 we calculate the effect of various imperfections in an experimental realization of our proposal, and in chapter 6 we describe a generalization of the work in chapter 4.

Part III is concerned with neutral atoms and spin squeezing. Chapter 7 introduces spin squeezing and the basic physics of our neutral atom proposals. We describe how neutral atoms in optical lattices can be used to create spin squeezed states and perform quantum simulations of ferro-magnetism in chapter 8, and in chapter 9 we present an efficient method for producing spin squeezed states by starting from a Bose–Einstein Condensate. Part III is concluded with a discussion of the connection between spin squeezing and entanglement in chapter 10.

Part IV contains a conclusion and finally in appendix A we give a summary of the thesis which is written for the university yearbook.

Chapter 2

Introduction to quantum computation

In this chapter we give a brief introduction to quantum computation. This introduction will include a description of the basic concepts of quantum computation, as well as a discussion of some of the experimental requirements for building such a computer. For a more comprehensive review see Refs. [22, 23].

2.1 Classical versus quantum computation

To get a better grasp of the novel principles of quantum computation we shall start with a very brief discussion of the classical theory of computation. The basic building block of a classical computer is the *bit* which is a variable that can be either 0 or 1. Physically, a bit may be represented by the voltage across a capacitor which is either 0 or 5 V. If one combines n bits there are 2^n possible combinations of zeros and ones, so that any integer ranging from 0 to $2^n - 1$ may be represented by these n bits (the binary number $\{b_{n-1}, b_{n-2}, ..., b_1, b_0\}$ represents the integer $x = \sum_{i=0}^{n-1} b_i 2^i$).

The task of a computer is to implement some algorithm $f(x)$ on a given input x, *i.e.*, to produce an output string of m bits for a given input of n bits according to the algorithm f. A *general purpose* computer is a device which is able to implement any such algorithm f. At first sight it may appear exceedingly difficult to build such a general purpose computer, however, computer design is simplified by the fact that any mapping from n to m bits may be accomplished by a sequence of NAND gates. The NAND gate is a *classical logic gate* involving only two bits, which produces the output 0 if and only if both inputs are 1 [22]. Hence, in order to build a general purpose computer all that

is required is the ability to perform NAND gates between any pair of bits. A similar result exists for the quantum computer.

The quantum mechanical equivalent of a bit is the quantum bit or the *qubit*. A qubit is a two-level quantum system with two states $|0\rangle$ and $|1\rangle$. Physically, a qubit may be represented by, *e.g.*, two states in an atom, the polarization of a photon, or the spin of an electron, etc. If a qubit is in one of the two internal states $|0\rangle$ or $|1\rangle$ it may be regarded as a classical bit, but an important difference arises between bits and qubits due to the ability of a qubit to be in a superposition of the two states

$$|\Psi\rangle = a|0\rangle + b|1\rangle, \tag{2.1}$$

where a and b are complex numbers fulfilling $|a|^2 + |b|^2 = 1$. It is important to realize that because the state in (2.1) may exhibit interferences between the two states $|0\rangle$ and $|1\rangle$ there is a major difference between the coherent superposition in (2.1) and a statistical mixture of $|0\rangle$ and $|1\rangle$. The classical bit obeys the rules of classical logic and is *either* 0 *or* 1, whereas the qubit acts according quantum logic and may be in *both* $|0\rangle$ *and* $|1\rangle$ at the same time. This difference between classical and quantum logic is at the heart of many of the 'paradoxes' in quantum mechanics, *e.g.*, Schrödingers cat. As we shall see below, quantum logic has a profound influence on the theory of computation.

Like the classical computer, the quantum computer is constructed by combining multiple qubits, and the most general state of the computer is a superposition of all possible binary states $\sum c_{b_{n-1},b_{n-2},....,b_0}|b_{n-1}, b_{n-2}, ..., b_0\rangle$, $b_i = 0$ or 1. Again, each binary state represents an integers x between 0 and $2^n - 1$, and the state of the computer may also be considered as a superposition of all number states $\sum c_x|x\rangle$.

In quantum mechanics, time evolution is described by unitary operators, and the action of the quantum computer is to implement a given unitary operation U on the initial state $|\psi_i\rangle$, so that it produces the final state $|\psi_f\rangle$ which may be measured by the experimentalist

$$|\psi_f\rangle = U|\psi_i\rangle. \tag{2.2}$$

The construction of a general purpose quantum computer thus requires the ability to implement any unitary operator on the mutual state of all the qubits in the computer. Fortunately, there exists a result similar to the classical theorem that any classical algorithm may be implemented with NAND gates: Any unitary operator on n qubits may be implemented by applying rotations on single qubits and two-qubit CONTROL-NOT gates [24]. By single qubit rotations we mean any unitary operator acting on a single qubit. It is called rotations because for a spin 1/2-particle any unitary operation corresponds to a rotation of the spin, or equivalently to a rotation on the Poincare-sphere if the qubits are represented by the polarization of single photons. Throughout

this thesis the logical states $|0\rangle$ and $|1\rangle$ are represented by the internal states of a two-level atom or ion and all single particle rotation can be obtained by illuminating the atom with light which is resonant with the transition between the two levels. In the experimental situations considered in this thesis, the single particle rotations are much easier to implement than the two particle gates, and we shall assume that the experimentalist is capable of producing any single-particle rotation. The CONTROL-NOT gate acts on two qubits and flips the state of the second qubit if the first qubit is in $|1\rangle$, *i.e.*, it implements the unitary transformation

$$\begin{array}{ll} |00\rangle \rightarrow |00\rangle & |01\rangle \rightarrow |01\rangle \\ |10\rangle \rightarrow |11\rangle & |11\rangle \rightarrow |10\rangle. \end{array} \tag{2.3}$$

The CONTROL-NOT gate is the gate that is usually referred to in the literature because it has some simple properties for building a large unitary operator U. However, there is no fundamental reason for choosing this gate; many other gates will also suffice. In fact, it has been shown [25–27] that any two qubit operation which doesn't reduce to a product of single qubit rotations is sufficient for quantum computation. Thus, the implementation of any unitary operation on the qubits has been reduced to a problem of applying rotations on each qubit and producing some kind of controlled interaction between pairs of qubits.

To get an idea about the difference between classical and quantum computation, let us consider a specific example. Suppose that we wish to evaluate a function $f(x)$ for all inputs x, and consider a quantum computer with $n+m$ qubits, where the first n qubits are assigned as input bits, and the remaining m bits are reserved for the output of the function. Initially all bits are assumed to be in the $|0\rangle$ state, so that the state of the computer is $|\Psi\rangle = |00...0\rangle_i|00...0\rangle_o$, where subscripts i and o refer to input and output bits. We first prepare the input bits in a superposition of all possible number states $|\Psi\rangle = \sum_{x=0}^{2^n-1} 2^{-n/2}|x\rangle_i|0\rangle_o$ (below, we describe how such a superposition may be achieved), and then apply a unitary operator U_f which evaluates the function $f(x)$

$$|\Psi\rangle = U_f \sum_{x=0}^{2^n-1} 2^{-n/2}|x\rangle_i|0\rangle_o = \sum_{x=0}^{2^n-1} 2^{-n/2}|x\rangle_i|f(x)\rangle_o. \tag{2.4}$$

The operator U_f can be constructed from fundamental two qubit gates using results from classical computer science, and the function $f(x)$ is evaluated for all x in a single step. On the classical computer each inputs have to be evaluated one at a time. The use of superpositions allows a quantum parallelism which may speed up computation, but problems arise as we try to read out the result of the computation. If we perform a measurement on the state in Eq. (2.4), the

wavefunction is collapsed onto $|\Psi\rangle = |y\rangle_i |f(y)\rangle_o$, where y is a random number, and the advantage of quantum parallelism is lost. Circumventing this read-out problem is the task of quantum algorithms.

2.2 Algorithms

From a computational viewpoint it is quantum algorithms that makes quantum computation interesting. By a clever design of a quantum algorithm a quantum computer may solve certain computational tasks much faster than any classical computer. It is the appearance of quantum algorithms which has boosted the interest in quantum computation in recent years. Specifically Shor's algorithm [28] (subsection 2.2.2), which allows an exponential speed up of a highly non-trivial problem, has created a lot of interest in the field. We start our description of quantum algorithms with a quite detailed discussion of Grover search [29], which illustrates the essential features of quantum computation: superposition and interference.

2.2.1 Grover search

Grover search is an algorithm for searching an unstructured database. Suppose, for instance, that you wish to find the owner of a given telephone number and you only have access to a phone book which is sorted in alphabetic order. This is a very time consuming task, because you have to check every entry of the book until you find a match, so that if there are N possible entries in your database you need an average of $N/2$ queries to find the desired person. In Grovers quantum algorithm [29] the number of steps required to search the database only increases proportional to $\sqrt{N}$, and for very large N, $\sqrt{N}$ is considerably below N, so that the quantum computer outperforms the classical counterpart. It will be convenient to have a formulation of the problem in mathematical terms. In an abstract notation, the problem may be stated as 'finding the position x_0 where a given function $f(x)$ differs from zero', *i.e.*, $f(x_0) = 1$ and $f(x) = 0$ for all other x.

The first step in the Groover search is to prepare the computer in an equal superposition of all possible inputs. This is done by applying the unitary Walsh-Haddamar transformation

$$W: \begin{array}{l} |0\rangle \rightarrow (|0\rangle + |1\rangle)/\sqrt{2} \\ |1\rangle \rightarrow (|1\rangle - |0\rangle)/\sqrt{2} \end{array} \tag{2.5}$$

to a string of qubits initially in the $|0\rangle$ state. The resulting product state

$$|\Psi\rangle = 2^{-n/2}(|0\rangle_{n-1} + |1\rangle_{n-1})(|0\rangle_{n-2} + |1\rangle_{n-2})...(|0\rangle_0 + |1\rangle_0) \tag{2.6}$$

is an equal superposition of all possible binary state $|b_{n-1}, b_{n-2}..., b_0\rangle$, or equivalently a superposition of all possible number states $|x\rangle$, $x = 0, 1, ..., 2^n - 1$. For simplicity we assume that the number of inputs N may be written as 2^n.

The computer is now in a superposition of all possible elements x, but this has not helped solving our problem because a measurement on the computer will merely collapse the state to a random element. The next step is to enhance the amplitude of the component with $f(x) = 1$ by first applying a phase change operator U_f which rotates the phase of a quantum state by π if $f(x) = 1$. Grover's algorithm then applies an 'inversion about the mean', where the amplitude with the sign changed will grow in comparison with the other amplitudes. In the $n-$qubit computer with $N = 2^n$ amplitudes c_x, the operation can be written $c_x \rightarrow \frac{1}{N}\sum_{x'} c_{x'} - (c_x - \frac{1}{N}\sum_{x'} c_{x'})$. The sum of all amplitudes of the state vector $|\Psi\rangle$ can be obtained as any component in the vector $M|\Psi\rangle$, where M is the $N \times N$ matrix with unit elements in all positions. The inversion about the mean is therefore given by the unitary matrix [29]

$$U_G = \frac{2}{N}M - I, \tag{2.7}$$

where I is the $N \times N$ identity matrix.

For simplicity we shall only go into details about this enhancement procedure in the simple case with only 4 inputs $|0\rangle...|3\rangle$ (two qubits). Suppose that the entry we are searching for is $x_0 = 2$. After the application of the operator U_f the wavefunction is

$$|\Psi\rangle = \frac{1}{2}(|0\rangle + |1\rangle - |2\rangle + |3\rangle). \tag{2.8}$$

When we apply the operator U_G, the amplitudes of the three components of the wavefunction with $f(x) = 0$ vanish exactly

$$c_{x\neq x_0} = (-1 + \frac{2}{4}) \cdot \frac{1}{2} + \frac{2}{4} \cdot \frac{1}{2} + \frac{2}{4} \cdot (-\frac{1}{2}) + \frac{2}{4} \cdot \frac{1}{2} = 0, \tag{2.9}$$

and we are left with the state $|x_0\rangle$. By measuring the state of each qubit, we can read the result x_0 and we have searched the database using only a single evaluation of the function $f(x)$. No classical computer is able to do this.

In the general case with N possible inputs, the amplitudes on all other components does not vanish after a single application of U_f and U_G. However, application of U_f and U_G does increase the amplitude on $|x_0\rangle$, and after $O(\sqrt{N})$ applications of U_f and U_G the amplitude on $|x_0\rangle$ is close to unity and the result may be read with almost unit probability [29]. In chapter 6 we describe how Grovers algorithm may be implemented in an ion trap.

2.2.2 Factorization

Grover's algorithm has attracted a lot of interest in recent years and it has been included here due to the simplicity of the algorithm. However, it was the discovery of Shor's algorithm [28] a few years earlier, which really started the interest in quantum computation. Here we shall only make a brief description of the problem and not go into any details about the algorithm. Suppose that you are given a n-digit number M which is the product of two primes $M = P_1 \times P_2$, and you wish to find the two primes, *i.e.*, to factorize M. The known classical algorithms essentially just divide M by a large number of integers, so that the computational time increases exponentially with the number of bits n, and the problem very quickly becomes intractable. On the quantum computer, Shor's algorithm uses the fact that factorization may be reduced to a problem of finding the period of a function, and then exploits quantum parallelism to perform an extremely fast Fourier transformation, so that the required time only grows polynomial in n, making the algorithm much faster for large n.

The factorization problem may seem of purely mathematical interest, but it is also extremely interesting from a commercial perspective because it is at the heart of many cryptographic schemes. Suppose that two parties Alice and Bob try to perform private communication without eavesdropping from an adversary. The way this is typically achieved today, is that Alice publicly announce a large number M which is the product of two primes which are only known to Alice. Bob encodes his message using existing classical algorithms and the public number M, in such a way that decoding the message requires knowledge of the two primes. He then communicates the encrypted message to Alice who decrypt the message using her two secret primes. As long as nobody, except Alice, knows these two primes, the protocol is secure against eavesdropping. The construction of a large scale quantum computer will make factorization an easy problem and the security of the scheme will be destroyed. This is the background for much of the interest in quantum computation as well as the motivation for much of the funding in this field[1].

2.2.3 Quantum simulation

From a physicists point of view, an interesting application of the quantum computer is to use it for solving quantum physics problems. Simulation of quantum many-body problems on a classical computer is difficult because the size of the Hilbert space grows exponentially with the number of particles. As suggested by Feynman [33] the growth in computational requirements is only linear on a quantum computer, which is itself a quantum many-body system, and such a

[1] On the other hand, quantum communication enables the construction of quantum cryptographic schemes [30, 31], which are provably secure against any attacks [32].

computer containing only a few tens of qubits may outperform a classical computer. Also, a quantum computer aimed at the solution of a quantum problem might be easier to realize in practice than a general purpose quantum computer, because the desired solution is governed by physical interactions which are constrained, *e.g.*, by locality [33, 34] and symmetry. In chapter 8 we give an explicit proposal for the construction of a *quantum simulator*. In this proposal the symmetry among the qubits removes the necessity of resolving the individual qubits experimentally and the locality of the underlying physical problem means that we only need gates between adjacent atoms.

2.3 Entanglement

The above description has focused on quantum computation from a computational viewpoint. In this section we put quantum computation into a more physical context; that is the physics of entanglement, which has been a source of controversy and paradoxes since the early days of quantum mechanics. Quantum computation has a prominent position in the theoretical and experimental exploration of the mind-boggling effects of entanglement.

Two quantum systems a and b are said to be entangled if the wavefunction cannot be written as a product state[2] $|\Psi\rangle \neq |\phi_a\rangle|\phi_b\rangle$. For instance, in conventional spectroscopy N atoms are prepared in the same quantum state so that the combined wavefunction may be written as $|\Psi\rangle = |\phi\rangle^N$, and this system is not entangled. Consider the singlet quantum state

$$|\Psi_{EPR}\rangle = \frac{1}{\sqrt{2}}(|01\rangle - |10\rangle). \tag{2.10}$$

(The term singlet refers to spin 1/2 particles. If the qubits are represented as spins, this state has zero total angular momentum.) The state in Eq. (2.10) cannot be written as a product state, it is entangled. $|\Psi_{EPR}\rangle$ is the discrete equivalent of the state considered by Einstein, Podolsky and Rosen (EPR) in a celebrated paper [35]. In this paper the authors argued that quantum mechanics cannot be a complete theory, because a measurement on one of the entangled particles leads to a knowledge about the state of the other. Their claim is that this may be used to measure non-commuting observables simultaneously, contrary to the fundamental principles of quantum mechanics. The arguments of EPR are based on assumptions of *locality* and *realism*, however, it has been shown that such assumptions are in conflict with the quantum correlation in the state $|\Psi_{EPR}\rangle$, and experiments using such states have been employed to rule out all local realism descriptions of Nature [17]. States like

[2]This definition applies to pure quantum states. The definition for mixed states is given in chapter 7.

$(|000\rangle + |111\rangle)/\sqrt{2}$ with three particles, the so-called GHZ states [36, 37], and with even more particles allow a closer scrutiny of the role of quantum correlations. In the experiment presented in Ref. [38] such three particle entangled states were produced and the correlation between the particles showed a striking conflict with the prediction of local realism. In this thesis we shall give several proposal for generating multi-particle entangled states.

The development of quantum computers is closely connected to the exploration of entanglement, since such computers will naturally produce multi-particle entangled states. As the number of qubits in the computer increases, the state of the computer approaches the situation considered in the Schrödinger cat paradox [39]. In this famous paradox, a cat is placed in a superposition of being dead and alive, which clashes with our every-day experience where superpositions are not present. Today, experimentalist are trying to realize the paradox by producing superpositions of states of large mesoscopic separation[3]. In the previous 'Schrödinger kitten' experiments, the vibrational motion [40] of a trapped ion, a single mode of the electro-magnetic field [41], the position of a C_{60} molecule [42], and the current in a superconductor [43] have been placed in a superposition of mesoscopicly distinguishable states. A large scale quantum computer may produce a different type of cat where a large number of qubits are placed in a superposition of being all $|0\rangle$ and all $|1\rangle$, and this may provide new insight on the theory of measurement and the foundation of quantum mechanics. In chapter 4 we give an experimentally feasible proposal for the constructions of such states. Following this proposal the experimentalist have been able to produce a four particle entangled state $(|0000\rangle + |1111\rangle)/\sqrt{2}$ [44]. This is the largest number of particles which has been entangled so far.

2.4 Coherence and decoherence

The actual construction of a quantum computer is an extremely demanding experimental challenge. One major problem is to avoid decoherence of the state of the computer. To maintain a coherent evolution of the quantum state the influence of the environment has to be very low. Interaction with the environment will generally lead to entanglement between the environment and the computer. Once the qubits are entangled with the environment, they can no longer produce interference effects and the advantages of quantum computation are lost.

To be useful for quantum computation the qubits have to be chosen so that they interact very weakly with the environment. This demand, however, conflicts with another requirement of quantum computation: To create two qubit gates we need to engineer an interaction such that the evolution of one

[3] It would properly be considered to be political incorrect to perform the experiment with a real cat. No cats were harmed during the production of this thesis.

qubit depends on the state of the other. For weakly interacting particles such a controlled interaction between individual quantum systems is not a trivial thing to construct in the laboratory.

Quantum error correction

The environment also affects classical computers, but classical computation is quite noise insensitive due to the use of error correcting codes. If there is a certain probability P that each of the n bit will be flipped during a computation, the probability to have no flips is $(1-P)^n$. Hence the probability for the computation to be successful decreases exponentially with the number of bits if error correction is not used. By using error correction the probability to avoid errors can be made arbitrarily large making computation tractable even with a large number of bits. For instance, the simple triple encoding $b \rightarrow bbb$ may be used to protect a bit against bit-flips. If the probability P for a bit to be flipped is small it is very unlikely that two bits will be flipped $\sim P^2$. If we see an output 101 we conclude that the input was probably 1 and by flipping the second bit we recover the correct state.

Error correction of quantum information is considerably more complicated than in the classical case because quantum mechanics does not allow copying of a single quantum state [45]. A naive code like $|0\rangle + |1\rangle \rightarrow |000\rangle + |111\rangle$ will protect against bit-flips, but it does not provide any protection against phase errors. A few years ago it was shown that despite these problems, it is still possible to construct quantum error correcting codes that protects against both bit flips and phase errors [46, 47]. With these codes quantum computation can be stabilized against errors and a large scale quantum computer may be constructed even with a non vanishing probability of errors on each bit. Current experiments are, however, still far away from the low noise regime where error correcting may be employed to further reduce the noise and it is a tremendous experimental challenge to maintain coherence during the implementation of even a few gates.

In some cases the character of the noise is such that the full generality of quantum error correcting codes is not required. If simplifying physical assumptions are applicable more suitable codes may be developed for the problem at hand [48]. In Ref. [1], for instance, we explicitly use some restrictions on the noise to ensure a perfect transmission in a quantum communication scenario.

2.5 Experimental proposals

The construction of quantum computers could have a large commercial potential and the physics of entanglement is also very interesting from a fundamental physics point our view. With this background it is not surprising that a number

of proposals for the construction of a quantum computer have appeared from several different branches of physics and we shall only discuss a few of them here. For a review of some of the proposals see Ref. [49].

So far the only technology which has been used to implement a quantum algorithm is NMR in molecules [18–20]. These experiments have played an important role by demonstrating that quantum computation is possible and they have provided inspiration for further explorations in the field. But as mentioned in chapter 1 it is very hard to scale this approach up to a large number of qubits [21], and it is therefore necessary to look for different approaches to quantum computation.

Traditionally, the control and detection of individual quantum systems has been studied intensively in the field of quantum optics and for several years the experimental explorations of entanglement have been dominated by quantum optics. By using down-conversion one can create entangled beams of photons [50, 51] and this has lead to experimental implementation of some simple quantum information protocols like for instance quantum teleportation [52–55]. Although down-conversion has been very successful in generating few particle entangled states it is very difficult to imagine a large scale quantum computer which operates by using only down conversion. To create a photonic quantum computer one strategy could be to encode the information in different quadratures of the quantized field (these quadratures behave like position and momentum). If a sufficiently strong non-linearity can be constructed this encoding may allow the construction of a continuous variable quantum computer [56]. By encoding the qubits in two orthogonal states of single photons, it is also possible to construct a quantum computer without having a non-linearity if one can produce very efficient sources and detectors for single photons [57]. Other quantum optics proposals involve trapped atoms and ions which are connected through the interaction between the particles or by their interaction with light. These proposals are discussed in chapters 3 and 7 in connection with the description of our work with atoms and ions.

The current classical computers are constructed in solid state devices. If one could also implement a quantum computer in solid state it would have the advantage that one can use the well developed technologies for the construction of classical computers to miniaturize the setup, and this could permit the scaling from a few bits to a large quantum computer. On the other hand a qubit in a solid state device is probable to be more strongly coupled to the surroundings due to the coupling to, *e.g.*, phonons. Several proposal for solid state quantum computers have appeared including impurities in Silicon [58], quantum dots [59, 60], and Josephson-junctions in superconducters [61]. Unfortunately these proposals are far from being realizable with the current technology. The most advanced of these technologies are currently at a stage where they are controlling a single bit [62, 63].

It is difficult to predict which of these technologies (if any) that will dominate in the future. Presently it appears that the trapped atoms and ions considered in this thesis are not much worse candidates than any of the other proposals. Furthermore, the quantum optics proposals are also important due to their applicability in quantum communication schemes. Quantum communication is performed with photons due to their ability to travel at enormous velocities through optical fibers. However, to communicate over long distances it is essential to have repeater stations equiped with small quantum processors which corrects for errors in the transmission [64]. The necessity of being able to link a quantum computer with a photonic quantum communication channel strongly motivates the construction of a quantum optics quantum computer.

2.6 RISQ – Reduced Instruction Set Quantum computers

Despite the dedicated efforts to construct a quantum computer it is possible that we will never see a large scale quantum computer. The practical difficulties may be so large that the possible gain by using a quantum computer does not justify further explorations in this direction. Even if this may eventually be the case it is our opinion that quantum computation is still worth investigating. By attempting to create a quantum computer we are exploring a completely new field and we are certainly going to discover a lot of interesting new physics in the process. And even though we may not be able to construct a full general purpose quantum computer it is very likely that the procedures and techniques which are developed for quantum computation may be useful for something else. This is the idea behind the RISQ (*reduced instruction set quantum computers*) concept which we introduced in Ref. [8].

The construction of a full scale quantum computer is terribly difficult experimentally, but in the RISQ approach one simply ignores some of the difficult parts and investigate whether the remaining entangling capabilities are useful for something. A major part of the work presented in this thesis follows this approach. Specifically, we investigate the experimental possibilities for producing interesting states and effects without accessing the qubits individually. In a quantum computer each qubit have different meanings and it is necessary to be able to control and detect the state of each individual qubit. But in several experimental setups it is very difficult to resolve the qubits individually and we have investigated what might be achieved by only addressing the qubits collectively. We have shown that by illuminating a collection of atoms or ions with broad beams of light interacting with all particles in the sample it is possible to create multi-particle entangled states (chapters 4, 8, and 9) and simulate the quantum evolution of a ferro-magnet (chapter 8). It is our hope that these

simpler experimental schemes can be implemented on systems where the technology does not yet permit the construction of a full scale quantum computer. In a premature quantum computer the collective properties investigated here, *e.g.* spin squeezing, provides an experimental signature of the underlying interactions and could be used as a diagnostic tool in the future development of the quantum computer.

Part II

Ion traps

Chapter 3

Introduction to ion traps

In the following chapters we present our work on quantum computation and multi-particle entanglement in linear ion traps [2, 3, 5, 6, 10, 12, 13]. The theory presented here, has been successfully implemented by the ion trapping group at NIST in Boulder, USA. By using our proposal they have been able to produce four-particle entangled states [44], implement a decoherence-free quantum memory [65], and violate Bells-inequality with efficient detectors [66]. In the remainder of this chapter we give a brief introduction to the physics of ion traps. A more detailed description of ion traps and their applications in quantum information can for instance be found in Ref. [67].

In chapter 4 we present our gate under ideal conditions. In chapter 5 the effect of various imperfections is analyzed, and we estimate the deviation from the ideal behaviour due to these imperfections in an actual experiment. Finally, in chapter 6 we extend the results of chapter 4 and propose a method to produce multi-particle logic gates and implement Grover search in a very direct way.

3.1 Construction of an ion trap

The construction of an ion trap is complicated by the Laplace equation which reads $\vec{\nabla}^2\Phi = 0$, where Φ is the electrostatic potential. A stable trap requires that the potential energy has a local minimum at the position of the trap, but since the potential energy is proportional to the electrostatic potential it is impossible to make a trap by electrostatic fields due to the Laplace equation. To create a stable three dimensional trap, time varying fields have to be applied.

In Fig. 3.1 we show a schematic drawing of a linear ion trap (other designs than the one presented in the figure are possible). The trap consists of four rods and some end cap electrodes. An oscillating potential U_{RF} is applied to the four rods, and for suitable values of the frequency and strength of U_{RF} the

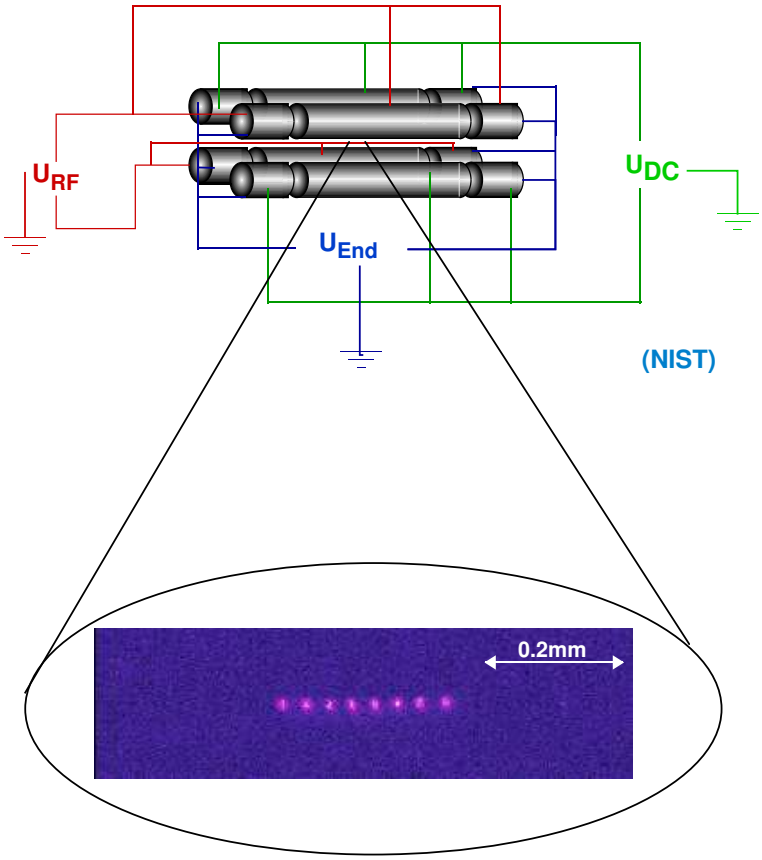

Figure 3.1: A linear ion trap is produced by a combination of static ($U_{\mathrm{End}}, U_{\mathrm{DC}}$) and time varying ($U_{\mathrm{RF}}$) potentials. The picture shows 8 trapped ions, which are cooled to a temperature where a one dimensional crystal is formed. (Picture courtesy of Liv Hornekær)

oscillating potential creates an effective confining transverse potential. On top of movement in the effective potential, the ions also perform a micro-motion with the frequency the applied potential. The amplitude of the micro-motion can be made arbitrarily small, so that for time scales which are long compared to the period of the oscillation of the potential, we can neglect the small micro-motion and consider the confining fields as a static harmonic potential. The oscillating potential only confines the ions in the transverse direction and to obtain confinement in the longitudinal direction an additional potential U_{End} has to be applied to the end cap electrodes.

At sufficiently low temperature the ions freeze into a crystal structure where the ions are located such that the Coulomb repulsion among the ions equilibrates the confining force from the trapping potential. The required low temperatures can be obtained by laser cooling the ions and ion crystals with any number of ions up to 10^5 have been produced experimentally [68]. It is even possible to produce crystals which contain different ion species [69]. In the following we consider the situation where the transverse potential is much stronger than the longitudinal potential. In this situation the ions form a one-dimensional crystal, as the one shown in Fig. 3.1, and we shall neglect the transverse dimensions.

The vibrations of the N ions around their equilibrium position are strongly coupled due to the Coulomb interaction between the ions. If the amplitude of the oscillations are much smaller than the separation between the ions, we may describe the vibrations in the harmonic oscillator approximation. By replacing the excursion x_j of the jth ion from its equilibrium position by a suitable linear combination of N coordinates q_l

$$x_j = \sum_{l=1}^{N} b_j^l q_l, \tag{3.1}$$

where b_i^l obeys the orthogonality conditions $\sum_{j=1}^{N} b_j^l b_j^{l'} = \delta_{l,l'}$ and $\sum_{l=1}^{N} b_j^l b_{j'}^l = \delta_{j,j'}$ [70], the vibrational Hamiltonian may be diagonalized to form a non-degenerate set of N collective vibrational modes, just like the phonon modes in an ordinary crystal. The mode with the lowest frequency is the center of mass mode ($l = 1$), where all ions participate equally in the vibration, $b_j^1 = 1/\sqrt{N}$ for all j. The frequency of this mode is equal to the oscillation frequency of a single ion in the trap.

3.2 Ion traps and quantum computation

The ion trap was originally proposed for quantum computation by Cirac and Zoller [71]. In the ion trap quantum computer each qubit is represented by the internal states of an ion, and by using long lived states, like for instance

hyperfine structure states, the qubits may be very effectively shielded from the surroundings. To represent the logical computational states $|0\rangle$ and $|1\rangle$ of the jth bit, the ion trap quantum computer uses two internal levels in the jth ion $|e\rangle_j$ and $|g\rangle_j$. Throughout this thesis such two-level systems are described by the Pauli operators σ_{zj}, σ_{+j}, and σ_{-j}, which have the properties $\sigma_{zj}|e\rangle_j = |e\rangle_j$, $\sigma_{zj}|g\rangle_j = -|g\rangle_j$, $\sigma_{+j}|g\rangle_j = |e\rangle_j$, and $\sigma_{-j}|e\rangle_j = |g\rangle_j$.

To implement gates between the bits, it was proposed to apply laser light to the ions in the trap [71]. Due to the recoil of an ion upon absorption of a photon, the laser light can be used to couple the internal and motional states of the ions. Since the motion of the different ions are strongly coupled by the Coulomb interaction, this coupling of internal and external states provides a means of implementing gates, as we will discuss below.

If the jth ion in the trap is illuminated by laser light with a frequency ω_j and an intensity parameterized by the resonant Rabi frequency Ω_j, the interaction may be described by the Hamiltonian (in the rotating wave approximation with respect to the ionic resonance frequency ω_{eg} and using $\hbar = 1$)

$$\begin{aligned} H =& H_0 + H_{\text{int}} \\ H_0 =& \sum_{l=1}^{N} \nu_l (a_l^\dagger a_l + 1/2) + \omega_{eg} \sum_{j=1}^{N} \sigma_{zj}/2 \\ H_{\text{int}} =& \sum_{j=1}^{N} \frac{\Omega_j}{2} (\sigma_{+j}\ \mathrm{e}^{i(\sum_{l=1}^{N} \eta_{j,l}(a_l + a_l^\dagger) - \omega_j t)} + h.c.), \end{aligned} \tag{3.2}$$

where ν_l and $a_l^\dagger$ and a_l are the frequency and ladder operators of the lth mode. The exponential $\mathrm{e}^{i(\sum_{l=1}^{N} \eta_{j,l}(a_l + a_l^\dagger)}$ represents the recoil of the ion upon absorption of the of a photon e^{ikx_j}, where k is the component of the wave vector of the incident laser light along the trap axis. To obtain the form in Eq. (3.2), x_j has been replaced by the collective coordinates q_l in Eq. (3.1), and q_l has been replaced by the ladder operators $q_l = \sqrt{\frac{\hbar}{2M\nu_l}}(a_l + a_l^\dagger)$. The constant $\eta_{j,l}$ is referred to as the Lamb-Dicke parameter and it is given by $\eta_{j,l} = \eta \frac{\sqrt{N} b_j^l}{\sqrt{\nu_l/\nu}}$, where ν and $\eta = k\sqrt{\frac{\hbar}{2NM\nu}}$ are the frequency and Lamb-Dicke parameter of the center-of-mass mode and M is the mass of the ions. For $N \leq 10$ the values of ν_l/ν and b_j^l may be found in Ref. [70]. In a practical realization, one might use Raman transitions between low lying states of the ions due to their long coherence time. By appropriate redefinition of the symbols, our formalism also describes this implementation [72].

By choosing the frequency of the laser equal to the resonance frequency of an internal transition in an ion plus or minus a vibrational frequency, the laser is exactly on resonance with an excitation of the internal transition and

a simultaneous change in the vibrational motion, and the laser may be used to selectively excite a single collective mode. Consider for example laser light of frequency $\omega = \omega_{eg} - \nu_k$ which is resonant to the kth lower sideband. In ion trap quantum computation one usually assumes $\eta_{j,l}\sqrt{n_l + 1} << 1$, where n_l is the vibrational quantum number of the lth mode. In this limit we may perform the 'Lamb-Dicke approximation' and expand the exponential in Eq. (3.2) in powers of the Lamb-Dicke parameter. Changing to the interaction picture with respect to H_0, the Hamiltonian describing this situation becomes

$$H'_{\rm int} = \sum_{j=1}^{N} \frac{\Omega_j}{2} \left[\sigma_{+j} \left(\mathrm{e}^{i\nu_k t} + i \sum_{l=1}^{N} \eta_{j,l} (a_l \mathrm{e}^{-i(\nu_l - \nu_k)t} + a_l^\dagger \mathrm{e}^{i(\nu_l + \nu_k)t}) \right) + h.c. \right] \tag{3.3}$$

to first order in $\eta_{j,l}$. If the strength of the laser is sufficiently small ($\Omega_j << \nu$) we can neglect all terms except the resonant contribution and (3.3) reduces to

$$H''_{\rm int} = \sum_{j=1}^{N} i \frac{\Omega_j}{2} \eta_{j,k} (\sigma_{+j} a_k - \sigma_{-j} a_k^\dagger). \tag{3.4}$$

Note, that the 'carrier term' which is the first term inside the parenthesis in Eq. (3.3) and which represents a change in the internal state of the ion without change in the vibrational motion, is the dominant contribution for short times $t \lesssim 1/\nu$ because we have assumed $\eta_{j,l}\sqrt{n_l + 1} << 1$. For longer times $t \sim 1/\eta\Omega$ the terms in Eq. (3.4) are dominant[1]. The validity of the omission of the carrier term and the Lamb-Dicke approximation will be studied in chapter 5. The Hamiltonian (3.4) is the well studied Jaynes-Cummings Hamiltonian which is used to describe the interaction of atoms with a single mode of a quantized electro-magnetic field. From the form of Eq. (3.4) one sees that light on the lower sideband can be used to transfer excitations from the atoms to the vibrational motion. This kind of coupling of internal and external degrees of freedom has been extensively used for precise control of the quantum state of trapped ions [40, 72], and it is also useful for quantum computation.

As described in chapter 2, a quantum computer requires single qubit rotations and two qubit gates. In the ion trap scheme it is suggested to achieve this by focusing a laser onto each ion and exploiting the collective vibrations for the interaction between the ions. In the original proposal the system is restricted to the joint motional ground state of the ions. By focusing a laser onto a particular ion and tuning the frequency to a sideband as it is assumed

[1] In the original proposal [71] the carrier term is suppressed by assuming that the light makes a standing wave with a node at the position of the ions. This configuration is an advantage because it removes the unwanted carrier term and all other terms with an even power of $\eta_{j,l}$. In this work we assume running waves which are easier to implement in practice.

in Eqs. (3.3) and (3.4), a vibration is excited if the particular ion is in the internal state $|e\rangle_j$. Subsequent laser irradiation of another ion interchanges the internal states of that ion if and only if the vibrational motion is excited. At the end of the gate the vibrational excitation is removed and additional gates may be implemented. This procedure implements a CONTROL-NOT operation and combined with single particle rotations, which may be obtained by choosing the frequency of the laser to be equal to the transition frequency ω_{eg}, we have the necessary ingredients to implement any quantum algorithm. To read out the final state after the computation a shelving scheme can be used [73]. A strong laser couples one of the internal states say $|g\rangle$ to a third state $|a\rangle$. If a suitable closed transition is used, the excited state $|a\rangle$ decays back to the state $|g\rangle$, which is then reexcited by the strong laser. In this way several photons are scattered of the ion if it is in the state $|g\rangle$ whereas no photons are scattered if it is in the state $|e\rangle$. In this way one can distinguish the two outcomes $|e\rangle$ and $|g\rangle$ and read out the result of the computation.

The original ion trap proposal was one of the first realistic proposals for implementing a quantum computer experimentally, and it triggered a lot of both experimental and theoretical work in the field. There are, however, severe experimental challenges in the proposal. The proposal requires that the vibrational state is cooled to the ground state, but for various technical reasons the vibrations of the ions are subject to heating. This makes ground state cooling a difficult task, but for a few ions, cooling to the ground state of the vibration has been accomplished [44, 74, 75]. Ground state cooling is easiest in traps with a high trap frequency so that the separation between the energy levels is large. At high frequencies the separation between the ions is small because the strong confining forces from the trap push the ions together. This creates a new problem because it is difficult to focus a laser onto a single ion when the separation of the ions is small. In the experiment in Ref. [74] the separation between the ions was only 2 μm whereas the laser beam waist was 20 μm, making it impossible to address the individual ions. Instead of addressing the individual ions with lasers, an alternative method is to make the micro motion different for the ions in the trap [76]. This technique has enabled the production of a two particle entangled state by following the original scheme [77].

To circumvent the problems of ground state cooling and individual addressing, we have developed an alternative implementation of quantum gates by using bichromatic light with two different frequencies. Our gate is both insensitive to the vibrational state and robust against changes in the vibrational motion occurring during operation (heating), as long as the ions are in the Lamb-Dicke regime. At the same time our gate also has advantages in situations without individual access. Without any need for individual addressing, our gate can be used to create a maximally entangled state of any number of particles by illuminating all the ions in the trap with a single broad beam of

bichromatic light. Our gate will be described in the following chapter.

Our scheme is not the only alternative to the original proposal. It has been proposed [78] to use widely separated vibrational states and to focus a laser laser beside the initial position of the ions. In this proposal the vibration of one ion pushes another ion into the focus of the laser such that the second ion is flipped conditioned on the movement of the first ion. This scheme also works if the vibrational mode is not cooled to the ground state, but it can not be generalized beyond 2 or 3 qubits. Another 'hot ion' scheme [79] involves adiabatic passage between even and odd numbers of vibrational excitation combined with phase flips which are conditioned on the vibrational state. This scheme is slow due to the adiabatic passage and is not applicable during heating. Milburn has proposed an alternative implementation of quantum gates which exploits the fact that the commutator of position and momentum is a constant [80]. As we will show later, this proposal is actually a different limit of our original proposal [2, 3], and the combination of our proposal with the proposal of Milburn enables a faster operation of the gate. In Ref. [81] it is proposed to use strong fields such that the Rabi frequency Ω is resonant with the vibrational motion. In this way it is possible to transfer excitation between the dressed states and the vibrational motion and implement a scheme similar to the original scheme. By tuning the dressed state off-resonance with the vibrational motion this scheme is turned into a new variant of our proposal and it becomes insensitive to the vibrational state [82]. Recently it has been proposed [83] that the coupling of internal and external states may be achieved by using a combination of inhomogeneous magnetic fields and micro-wave fields.

All the methods involving only linear ion traps have the drawback that they are not directly scalable to any number of ions. With increasing number of ions in the trap, the ratio of the radial frequency to the axial frequency of the ions has to been increased in order to avoid a phase transition from a linear string of ions to a zig-zag configuration [84] and this will limit the number of ions that can be processed in a single trap. Instead it has been suggested to use ions trapped in separate traps [85]. These traps can either contain small ion trap processors which are connected by optical means [86] or one can use a movable ion which interacts with stationary qubits in different traps [87, 88]. In this way the ion trap quantum processor is in principle scalable to any number of ions.

Chapter 4

The bichromatic gate

In this chapter we describe our bichromatic gate. In section 4.1 we present our original proposal which suggests a gate which is rather slow but has the attractive feature that it is insensitive to heating as we show in section 4.2. In section 4.3 we show how our our proposal enables the production of some very interesting multi-particle entangled states, and finally in section 4.4 we show how our procedure can be derived in a more general way. This derivation enables a faster gate operation than in section 4.1. In this chapter we make several approximations. The validity of these idealizations in an actual experiment is the subject of chapter 5.

4.1 Slow gate

Like in the original ion trap scheme [71], we address each ion with a single laser, but quantum logic gates involving two ions are performed through off-resonant laser pulses. For the laser addressing the first ion, we choose a detuning close to the upper sideband, *i.e.*, close to resonance with a joint vibrational and internal excitation of the ion. We choose the detuning of the laser addressing the second ion to be the negative of the detuning of the first laser, see Fig. 4.1 (a). As shown in Fig. 4.1 (b), this laser setting couples the states $|ggn\rangle \rightarrow \{|egn+1\rangle, |gen-1\rangle\} \rightarrow |een\rangle$, where the first (second) letter denotes the internal state e or g of the first (second) ion and n is the quantum number for the relevant vibrational mode of the trap. We choose the laser intensity to be much less than the detuning ($\Omega << \delta$) so that we can neglect the direct coupling from $|ggn\rangle$ to $|egn\rangle$ and $|gen\rangle$, and we also choose the detuning from the sidebands so large that the intermediate states $|egn+1\rangle$ and $|gen-1\rangle$ are not populated in the process ($\nu_k - \delta >> \eta\Omega$). As we shall show below, the internal state transition $|ggn\rangle \rightarrow |een\rangle$ is insensitive to the vibrational quantum number

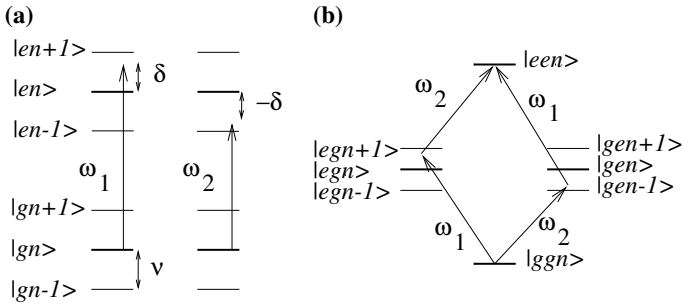

Figure 4.1: Energy levels and laser detunings. **(a)** Two ions with quantized vibrational motion are illuminated with lasers detuned close to the upper and lower sidebands. **(b)** The ions oscillate in collective vibrational modes, and two interfering transition paths are identified.

n, and it may be applied even when the ions exchange vibrational energy with a surrounding reservoir.

If we tune the lasers sufficiently close to a sideband, we can neglect all other vibrational modes and concentrate on one collective degree of vibrational excitation of the ions. In this case the Hamiltonian (3.2) reduces to

$$\begin{aligned} H &= H_0 + H_{\rm int} \\ H_0 &= \nu(a^\dagger a + 1/2) + \omega_{eg} \sum_j \sigma_{zj}/2 \\ H_{\rm int} &= \sum_j \frac{\Omega_j}{2}(\sigma_{+j}\ {\rm e}^{i(\eta(a+a^\dagger)-\omega_j t)} + h.c.), \end{aligned} \tag{4.1}$$

Here we assume that we tune the lasers close to the center-of-mass vibrational mode where the coupling of the recoil to the vibration is identical for all ions, and to simplify the notation we have omitted the subscript referring to the mode number on a, ν and η. The expressions derived below can easily be generalized to any other mode. We consider an ion trap operating in the Lamb-Dicke limit, where the Lamb-Dicke parameter η is much smaller than unity for all ions and the ions are cooled to a regime with vibrational quantum numbers n ensuring that $\eta\sqrt{n+1}$ is well below unity. Note that this may still allow n-values well above unity. In our analytical calculations we use an expansion of $H_{\rm int}$ to second order in η, but in our numerical treatment we apply the full Hamiltonian (4.1).

We wish to perform an operation on the mutual state of two ions 1 and 2 selected freely within the string of ions, and we assume that $\Omega_1 = \Omega_2 = \Omega$. With the choice of detunings described above, the only energy conserving transitions

are between the states $|ggn\rangle$ and $|een\rangle$. The Rabi frequency $\tilde{\Omega}$ for the transition between these states, via intermediate states m, can be determined in second order perturbation theory,

$$\left(\frac{\tilde{\Omega}}{2}\right)^2 = \left|\sum_m \frac{\langle een|H_{\rm int}|m\rangle\langle m|H_{\rm int}|ggn\rangle}{E_{ggn}+\omega_j-E_m}\right|^2, \tag{4.2}$$

where the laser energy ω_j is the energy of the laser addressing the ion which is excited in the intermediate state $|m\rangle$. If we restrict the sum to $|egn+1\rangle$ and $|gen-1\rangle$, we get

$$\tilde{\Omega} = -\frac{(\Omega\eta)^2}{2(\nu-\delta)}, \tag{4.3}$$

where $\delta = \omega_1 - \omega_{eg}$ is the detuning of the laser addressing the first ion. If the additional far off-resonant coupling to the lower (higher) sideband of ion 1 (2) is included, $2(\nu-\delta)$ in Eq. (4.3) is replaced by $(\nu^2-\delta^2)/\nu$.

The remarkable feature in Eq. (4.3) is that it contains no dependence on the vibrational quantum number n. This is due to interference between the two paths indicated in Fig. 4.1 (b). If we take the path where ion No. 1 is excited first, we have a factor of $n+1$ appearing in the numerator ($\sqrt{n+1}$ from raising and $\sqrt{n+1}$ from lowering the vibrational quantum number). In the other path we obtain a factor of n. Due to the opposite detunings, the denominators in Eq. (4.2) have opposite signs and the n-dependence disappears when the two terms are subtracted. The coherent evolution of the internal atomic state is thus insensitive to the vibrational quantum numbers, and it may be observed with ions in any superposition or mixture of vibrational states.

From the above arguments we expect to see perfect sinusoidal oscillations between the population of the internal states $|gg\rangle$ and $|ee\rangle$. To confirm the validity of our pertubative analysis we have performed a direct numerical integration of the Scrödinger equation with the Hamiltonian (4.1) to all orders in η. We have considered a situation, where both ions are initially in the internal ground state. For the vibrational state, we have investigated a number of different states, including Fock, coherent and thermal states, all yielding qualitatively similar results. The outcome of the computation for a coherent state of vibrational motion can be seen in Fig. 4.2, where we show the evolution of relevant terms of the atomic internal state density matrix $\rho_{ij,kl} = {\rm Tr}_n(\rho^{tot}|kl\rangle\langle ij|)$, where $i,j,k,l = e$ or g, ρ^{tot} is the density matrix for the total system consisting of the internal and vibrational states, and ${\rm Tr}_n$ denotes the partial trace over the unobserved vibrational degrees of freedom. The figure clearly shows that we have Rabi oscillations between the atomic states $|gg\rangle$ and $|ee\rangle$, and the values of the off diagonal element $\rho_{gg,ee}$ confirm that we have a coherent evolution of the internal atomic state which is not entangled with the vibrational motion. Superimposed on the sinusoidal curves are small oscillations with a high frequency due to off-resonant couplings from $|ggn\rangle$ to $|egn+1\rangle$, $|gen-1\rangle$, $|egn\rangle$,

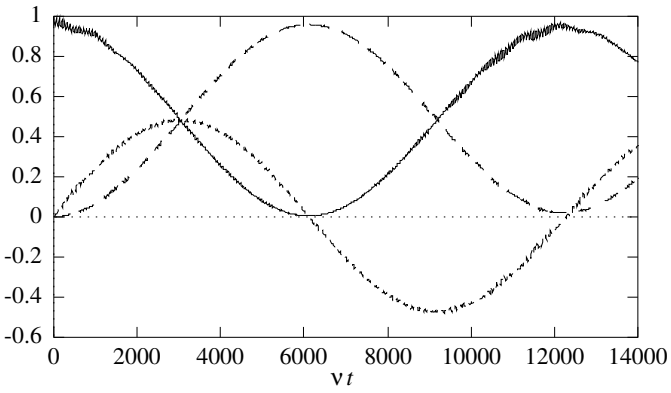

Figure 4.2: Rabi oscillations between $|gg\rangle$ and $|ee\rangle$. The figure shows the time evolution of the internal atomic density matrix elements $\rho_{gg,gg}$ (full line), $\rho_{ee,ee}$ (long dashed line) and $\mathrm{Im}(\rho_{gg,ee})$ (short dashed line). The magnitude of $\mathrm{Re}(\rho_{gg,ee})$ is below 0.03 and is not shown. In the initial state, the ions are in the internal ground state and a coherent vibrational state with mean excitation $\bar{n} = 2$. Parameters are $\delta = 0.90\ \nu$, $\Omega = 0.10\ \nu$, and $\eta = 0.10$.

and $|gen\rangle$. The magnitude of these oscillation and the deviation from ideal transfer between $|gg\rangle$ and $|ee\rangle$ can be suppressed by decreasing Ω.

The analysis given so far is sufficient for creation of internal state entanglement, completely decoupled from the external motion of the ions. By optical pumping we can prepare a state $\rho^{tot} = |gg\rangle\langle gg| \otimes \rho_{vib}$, and if we apply radiation fields corresponding to a pulse of duration $t = \frac{\pi}{2|\Omega|}$, our system is described by the density operator $\rho^{tot} = |\psi\rangle\langle\psi| \otimes \rho_{vib}$, where $|\psi\rangle$ is a maximally entangled EPR-state $(|gg\rangle - i|ee\rangle)/\sqrt{2}$.

$|eg\rangle$ and $|ge\rangle$

To be relevant for quantum computation, we also need a controlled coherent evolution of the states $|eg\rangle$ and $|ge\rangle$. Since these states do not fulfill any resonance condition one might expect that they are unaffected by the laser pulses. But due to n-dependent perturbations of the energy levels by the lasers this is not the case. Keeping only the most important terms, we get the energy shifts from perturbation theory

$$\begin{aligned}
\Delta E_{ggn} &= \Delta E_{een} = -\frac{(\eta\Omega)^2}{4}\frac{1}{\nu-\delta} \\
\Delta E_{egn} &= \frac{(\eta\Omega)^2}{2}\frac{n}{\nu-\delta} - \frac{\Omega^2}{2\delta} \\
\Delta E_{gen} &= -\frac{(\eta\Omega)^2}{2}\frac{n+1}{\nu-\delta} + \frac{\Omega^2}{2\delta}.
\end{aligned} \tag{4.4}$$

The energy shifts of the $|een\rangle$ and $|ggn\rangle$ are identical and independent of n, but since the energy shifts of $|egn\rangle$ and $|gen\rangle$, depend on the vibrational quantum number, the time evolution introduces phase factors $e^{-i\Delta E_{egn}t}$ which depend on n. At the time $t = T_{inv} = \frac{2\pi(\nu-\delta)}{\eta^2\Omega^2}$ where $|gg\rangle$ end $|ee\rangle$ are inverted, factors of $(-1)^n$ will tend to extinguish the coherence between internal states $|ee\rangle$ and $|eg\rangle$. This is shown in Fig. 4.3 where we start out with the first ion in a superposition $(|g\rangle + |e\rangle)/\sqrt{2}$ and the second ion in $|g\rangle$. The figure shows that the off-diagonal density matrix element $\rho_{gg,eg}$ quickly vanishes due to the entanglement with the vibrational motion. At time $t \approx 2T_{inv}$ the phase factors become independent of n and there is a revival of coherence.

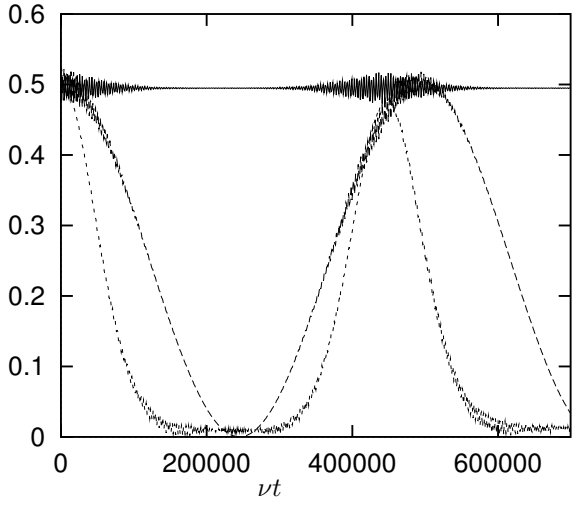

Figure 4.3: Decay and revival of the coherence between $|gg\rangle$ and $|eg\rangle$. The figure shows the evolution of $\rho_{eg,eg}$ (full line), $\rho_{gg,gg}$ (long dashed line) and the magnitude of the coherence $|\rho_{gg,eg}|$ (short dashed line), when ion 1 is initially in a superposition $(|e\rangle + |g\rangle)/\sqrt{2}$ and ion 2 is in $|g\rangle$. Parameters are $\delta = 0.96\ \nu$, $\Omega = 0.01\ \nu$, and $\eta = 0.10$.

The coherence between $|ee\rangle$ and $|eg\rangle$ can be restored by a trick resembling photon echoes [89]. Notice that the n-dependent part of ΔE_{egn} is minus the n-dependent part of ΔE_{gen}. If at any time $T/2$ we change the sign of the laser detuning δ, phase components proportional to n will begin to rotate in the opposite direction and at time T we will have a revival of the coherence. This is confirmed by our numerical solution of the Schrödinger equation presented in Fig. 4.4, where we change the laser detunings at the time $T_{inv}/2$, and at the time T_{inv} we have completed the transfer $(|gg\rangle+|eg\rangle)/\sqrt{2} \rightarrow (-i|ee\rangle+|eg\rangle)/\sqrt{2}$.

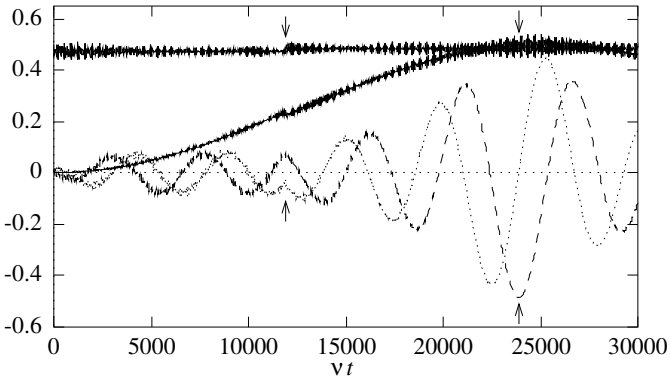

Figure 4.4: Revival of coherence at T_{inv}. Initially ion 1 is in a superposition $(|g\rangle + |e\rangle)/\sqrt{2}$ and ion 2 is in $|g\rangle$. The sign of δ is changed at $T_{inv}/2$ (left arrows), to ensure the perfect transition at T_{inv} (right arrows). The full lines represent populations of $|ee\rangle$ and $|eg\rangle$. The dotted and the dashed curves represent the real and imaginary part of the coherence $\rho_{ee,eg}$. Parameters are $\delta = 0.90\ \nu$, $\Omega = 0.05\ \nu$ and $\eta = 0.10$.

4.2 Heating

No particularly demanding assumptions have been made for the experimental parameters. With a vibrational frequency $\nu/2\pi = 200$ kHz, the transition shown in Fig. 4.2, require Rabi frequencies $\Omega/2\pi$ of modest 20 kHz, and the evolution from $|gg\rangle$ to $|ee\rangle$ is accomplished in 5 ms. This time scale is, however, longer than the time scale in the original ion trap proposal [71], due to the use of off-resonant interactions instead of resonant couplings. To be relevant for real computational tasks, it is necessary that our evolution is robust against decoherence effects on this longer time scale. An important source of decoherence is heating of the vibrational motion, and it is a major asset of our proposal that it can be made insensitive to the interaction with the environment. The arguments leading to Eq. (4.3) do not require that the ions remain in the same vibrational state, and the coherent oscillation from $|gg\rangle$ to $|ee\rangle$ may still be observed when the vibrational motion exchange energy with a thermal reservoir. The photon echo trick, however, is sensitive to heating: If the vibrational quantum number n changes its value at the time $T/2$ where the detunings are inverted, the second half of the gate, will no longer revert the phase evolution due to the new value of n and coherence is lost. If instead the detunings are inverted N times during a gate, the erroneous phase will only be of the order of the phase evolution during the time T/N, and the effect of the heating is reduced.

Rather than inverting the detunings a large number of times, we suggest to continuously apply lasers with both detunings $\pm\delta$ on both ions. With two fields

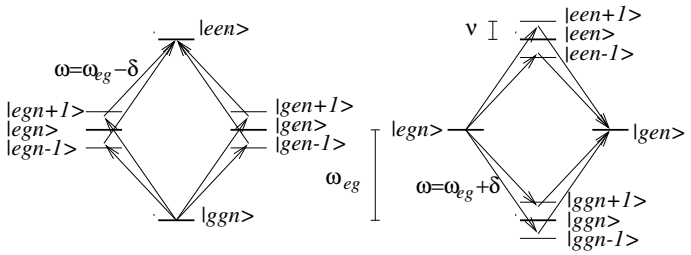

Figure 4.5: Illumination with bichromatic light. **(a)** Two additional transition paths exist between $|ggn\rangle$ and $|een\rangle$. The strengths of the additional paths are identical to the strength of the paths in Fig. 4.1 and the effective Rabi frequency in Eq. (4.3) is doubled. **(b)** Four similar transition paths are identified between states $|egn\rangle$ and $|gen\rangle$, yielding the same effective coupling among these states as between the states in part (a).

of opposite detunings and identical Rabi frequency Ω there are two contributing paths in addition to the two paths in Fig. 4.1, see Fig. 4.5 (a). The contribution from the two additional paths are identical to the two original paths, and the only modifications of the $|gg\rangle \leftrightarrow |ee\rangle$ Rabi frequency in Eq. (4.3) is multiplication by a factor of two. With bichromatic fields there also exists a resonant transition from $|eg\rangle$ to $|ge\rangle$, see Fig. 4.5 (b). The Rabi frequency of this transition is the negative of the Rabi frequency from $|gg\rangle$ to $|ee\rangle$ and the evolution will be described by

$$\begin{aligned}
|gg\rangle &\rightarrow \cos\left(\tfrac{\tilde{\Omega}t}{2}\right)|gg\rangle + i\ \sin\left(\tfrac{\tilde{\Omega}t}{2}\right)|ee\rangle \\
|ee\rangle &\rightarrow \cos\left(\tfrac{\tilde{\Omega}t}{2}\right)|ee\rangle + i\ \sin\left(\tfrac{\tilde{\Omega}t}{2}\right)|gg\rangle \\
|ge\rangle &\rightarrow \cos\left(\tfrac{\tilde{\Omega}t}{2}\right)|ge\rangle - i\ \sin\left(\tfrac{\tilde{\Omega}t}{2}\right)|eg\rangle \\
|eg\rangle &\rightarrow \cos\left(\tfrac{\tilde{\Omega}t}{2}\right)|eg\rangle - i\ \sin\left(\tfrac{\tilde{\Omega}t}{2}\right)|ge\rangle.
\end{aligned} \tag{4.5}$$

To validate that the evolution in Eq. (4.5) is in fact stable against heating, we introduce a thermal reservoir described by relaxation operators $C_1 = \sqrt{\Gamma(1+n_{th})}a$ and $C_2 = \sqrt{\Gamma n_{th}}a^\dagger$, where Γ characterizes the strength of the interaction and n_{th} is the mean vibrational number in thermal equilibrium. We analyse the dynamics of the system using Monte Carlo wavefunctions [90], which evolve with a non-Hermitian Hamiltonian interrupted by jumps at random times. The result of the computation can be seen in Fig. 4.6, where we show (left) the result of a single Monte Carlo realization with quantum jumps indicated by arrows and (right) the average over 10 realizations. In the figure we have chosen $n_{th} = 2$. This rather low value could represent a heating mechanism counteracted by laser cooling on a particular ion reserved for this purpose.

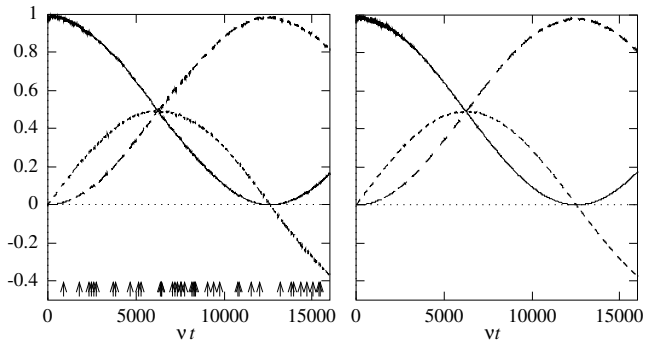

Figure 4.6: Rabi oscillations in a heating trap. The left panel shows the result of a single Monte Carlo realization with a total of 39 jumps occurring at times indicated by the arrows. The right panel is an average over 10 realizations. The curves represent $\rho_{gg,gg}$ (full line), $\rho_{ee,ee}$ (long dashed) and $\mathrm{Im}(\rho_{gg,ee})$ (short dashed). Parameters are $\delta = 0.90\ \nu$, $\Omega = 0.05\ \nu$, $\eta = 0.1$, $\Gamma = 2 \cdot 10^{-4}\ \nu$, and $n_{th} = 2$.

In the simulations 34 vibrational quanta are exchanged with the reservoir on average, and we wish to emphasize that with the proposed scheme, the gate is almost unaffected even though the duration of the gate is much longer than the coherence time of the channel used to communicate between the qubits. In chapter 5 we calculate the effect of heating analytically.

4.3 Multi-particle entanglement

Access to the individual ions is required for the construction of a general purpose quantum computer. As discussed in chapter 3, such individual access is problematic in traps with high trapping frequencies where the cooling to the Lamb-Dicke limit is easier to perform. It is a major asset of our proposal that our gate is capable of producing multi-particle entangled states even in situations where there is no access to the individual ions.

Suppose that there are only two ions in the trap and that we illuminate the ions with a broad beam of bichromatic light. If the beam has the same intensity in both colours, this is exactly the situation depicted in Fig. 4.5, and the evolution of the internal state of the ions is described by Eq. (4.5). If the ions are initially prepared in the ground state $|gg\rangle$, an EPR-state $(|gg\rangle - i|ee\rangle)/\sqrt{2}$ may be generated. Incidentally, it turns out that we may also generate maximally entangled states

$$|\Psi\rangle = \frac{1}{\sqrt{2}}\big(\mathrm{e}^{i\phi_g}|gg...g\rangle + \mathrm{e}^{i\phi_e}|ee...e\rangle\big), \tag{4.6}$$

for any number of ions (N), by simply illuminating all ions with the bichromatic

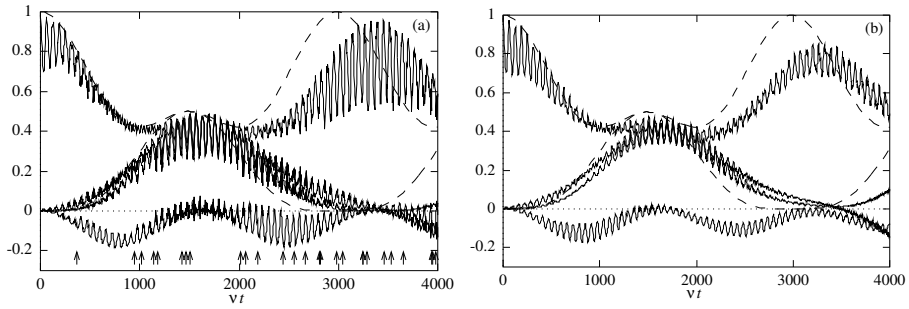

Figure 4.7: Generation of a state like Eq. (4.6) by illuminating 4 ions with a broad laser beam. The physical parameters are $\delta = 0.90\nu$, $\Omega = 0.10\nu$, $\eta = 0.10$, $\Gamma = 0.0001\nu$, and $n_{th} = 5$. (a) Single Monte Carlo realization with quantum jumps in the vibrational states at instants of time, indicated by arrows in the figure. (b) Average over 10 realizations. The first full curve (counted from above at $\nu t < 1000$) is the population of the joint ground state, the second one is the imaginary part of the internal density matrix element between the joint ground and the joint excited state, the third one is the population of the joint excited state, and the fourth one is the real part of the off-diagonal density matrix element. The dashed curves are equivalent to the $N = 4$ curves of Fig. 4.8, obtained by application of the spin Hamiltonian (4.8).

light. The states in Eq. (4.6) have several very interesting applications both in fundamental physics and technology. They are Schrödinger cat superpositions of states of mesoscopic separation, and they are ideal for spectroscopic investigations. In current frequency standards each atom or ion evolves individually, so that the improvement in frequency uncertainty, as the number of particles (N) is increased, is of statistical nature, *i.e.*, the uncertainty behaves like $\frac{1}{\sqrt{N}}$. By binding the ions together as in Eq. (4.6) the phase evolution of the excited state $|ee...e\rangle$ is increased by a factor of N, and consequently the frequency uncertainty is proportional to $\frac{1}{N}$ resulting in an improved sensitivity [91]. Note however, that it has been shown that if the duration of the measurement is comparable to the decoherence time of the internal state, the increased vulnerability of the state (4.6) to decoherence will remove this gain in sensitivity [92]. We shall return to the question of improving frequency standards in part III where we propose different methods to produce multi-particle entangled states.

In Fig. 4.7 we show a simulation for four ions initially in the ground state $|g\rangle$. At $t = 0$ the ions are illuminated by a broad beam of bichromatic light, and at $\nu t \approx 1500$ a state closely resembling, the state in Eq. (4.6) is generated. Again, we emphasize that no particular demanding experimental assumptions have been made. In particular, the internal state generation is robust against the heating of the external motion. Below, we show that states like (4.6) may be generated for any number of ions without access to the individual ions.

To describe the dynamics leading to the generation of states like Eq. (4.6)

it is convenient to apply the spin-representation, where the kth ion is represented as a spin 1/2 particle with the two eigenstates of the $j_{z,k}$ operator, $|jm\rangle_k = |1/2, 1/2\rangle_k$ and $|1/2, -1/2\rangle_k$, representing $|e\rangle_k$ and $|g\rangle_k$. In the spin-representation the time evolution described in Eq. (4.5) is identical to time evolution $\exp(-iHt)$ with the Hamiltonian

$$H = -\frac{\tilde{\Omega}}{2}\left(j_{+,k}j_{+,l} + j_{-,k}j_{-,l} - j_{+,k}j_{-,l} - j_{-,k}j_{+,l}\right) = 2\tilde{\Omega}j_{y,k}j_{y,l}, \tag{4.7}$$

where k (l) refers to the number of the first (second) atom in Eq. (4.5). In section 4.1 the center-of-mass mode was only used for convenience; other modes could also be used to implement gates between two ions. To create states like (4.6) it is necessary that transitions like those described in Eq. (4.5) occur between all pairs of ions with the same effective Rabi frequency $\tilde{\Omega}$, and we have to use the center-of-mass mode, where all ions participate equally[1]. With identical intensity illuminating all ions and using the center-of-mass vibrational motion, the action of our external driving field is completely symmetric with respect to interchange of the ions, and the Hamiltonian describing the evolution of all ions in the trap is obtained by summing the Hamiltonian (4.7) over all pairs k and l

$$H = \sum_{\text{All pairs } k,l} 2\tilde{\Omega}j_{y,k}j_{y,l} = \tilde{\Omega}J_y^2. \tag{4.8}$$

Here we have introduced a collective spin operator which is just the sum of the individual particle spin operators $J_\xi = \sum_k j_{\xi,k}$ ($\xi = x, y, z$). In the remainder of this thesis these operators will used several times to express collective properties of two-level systems. Strictly speaking, the last equality in Eq. (4.8) is not correct since the product of two J_y operators involves the sum of $j_{y,k}^2$ which is not present on the left side. However, since $j_{y,k}^2 = 1/4$ for spin 1/2 particles these terms only add a constant which is of no relevance to the time evolution, and this is omitted from the equation for simplicity. A more rigorous derivation of this Hamiltonian will be presented in section 4.4.

States with N_e excited ions which are symmetric with respect to interchange of the ions may be described by the eigenstates $|JM\rangle = |N/2, N_e - N/2\rangle$ of the J_z operator $J_z|JM\rangle = M|JM\rangle$. Initially all ions are in the ground state $|g\rangle$ corresponding to the spin state $|N/2, -N/2\rangle$, and since the interaction only involves the J_y-operator which conserves the total angular momentum, the quantum state remains in the $J = N/2$ subspace (any interaction which is symmetric with respect to interchange of the particles conserves the total angular momentum).

[1] Actually it is sufficient that the magnitude of $|\eta_{j,l}|$ is the same for all ions j. In the experiment in Ref. [44] a higher mode where the sign of $\eta_{j,l}$ changes with j was used because the heating rate of this mode was lower than the heating rate of the center-of-mass mode.

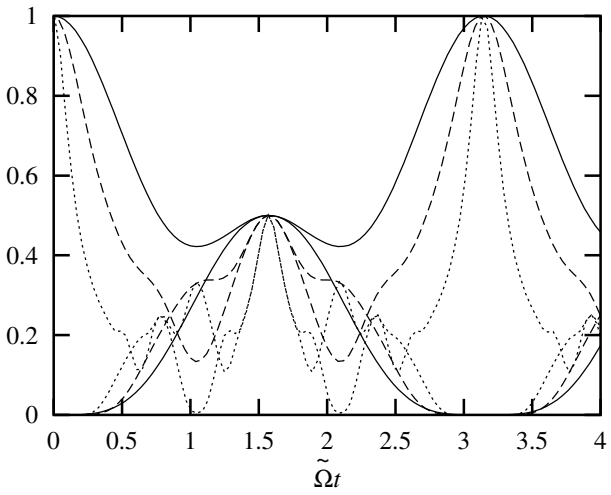

Figure 4.8: Time evolution of the population of the joint ionic ground state $|gg...g\rangle = |N/2, -N/2\rangle$ (curves starting from the value of unity at $t = 0$), and the joint ionic excited state $|ee...e\rangle = |N/2, N/2\rangle$. Results are presented for different values of the number of ions: N=4 (solid curves), N=8 (dashed curves), and N=20 (dotted curves). At $t = \pi/(2\tilde{\Omega})$ the states are in a 50-50 superposition and the state (4.6) is obtained.

Time evolution is accommodated by application of the operator $U(t) = \exp(-i\tilde{\Omega}J_y^2 t)$ to the initial state $|N/2, -N/2\rangle$ and the population becomes distributed on all $|J, M\rangle$ states, with M differing from $-N/2$ by an even number. If N is even, population is transferred all the way to the state $|N/2, N/2\rangle$, which is the second component of (4.6). Moreover, at the instant $t = \pi/(2\tilde{\Omega})$, the state is precisely of the form (4.6), with[2] $\phi_g = -\pi/4$ and $\phi_e = \pi/4$. We show in Fig. 4.8. the time evolution of the populations of the two extremal states for different (even) numbers of ions. At $t = \pi/(2\tilde{\Omega})$ and at later odd multiples of this value, both populations equal one half. For comparison, we have also plotted the time evolution with the Hamiltonian (4.8) in Fig. 4.7. The two approaches are roughly in agreement with the parameters chosen, and the difference between the curves can be diminished with other physical parameters.

This result can be understood from the rotation properties of angular momenta. The initial state can be expanded on eigenstates of J_y: $|N/2, -N/2\rangle = \sum_M c_M |N/2, M\rangle_y$. To find the relation to a similar expansion of $|N/2, N/2\rangle$,

[2]These phases are actually at variance with the result in Fig. 4.7. This is because $\tilde{\Omega}$ is negative in this simulation, so that the stated values of ϕ_g and ϕ_e are obtained by propagating the wavefunction backwards in time. By propagating forward we get the negative of the phases, as may be deduced from Fig. 4.7.

we note that up to a phase factor, $|JM\rangle$ may be obtained by rotating $|J-M\rangle$ around the y-axis by an angle π, and with the conventional choice of phases we get $|JJ\rangle = (-1)^{2J}\exp(-i\pi J_y)|J-J\rangle$ [93]. This rotation is easily performed in the y basis where the operator is diagonal, and it follows that $|N/2,N/2\rangle = \sum_M c_M \mathrm{e}^{i\pi(N-M)}|N/2,M\rangle_y$. Inserting the values for ϕ_g and ϕ_e mentioned above, we can therefore write the state (4.6) as $\sum_M c_M(\mathrm{e}^{-i\pi/4} + (-1)^M\mathrm{e}^{i\pi/4})/\sqrt{2}|N/2,M\rangle_y$ (N even). The net factors multiplying the initial amplitudes c_M are unity for M even and $-i$ for M odd. The action of $U(t)$ in the J_y basis amounts to a multiplication of each amplitude c_M by $\exp(-i\tilde{\Omega}M^2t)$, and for $t=\pi/(2\tilde{\Omega})$ this factor just attains the desired value of unity for M even and $-i$ for M odd, such that a state like (4.6) is created. Mathematically, our analysis above resembles the one for production of superpositions of states of mesoscopic distance by propagation of an optical field through an amplitude dispersive medium [94].

The pairwise interaction between the ions does not produce a coherent coupling of the two components in (4.6) if N is odd. In this case, however, states like (4.6) with $\phi_g = -\pi/8$ and $\phi_e = 7\pi/8$ may be produced by applying a linear coupling $H=\xi J_y$ for the duration $t=\pi/(2\xi)$ in addition to our quadratic term (4.8). With an odd number of ions and the above phases, the state in Eq. (4.6) may be written as $\sum_M c_M(\mathrm{e}^{-i\pi/8} - \mathrm{e}^{i(7\pi/8-M\pi)})/\sqrt{2}|N/2,M\rangle_y$, where we apply the same expansion on eigenstates of J_y as above. Depending on the value of M, the quantity in the parenthesis attains the values $\mathrm{e}^{-i3\pi/8}$ and $\mathrm{e}^{i\pi/8}$, which is exactly the same as the value obtained from the time evolution operator $U=\exp(-i\pi/2(M_y^2+M_y))$. Since J_y and J_y^2 commute, the linear Hamiltonian may actually be applied before, after, or simultaneously with the quadratic one. This additional operation is easy to implement in the ion trap, where one only needs to drive the ions on the atomic resonance frequency ω_{eg}.

4.4 Fast gate

Experimental implementation of scheme presented so far has been attempted without success. The insensitivity to heating makes the proposal robust against the main source of noise, but unfortunately the gate time is so long that other sources of noise like fluctuating magnetic fields begin to be important [95]. To achieve a faster gate operation the gate has to be combined with a recent proposal by Milburn [80]. The revised proposal presented below, allows for a faster gate operation at the expense of being more sensitive to heating, and it has been successfully used to create four particle entangled states experimentally [44]. In future experiments with longer coherence times it might be an advantage to use the slow operation which is more robust against heating.

Milburn [80] proposed a realization of a multi-bit quantum gate in the ion trap, which also operates when the ions are vibrationally excited: Adjusting

the phases of laser fields resonant with sideband transitions, one may couple internal state operators to different quadrature components, *e.g.*, position and momentum, X and P, of the oscillatory motion. In Ref. [80] it is proposed to use the two Hamiltonians $H_1 = \lambda_1 J_z P$ and $H_2 = \lambda_2 J_z X$. By alternating application of the Hamiltonians H_1 and H_2 for a time τ, we may obtain the *exact* propagator

$$e^{iH_2\tau}e^{iH_1\tau}e^{-iH_2\tau}e^{-iH_1\tau} = e^{-i\lambda_1\lambda_2 J_z^2\tau^2} \tag{4.9}$$

because the commutator of the oscillator position and momentum is a number. The interaction between the ions contained in J_z^2 has been established via the vibrational degrees of freedom, but after the gate this motion is returned to the initial state and is not in any way entangled with the internal state dynamics. Milburn also considers the possibility of coupling different individual internal state operators successively to X and P, so that the commutator term provides the product of such operators.

We shall now demonstrate that our bichromatic excitation scheme is closely related to the proposal by Milburn, and that gate operation more rapid than concluded previously is possible. We now consider the interaction without restricting the parameters to a regime where no population is transfered to states with different n, *i.e.*, we shall omit the assumption $\eta\Omega << \nu - \delta$ which was used in section 4.1. For this purpose it is convenient to change to the interaction picture with respect to H_0. In the Lamb-Dicke limit with lasers detuned by $\pm\delta$ the interaction Hamiltonian becomes

$$\begin{aligned} H_{\rm int} = 2\Omega J_x \cos\delta t - \sqrt{2}\eta\Omega J_y[x(\cos(\nu-\delta)t + \cos(\nu+\delta)t) \\ + p(\sin(\nu-\delta)t + \sin(\nu+\delta)t)], \end{aligned} \tag{4.10}$$

where we have introduced the dimensionless position and momentum operators, $x = \frac{1}{\sqrt{2}}(a + a^\dagger)$ and $p = \frac{i}{\sqrt{2}}(a^\dagger - a)$, and the collective spin operators.

Choosing not too strong laser intensities $\Omega << \delta$ and tuning close to the sidebands $\nu - \delta << \delta$ we may neglect the J_x term and the terms oscillating at frequency $\nu + \delta$ in Eq. (4.10), and our interaction is a special case of the Hamiltonian

$$H_{\rm int} = f(t)J_y x + g(t)J_y p. \tag{4.11}$$

The exact propagator for the Hamiltonian (4.11) may be represented by the ansatz

$$U(t) = \mathrm{e}^{-iA(t)J_y^2}\mathrm{e}^{-iF(t)J_y x}\mathrm{e}^{-iG(t)J_y p}, \tag{4.12}$$

and the Schrödinger equation $i\frac{d}{dt}U(t) = H_{\rm int}U(t)$ then leads to the expressions

$$\begin{aligned} F(t) &= \int_0^t f(t')dt' \\ G(t) &= \int_0^t g(t')dt' \\ A(t) &= -\int_0^t F(t')g(t')dt'. \end{aligned} \tag{4.13}$$

From (4.10) follows that $f(t) = -\sqrt{2}\eta\Omega\cos(\nu-\delta)t$ and $g(t) = -\sqrt{2}\eta\Omega\sin(\nu-\delta)t$, and we get

$$\begin{aligned} F(t) &= -\frac{\sqrt{2}\eta\Omega}{\nu-\delta}\sin\left((\nu-\delta)t\right) \\ G(t) &= -\frac{\sqrt{2}\eta\Omega}{\nu-\delta}[1-\cos((\nu-\delta)t)] \\ A(t) &= -\frac{\eta^2\Omega^2}{\nu-\delta}\left[t - \frac{1}{2(\nu-\delta)}\sin(2(\nu-\delta)t)\right]. \end{aligned} \tag{4.14}$$

In the xp phase space the operator U performs translations $(x,p) \rightarrow (x + J_yG(t), p - J_yF(t))$ entangled with the internal state of the ions.

Apart from a change of basis from J_z to J_y the interaction considered by Milburn [80] may also be put in this form, with $f(t)$ and $g(t)$ alternating between zero and non-vanishing constants. Within the present formulation, the trick in Ref. [80] is to use functions $f(t)$ and $g(t)$ such that $F(t)$ and $G(t)$ both vanish after a period τ. At this instant the vibrational motion is returned to its original state, the propagator reduces to $U(\tau) = \mathrm{e}^{-iA(\tau)J_y^2}$, and we are left with an internal state evolution which is independent of the external vibrational state as in Eq. (4.3). This is the same propagator as the one that was shown to produce multi-particle entangled states in section 4.3. According to (4.13) the acquired factor $A(\tau)$ is equal to the area swept by the line segment between $(G(t),0)$ and $(G(t),-F(t))$, as shown in Fig. 4.9. If $(G(t),-F(t))$ forms a closed path, $A(t)$ is plus (minus) the enclosed area if the path is traversed in the (counter) clockwise direction. In the proposal by Milburn successive constant Hamiltonians proportional to x and p are applied and the area enclosed by $(G(t),-F(t))$ is rectangular. In our proposal the area is a circle of radius $\sqrt{2}\eta\Omega/(\nu-\delta)$, as illustrated in Fig. 4.9.

With the propagator in Eq. (4.12) we may calculate the time evolution of the system. Suppose that the ions are initially in the internal ground state and an incoherent mixture of vibrational state as described by the density matrix $\rho^{tot} = \sum_n P_n|g..gn\rangle\langle g..gn|$. The time evolution of the internal state density operator $\rho = \mathrm{Tr}_n(\rho^{tot})$ with any number of ions N may be found from

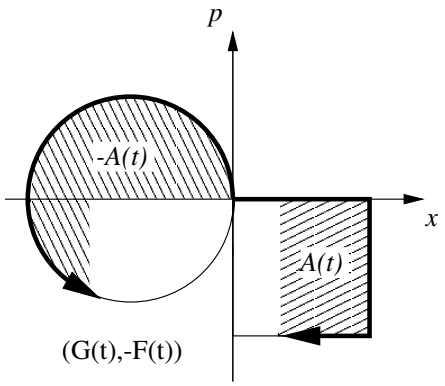

Figure 4.9: The paths traversed in phase space and the function $A(t)$ in Milburns proposal (rectangular path) and in our proposal (circular path).

$\rho_{a_1...a_N,b_1..b_N}(t) = \sum_n P_n \langle g..gn|U^\dagger(t)|b_1..b_N\rangle\langle a_1..a_N|U(t)|g..gn\rangle$ ($a_j, b_j = e$ or g), where we have used $\sum_n |n\rangle\langle n| = 1$ to remove one of the summations over vibrational states. Here we list the density matrix elements for the case of two ions $N = 2$:

$$
\begin{aligned}
\rho_{gg,gg} = \sum_n P_n \Big[& \frac{3}{8} + \frac{1}{2} \mathrm{e}^{-\frac{F(t)^2+G(t)^2}{4}} \\
& \times L_n\left(\frac{F(t)^2+G(t)^2}{2}\right) \cos\left(A(t) + \frac{1}{2}F(t)G(t)\right) \\
& + \frac{1}{8}\mathrm{e}^{-(F(t)^2+G(t)^2)} L_n\big(2(F(t)^2+G(t)^2)\big)\Big] \\
\rho_{ee,ee} = \sum_n P_n \Big[& \frac{3}{8} - \frac{1}{2} \mathrm{e}^{-\frac{F(t)^2+G(t)^2}{4}} \\
& \times L_n\left(\frac{F(t)^2+G(t)^2}{2}\right) \cos\left(A(t) + \frac{1}{2}F(t)G(t)\right) \\
& + \frac{1}{8}\mathrm{e}^{-(F(t)^2+G(t)^2)} L_n(2(F(t)^2+G(t)^2))\Big] \\
\rho_{gg,ee} = \sum_n P_n \Big[& \frac{1}{8}(1 - \mathrm{e}^{-(F(t)^2+G(t)^2)} L_n(2(F(t)^2+G(t)^2))) \\
& - \frac{i}{2}\mathrm{e}^{-\frac{F(t)^2+G(t)^2}{4}} L_n\left(\frac{F(t)^2+G(t)^2}{2}\right) \\
& \times \sin\left(A(t) + \frac{1}{2}F(t)G(t)\right)\Big],
\end{aligned}
\tag{4.15}
$$

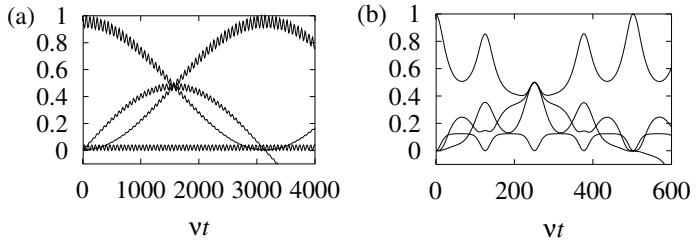

Figure 4.10: Time evolution of density matrix elements for two ions calculated from Eq. (4.15). (a) Weak field regime (b) Fast gate. The first curve (counting from above at $\nu t \approx 1000$ in (a) and $\nu t \approx 130$ in (b)) represents $\rho_{gg,gg}$, the second is the imaginary part of $\rho_{gg,ee}$, the third is $\rho_{ee,ee}$, and the last curve is the real part of $\rho_{gg,ee}$. The ions are initially in the internal state $|gg\rangle$ and a thermal vibrational state with an average of 2 vibrational quanta. In (a) the physical parameters are $\delta = 0.9\nu$, $\eta = 0.1$, and $\Omega = 0.1\nu$. In (b) the physical parameters are $\delta = 0.95\nu$, $\eta = 0.1$, and $\Omega = 0.177\nu$. The parameters in (b) are chosen such that a maximally entangled state $\frac{1}{\sqrt{2}}(|gg\rangle - i|ee\rangle)$ is formed at the time $\nu t \approx 250$, where the circular path in Fig. 4.9 has been traversed twice.

where L_n is the nth order Laguerre polynomium.

These expressions can be evaluated in different regimes. In the weak field regime, $\eta\Omega << \nu - \delta$, the xp phase space trajectory is a very small circle, which is traversed several times. $F(t)$ and $G(t)$ are negligible for all times, and $\mathrm{e}^{-iF(t)J_y x}\mathrm{e}^{-iG(t)J_y p}$ is approximately unity, such that we have an internal state preparation which is disentangled from the vibrational motion throughout the gate. Since $A(t) \approx -\eta^2\Omega^2 t/(\nu - \delta)$ if $(\nu - \delta)t >> 1$ the time evolution corresponds to the one obtained from an effective Hamiltonian $H = \tilde{\Omega}J_y^2$ with $\tilde{\Omega} = -\eta^2\Omega^2/(\nu - \delta)$, and Eq. (4.15) describes simple Rabi oscillations between the states $|gg\rangle$ and $|ee\rangle$. The expression for $\tilde{\Omega}$ derived here is twice as large as in the result in Eq. (4.3) because Eq. (4.3) assumes that each ion is only illuminated by a single frequency, whereas we now assume that all ions are illuminated by light detuned both above and below resonance. The Rabi oscillation is demonstrated in Fig. 4.10 (a) which shows the time evolution described by Eq. (4.15). The curves show sinusoidal Rabi oscillation from $|gg\rangle$ to $|ee\rangle$ superimposed by small oscillations due to the weak entanglement with the vibrational motion.

Outside the weak field regime the internal state is strongly entangled with the vibrational motion in the course of the gate. For successful gate operation we have to ensure that we return to the initial vibrational state at the end of the gate by choosing parameters such that $G(\tau) = F(\tau) = 0$, corresponding to $(\nu - \delta)\tau = K2\pi$, where K is an integer. A maximally entangled state is created if we adjust our parameters so that $A(\tau) = -\pi/2$. This is achieved if

the parameters are chosen in accordance with

$$\frac{\eta\Omega}{\nu-\delta} = \frac{1}{2\sqrt{K}}, \quad K = 1, 2, 3, \ldots . \tag{4.16}$$

By choosing a low value of K such that an entangled state is created after a few rounds in phase space we may perform a faster gate than considered in the weak field case. See Fig. 4.10 (b), where we have used $K = 2$, and where a maximally entangled state $\frac{1}{\sqrt{2}}(|gg\rangle - i|ee\rangle)$ is created at the time $\nu t \approx 250$.

By combining the requirement (4.16) with the condition $(\nu - \delta)\tau = K2\pi$ we may express the time for the state preparation as

$$\tau = \frac{\pi}{\eta\Omega}\sqrt{K}. \tag{4.17}$$

In order to avoid off-resonant excitations of the ions we must require $\frac{\Omega^2}{\nu^2} << 1$ and η^2 must be much less than unity to fulfill the Lamb-Dicke approximation (see chapter 5). For a given trap and/or laser intensity Eq. (4.17) sets a bound on the speed of the gate. In table 4.1 we give some numerical examples for the time of the gate for some typical experimental parameters.

So far we have demonstrated how our gate is capable of creating entanglement, but we have actually not yet discussed how our scheme can be used to construct a quantum computer. To show this, we demonstrate how we can implement a CONTROL-NOT operation, since any other operation can be constructed efficiently by CONTROL-NOT operations and single particle rotations as discussed in chapter 2. The CONTROL-NOT operation rotates the state of the second qubit if the first qubit is in the state $|1\rangle$. The operator $(\sigma_{z1} + 1)/2$ is a projector onto the space where the first ion is in $|1\rangle$ and the CONTROL-NOT operation can be written as

$$U_{\mathrm{CNOT}} = \mathrm{e}^{i\frac{\pi}{2}\frac{(\sigma_{z1}+1)}{2}\sigma_{x2}} = \mathrm{e}^{i\frac{\pi}{2}\frac{\sigma_{z1}\sigma_{x2}}{2}}\mathrm{e}^{i\frac{\pi}{4}\sigma_{x2}}. \tag{4.18}$$

Our interaction is of the form J_y^2, which is the same as $\frac{\sigma_{y1}\sigma_{y2}}{2}$ apart from irrelevant constant terms. By using single particle rotations before and after the application of the bichromatic gate, σ_{y1} and σ_{y2} can effectively be turned into σ_{z1} and σ_{x2}, and if we use $A(\tau) = -\pi/2$, the bichromatic gate implements the first exponential in U_{CNOT}. The last exponential is just a single particle rotation which can be applied before, after, or during the bichromatic gate, and the CONTROL-NOT operation can be constructed by a combination of a single bichromatic gate with $A(\tau) = -\pi/2$ and single particle rotations. The single particle operations may be performed much faster than the two qubit gates, so that the time required to perform a CONTROL-NOT operation is also given by (4.17). This method of writing logical gates as exponentials will also be used in chapter 6, where multi-bit gates are constructed.

Table 4.1: The time required to create the maximally entangled state $\frac{1}{\sqrt{2}}(|gg...g\rangle - i|ee..e\rangle)$ with a Lamb-Dicke parameter $\eta = 0.1$ for various trapping frequencies (ν) and laser intensities (Ω). The table shows the gate time if the entangled state is prepared after a single round in phase space. If the gate operation is accomplished after K rounds in phase space the time should be multiplied by $\sqrt{K}$.

$\frac{\Omega}{\nu}$	$\frac{\nu}{2\pi}$ =500 KHz	1 MHz	10 MHz
0.05	200 μs	100μs	10 μs
0.10	100 μs	50 μs	5 μs
0.20	50 μs	25 μs	2.5 μs

Chapter 5

Non-ideal conditions

In the previous chapter we made a number approximations in order to arrive at a solvable model. In this chapter we perform a more detailed analysis of the validity of these approximations and we estimate the effect of deviations from the ideal situation in an actual experiment. The general procedure in this chapter, is to change to the interaction picture with respect to the simple Hamiltonian (4.11) using the exact propagator in Eq. (4.12) and treat the small deviations from the ideal situation by perturbation theory. In section 5.1 we investigate the internal disturbances, which are due to a non-ideal interaction with the center-of-mass mode, *i.e.*, the approximations that we made to the Hamiltonian (4.1). These approximations are the omission of the direct coupling of internal states (subsection 5.1.1) and the Lamb-Dicke approximation (subsection 5.1.2). In section 5.2 we consider external disturbances which are not included in Eq. (4.1). We calculate the effect of spectator vibrational modes (subsection 5.2.1) and the effect of heating (subsection 5.2.2).

The figure of merit for the performance of the gate is taken to be the fidelity F of creation of the maximally entangled N-particle state $|\Psi_{max}\rangle = 1/\sqrt{2}(|gg...g\rangle - i|ee...e\rangle)$

$$F = \langle\Psi_{max}|\rho_{int}(\tau)|\Psi_{max}\rangle. \tag{5.1}$$

In the ideal case this state is created at the time when $A(\tau) = -\pi/2$, if the ions are initially in the $|gg...g\rangle$ state.

5.1 Internal disturbances

5.1.1 Direct coupling

Going from Eq. (4.10) to Eq. (4.11) we neglected a term $H_{\rm d} = 2\Omega J_x \cos(\delta t)$. This term describes direct off resonant coupling of $|g\rangle$ and $|e\rangle$ without changes

in the vibrational motion. For high laser power this term has a detrimental effect on the fidelity, which we calculate below.

Changing to the interaction picture, we may find the propagator $U_{\rm d}(t)$ from the Dyson series

$$U_{\rm d}(t) = 1 - i\int_0^t dt' H_{\rm d,Int}(t') - \int_0^t \int_0^{t'} dt' dt'' H_{\rm d,Int}(t') H_{\rm d,Int}(t'') + \dots \ , \quad (5.2)$$

where the interaction picture Hamiltonian $H_{\rm d,Int}$ is given by $H_{\rm d,Int}(t) = U^\dagger(t) H_{\rm d}(t) U(t)$. Since $H_{\rm d}(t)$ is oscillating at a much higher frequency than the propagator $U(t)$, we may treat $U(t)$ as a constant during the integration and we obtain

$$U_{\rm d}(t) = 1 - i\frac{2\Omega}{\delta}\sin(\delta t) U^\dagger(t) J_x U(t) - \frac{\Omega^2}{\delta^2}(1-\cos(2\delta t)) U^\dagger(t) J_x^2 U(t) + \dots \ . \quad (5.3)$$

Near the endpoint, $U(t) \approx {\rm e}^{i(\pi/2)J_y^2}$ and we obtain the fidelity

$$F \approx 1 - \frac{N\Omega^2}{2\delta^2}(1-\cos(2\delta\tau)), \quad (5.4)$$

where N is the number of ions participating in the gate. We plot in Fig. 5.1 the product of the fidelity due to the carrier (5.4) and the population of the EPR-state $\frac{1}{\sqrt{2}}(|gg\rangle - i|ee\rangle)$ expected from the time evolution in Eq. (4.15). The result agrees well with the result of a numerical integration of the Schrödinger equation with the Hamiltonian (4.10).

If the duration of the laser pulses can be controlled very accurately in the experiment, so that one fulfills both (4.16) and $2\delta\tau = 2K'\pi$, the effect of the direct coupling vanishes. If one cannot perform such an accurate control, the net effect of the direct coupling is to reduce the average fidelity by $\frac{N\Omega^2}{2\delta^2}$ (=0.03 for the parameters of Fig. 5.1).

5.1.2 Lamb-Dicke approximation

In chapter 4 we used the Lamb-Dicke approximation ${\rm e}^{i\eta(a+a^\dagger)} \approx 1 + i\eta(a+a^\dagger)$ to simplify our calculations. Now we investigate the validity of this approximation.

In the weak field case, we can use the exact matrix elements $\langle n|{\rm e}^{i\eta(a+a^\dagger)}|n+1\rangle = i\eta\frac{{\rm e}^{-\eta^2/2}}{\sqrt{n+1}} L_n^1(\eta^2)$, to obtain the effective Rabi frequency between $|ggn\rangle$ and $|een\rangle$

$$\begin{aligned}\tilde{\Omega}_n =& \tilde{\Omega}{\rm e}^{-\eta^2}\left[\frac{\left(L_n^1(\eta^2)\right)^2}{n+1} - \frac{\left(L_{n-1}^1(\eta^2)\right)^2}{n}\right] \\ \approx& \tilde{\Omega}\left[1 - \eta^2(2n+1) + \eta^4\left(\frac{5}{4}n^2 + \frac{5}{4}n + \frac{1}{2}\right)\right],\end{aligned} \quad (5.5)$$

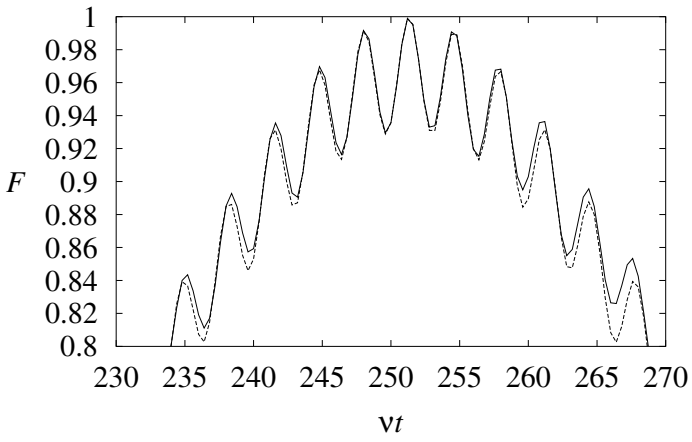

Figure 5.1: Population of the EPR-state $\frac{1}{\sqrt{2}}(|gg\rangle - i|ee\rangle)$ near the optimum. The full line is obtained by a numerical integration of the Hamiltonian (4.10) and the dashed line is the product of the expression in (5.4) and the expression for the fidelity obtained from Eq. (4.15). The parameters are the same as in Fig. 4.10 (b).

where $\tilde{\Omega}$ is given by $-\eta^2\Omega^2/(\nu-\delta)$, and where L_n^1 are the generalized Laguerre polynomials

$$L_n^\alpha(x) = \sum_{m=0}^{n} (-1)^m \begin{pmatrix} n+\alpha \\ n-m \end{pmatrix} \frac{x^m}{m!}. \tag{5.6}$$

The effective Rabi frequency is no longer independent of the vibrational quantum number n, and the internal state becomes entangled with the vibrational motion, resulting in a non-ideal performance of the gate. In Ref. [96, 97] it is proposed to use this n-dependent coupling to map out the vibrational state of the ion.

To illustrate the effect of deviations from the Lamb-Dicke approximation, we consider again the production of an EPR-state $\frac{1}{\sqrt{2}}(|gg\rangle - i|ee\rangle)$. With an n-dependent coupling strength the fidelity is

$$F = \frac{1}{2} + \frac{1}{2}\sum_{n=0}^{\infty} P_n \sin(\tilde{\Omega}_n t), \tag{5.7}$$

where P_n is the initial population of the vibrational state n. We show in Fig. 5.2 the evolution of the fidelity predicted by Eq. (5.7) and obtained by a direct integration of the full Hamiltonian in Eq. (4.1). Due to the deviation from the Lamb-Dicke approximation the effective Rabi frequency is reduced,

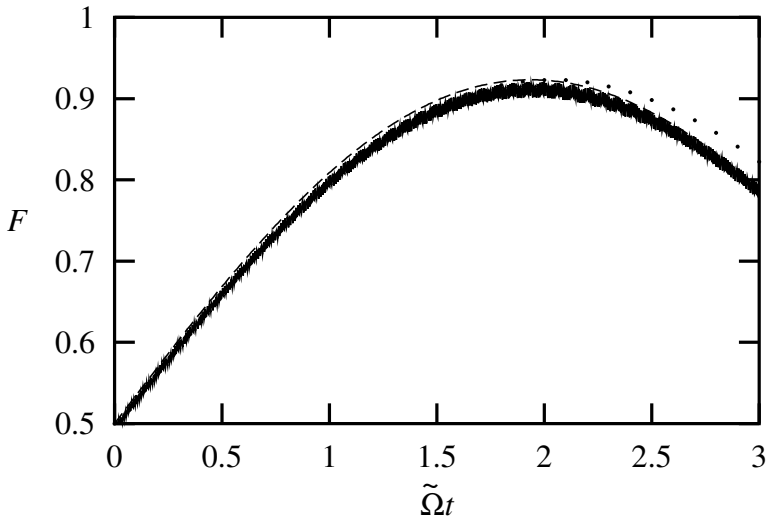

Figure 5.2: Evolution of the population of the EPR-state $\frac{1}{\sqrt{2}}(|gg\rangle - i|ee\rangle)$ for a vibrational thermal state with an average of 5 vibrational quanta and $\eta = 0.20$. The dotted line is the prediction from Eq. (5.7) and the solid line is the result of a numerical integration of the Hamiltonian (4.1) with parameters $\Omega = 0.02\nu$ and $\delta = 0.9\nu$. The discrepancy between the two curves at $\tilde{\Omega}t \gtrsim 2$ is due to additional off-resonant couplings which may be taken into account by multiplying the coupling strength by $\frac{2\nu}{\nu+\delta}$ (dashed curve).

cf., Eq. (5.5), and the optimal gate performance is achieved with a duration that is longer than $\pi/(2\tilde{\Omega})$. The spreading of the values of $\tilde{\Omega}_n$, causes entanglement with the vibrational motion which reduces the fidelity. With the parameters in Fig. 5.2 the maximal obtainable fidelity is 0.92 obtained after a pulse of duration $\tau \approx 1.9/\tilde{\Omega}$.

With more than two ions, the time evolution of the system may be obtained by expanding the initial state $|gg...g\rangle$ on eigenstates of the J_y operator:

$$|gg...g\rangle = \frac{(-i)^N}{2^{N/2}} \sum_{k=0}^{N} (-1)^k \sqrt{\begin{pmatrix} N \\ k \end{pmatrix}} |M_y = N/2 - k\rangle. \tag{5.8}$$

In the J_y basis the propagator (4.12) is diagonal and in the weak field regime ($F(t)$, $G(t) \approx 0$) with n dependent coupling strengths we get the fidelity

$$F = \sum_{n=0}^{\infty} P_n \left| \frac{1}{2^N} \sum_{k=0}^{N} \begin{pmatrix} N \\ k \end{pmatrix} \mathrm{e}^{i(N/2-k)^2(\pi/2-\tilde{\Omega}_n t)} \right|^2. \tag{5.9}$$

In the limit of many ions ($N >> 1$) and near the optimum ($\tilde{\Omega}_n t \approx \pi/2$) we may approximate this expression by assuming that k is a continuous variable and replacing the binomial coefficient by a Gaussian distribution with the same width. In this limit the fidelity becomes

$$F = \sum_{n=0}^{\infty} P_n \frac{1}{\sqrt{1 + \frac{N(N-1)(\pi/2-\tilde{\Omega}_n t)^2}{4}}}. \tag{5.10}$$

Expanding this expression to lowest order in η and adjusting the pulse duration to take into account the reduction in the coupling strength, we find to lowest order in η

$$F = 1 - \frac{\pi^2 N(N-1)}{8}\eta^4 \mathrm{Var}(n) \tag{5.11}$$

at the optimum time

$$\tau_{opt} = \frac{\pi}{2\tilde{\Omega}}(1 + \eta^2(2\bar{n}+1)), \tag{5.12}$$

where $\bar{n}$ and $\mathrm{Var}(n)$ are the mean and variance of the vibrational quantum number.

In Eq. (5.10) and (5.11) we have replaced a quantity N^2 following from the Gaussian approximation to (5.9) by $N(N-1)$. With this substitution (5.10) and (5.11) describe the fidelity well for all values of N. With the parameters of Fig. 5.2, Eq. (5.11) yields $F = 0.88$ which is in good agreement with the numerical result in the figure.

The equations (5.5-5.12) were derived for weak fields, but they also provide an accurate description of the system outside this regime. To show this we note that with bichromatic light, H_{int} in Eq. (4.1) may be written as

$$\begin{aligned} H_{\mathrm{int}} = 2\Omega\cos(\delta t)\Big[& J_x \cos\Big(\eta\sqrt{2}(x\cos(\nu t) + p\sin(\nu t))\Big) \\ & - J_y \sin\Big(\eta\sqrt{2}(x\cos(\nu t) + p\sin(\nu t))\Big)\Big] \end{aligned} \tag{5.13}$$

in the interaction picture with respect to H_0. An expansion of the trigonometric functions in this Hamiltonian leads to Eq. (4.10) which formed the basis of the discussion in chapter 4. The term proportional to J_x is suppressed because it is far off resonance. The lowest order contribution of this term was treated in subsection 5.1.1, and we shall now consider corrections to the J_y term which may have significant effects. In the interaction picture with respect to the lowest order Hamiltonian (4.11), x and p are changed into $x + J_y G(t)$ and $p - J_y F(t)$ and to lowest non-vanishing order in η, the interaction picture Hamiltonian is

$$H_3 = \eta^3 J_y \frac{\sqrt{2}\Omega}{12}\Big[\cos((\nu-\delta)t)h_1(x,p) + \sin((\nu-\delta)t)h_2(x,p)\Big], \tag{5.14}$$

where

$$\begin{aligned} h_1(x,p) =& 3x^3 + xp^2 + pxp + p^2x \\ h_2(x,p) =& 3p^3 + px^2 + xpx + x^2p, \end{aligned} \tag{5.15}$$

and where we have used that $F(t)$ and $G(t)$ are proportional to η. To calculate the effect of the Hamiltonian in (5.14) we note that the propagator

$$U_{3,\mathrm{int}}(t) = \mathrm{e}^{\left[-i\frac{\sin((\nu-\delta)t)}{\nu-\delta}h_1(x,p)\right]}\mathrm{e}^{\left[-i\frac{1-\cos((\nu-\delta)t)}{\nu-\delta}h_2(x,p)\right]} \tag{5.16}$$

is consistent with the Hamiltonian (5.14) until order η^5, *i.e.*, $i\frac{dU_{3,\mathrm{int}}(t)}{dt} = (H_3 + O(\eta^6))U_{3,\mathrm{int}}$. (But the full Hamiltonian contains terms of order η^4 and η^5 which are not taken into account in $U_{3,\mathrm{int}}$. These terms are included below). We are interested in the propagator at times $\tau = K2\pi/(\nu-\delta)$ where the vibrational motion is returned to the initial state. At these instants the exponents in Eq. (5.16) vanish and the propagator reduces to $U_3(\tau) = 1$ such that it has no influence on the internal state preparation.

Expanding the Hamiltonian to order η^6 we obtain the propagator to the same order in η in the interaction picture with respect to H_0 in (4.1)

$$U_6(\tau) = \mathrm{e}^{-i\tilde{\Omega}\tau J_y^2\left[1-\eta^2(2n+1)+\eta^4\left(\frac{5}{4}n^2+\frac{5}{4}n+\frac{1}{2}\right)\right]}\mathrm{e}^{i\eta^5 J_y^3\frac{\sqrt{8}\Omega^3}{(\nu-\delta)^2}x\tau}\mathrm{e}^{-i\eta^6 J_y^4\frac{5\Omega^4}{2(\nu-\delta)^3}\tau} \tag{5.17}$$

valid at times $\tau = K2\pi/(\nu-\delta)$. The first exponential provides the time evolution with the modified effective Rabi frequency in Eq. (5.5). If we evaluate the propagator (5.17) in the weak field regime, the last two exponentials both vanish in the limit of large K when the requirement (4.16) is inserted, and the time evolution in (5.17) is consistent with Eqs. (5.5-5.11). The last two exponentials are also of minor importance for a different reason: In Eq. (5.5) η^2 appears in the combination $\eta^2 n$, whereas it appears as η^2 in the last two exponentials of (5.17) when the condition (4.16) is inserted. In situations where deviations from the Lamb-Dicke approximation are important $\eta^2 n \sim 1$, the deviation is typically caused by a high value of n rather than a large value of η ($\eta^2 << 1$). In this case one may neglect the last two exponentials and the effect of the non-Lamb-Dicke terms are the same as in the case of weak fields as described by Eqs. (5.5-5.12). To achieve the optimum operation of the gate with the parameters of Fig. 5.2 we have to ensure $\tilde{\Omega}\tau \approx 1.9$ and there is a small correction to the condition in Eq. (4.16).

5.2 External disturbances

So far we have considered a system described by the Hamiltonian (4.1), where only the center-of-mass motion is present in the ion trap, and where the coupling of this mode to the surroundings is negligible. In this section we shall

remove these two assumptions and consider the decrease in fidelity due to the presence of other modes in the trap and due to heating of the center-of-mass vibrational motion.

5.2.1 Spectator vibrational modes

With N ions in the trap, the motional state is described by $3N$ non degenerate vibrational modes. With a proper laser geometry or if the transverse potential is much steeper than the longitudinal potential, the coupling of the laser to transverse modes will be negligible and the only contribution is from the N longitudinal modes. With N vibrational modes in the trap we need the full Hamiltonian in Eq. (3.2).

The center-of-mass mode ($l = 1$), which is used to create the entangled states of the ions, has $b_i^1 = 1/\sqrt{N}$ for all ions and is well isolated from the remaining $N-1$ vibrational modes $\nu_{l>1} \geq \sqrt{3}\nu$, so that we could neglect the contribution from the other modes in the previous chapter. Here we shall estimate the effect of the presence of the spectator modes. They have both a direct effect, due to the off-resonant coupling to the other modes, and an indirect 'Debye-Waller' effect [67] because the coupling strength of the center-of-mass mode is reduced due to the oscillations in the spectator modes. Below we shall calculate the direct and indirect effects separately.

In the Cirac-Zoller scheme [71], the n-dependent AC Stark shifts caused by coupling to other vibrational modes lead to decoherence, unless these modes are cooled to the ground state. In our bichromatic scheme, these internal state level shifts depend much less on the vibrational excitation. The lowest order contribution of the direct coupling to the spectator modes may be found by expanding the exponentials as in Eq. (4.10)

$$H_{\text{int}} = 2\Omega J_x \cos\delta t + \sum_{l=1}^{N} \Theta_l [x_l f_l(t) + p_l g_l(t)], \tag{5.18}$$

where $f_l(t) = -\sqrt{2}\eta\Omega\sqrt{\nu/\nu_l}[\cos(\nu_l - \delta)t + \cos(\nu_l + \delta)t]$ and $g_l(t) = -\sqrt{2}\eta\Omega\sqrt{\nu/\nu_l}[\sin(\nu_l - \delta)t + \sin(\nu_l + \delta)t]$, and where the internal and external state operators are defined by $\Theta_l = \sqrt{N}\sum_{k=1}^{N} b_k^l j_{y,k}$ and $x_l = \frac{1}{\sqrt{2}}(a_l + a_l^\dagger)$ and $p_l = \frac{i}{\sqrt{2}}(a_l^\dagger - a_l)$. Since the ladder operators for different modes commute, we may find the propagator for this Hamiltonian using the steps that lead to Eq. (4.12)

$$U(t) = \prod_{l=1}^{N} U_l(t), \tag{5.19}$$

where

$$U_l(t) = \mathrm{e}^{-iA_l(t)\Theta_l^2}\mathrm{e}^{-iF_l(t)\Theta_l x_l}\mathrm{e}^{-iG_l(t)\Theta_l p_l} \tag{5.20}$$

with the functions F_l, G_l and A_l defined analogously to Eq. (4.13). Note, that this is an exact solution of the Hamiltonian (5.18) without the J_x term, so that to lowest order in the Lamb-Dicke parameter it includes all effects of the coupling to the other modes.

From the definition of Θ_l it is seen that $\Theta_1 = J_y$ and the propagator U_1 reduces to Eq. (4.12) in the rotating wave approximation. The other $N-1$ propagators in (5.19) cause a reduction of the fidelity due to the excursion into the $x_l p_l$ phasespace of these modes. Expanding the exponentials, using $\langle gg...g|\Theta_l\Theta_{l'}|gg...g\rangle = \delta_{l,l'}N/4$ and $\delta \approx \nu$, and averaging over time we find

$$F = 1 - \eta^2 N \frac{\Omega^2}{\nu^2} \sum_{l=2}^{N} \frac{\nu}{\nu_l}(2\bar{n}_l + 1)\frac{\nu_l^2/\nu^2 + 1}{(\nu_l^2/\nu^2 - 1)^2}, \tag{5.21}$$

where $\bar{n}_l$ is the mean vibrational excitation of the lth mode.

In addition to the direct coupling to the spectator vibrational mode, the fidelity is also reduced because the coupling strength is dependent on the vibration of the other modes. Unlike the direct coupling discussed above, this effect is not suppressed by the other modes being far off-resonant, and it may have an effect comparable to the direct coupling.

Due to the vibration of the ions the coupling of the kth ion to the sideband is reduced from $i\eta\sqrt{n+1}$ to $\langle n_1 n_2 ... n_N|\mathrm{e}^{i\sum_{l=1}^{N}\eta_{k,l}(a_l + a_l^\dagger)}|n_1+1 n_2 ... n_N\rangle \approx i\eta\sqrt{n+1}(1 - \sum_{l=1}^{N}\eta_{k,l}^2(n_l + 1/2))$. With this reduced coupling strength the effective propagator at times $\tau = K2\pi/(\nu - \delta)$ may be described by

$$U(\tau) = \mathrm{e}^{-iA(\tau)\Lambda^2}, \tag{5.22}$$

where $\Lambda = \sum_{k=1}^{N} j_{y,k}(1 - \sum_{l=1}^{N}\eta_{k,l}^2(n_l + 1/2))$. By expanding (5.22) around the optimum $A(t) \approx \pi/2$ we calculate the lowest order reduction in the fidelity

$$\begin{aligned} F =& 1 - \frac{\pi^2 N(N-1)}{8}\eta^4 \sum_{l=1}^{N} \frac{\mathrm{Var}(n_l)}{(\nu_l/\nu)^2} \\ &- \frac{\pi^2(N-2)}{16}\eta^4 \sum_{i,l,l'=1}^{N} \frac{(b_i^l)^2(b_i^{l'})^2 - 1/N^2}{\nu_l\nu_{l'}/\nu^2}\overline{n_l n_{l'}}. \end{aligned} \tag{5.23}$$

The expressions in Eqs. (5.21) and (5.23) may be simplified if the vibrational motion is in a thermal equilibrium at a given temperature. In a thermal state $\mathrm{Var}(n_l) = \bar{n}_l^2 + \bar{n}_l$, $\overline{n_l n_{l'}} = \bar{n}_l\bar{n}_{l'}$ for $l \neq l'$, and $\bar{n}_l \leq \bar{n}_1\nu/\nu_l$, and using these expressions we find the lower estimate for the fidelity

$$F \geq 1 - \eta^2 N \frac{\Omega^2}{\nu^2}(\bar{n}_1\sigma_1(N) + \sigma_2(N)) \tag{5.24}$$

for the direct coupling (5.21) and

$$\begin{aligned} F \geq & 1 - \frac{\pi^2 N(N-1)}{8}\eta^4(\bar{n}_1^2\sigma_3(N) + \bar{n}_1\sigma_4(N)) \\ & - \frac{\pi^2(N-2)}{16}\eta^4(\bar{n}_1^2\sigma_5(N) + \bar{n}_1\sigma_6(N)) \end{aligned} \tag{5.25}$$

for the Debye-waller coupling (5.23), where the sums $\sigma_1 ... \sigma_6$ may be derived from Eqs. (5.21) and (5.23). For example $\sigma_3(N) = \sum_{l=1}^{N} \frac{\nu^4}{\nu_l^4}$. With the mode functions and frequencies of Ref. [70] these sums are readily evaluated, and the results are shown in Fig. 5.3. From the figure it is seen that $\sigma_5, \sigma_6 << \sigma_3, \sigma_4$, so that the last term in Eq. (5.25) may be neglected. All the sums have a very rapid convergence and we may estimate the fidelity by replacing the sums with their large N values, *i.e.*

$$F \geq 1 - \eta^2 N \frac{\Omega^2}{\nu^2} 0.8(\bar{n}_1 + 1) \tag{5.26}$$

for the direct coupling (5.21) and

$$F \geq 1 - \frac{\pi^2 N(N-1)}{8}\eta^4(1.2\bar{n}_1^2 + 1.4\bar{n}_1) \tag{5.27}$$

for the Debye-Waller coupling (5.23).

We note that Eq. (5.27) is derived from terms beyond the Lamb-Dicke expansion and it incorporates the reduction of fidelity due to deviations from the Lamb-Dicke approximation in the center-of-mass mode, *cf.*, the formal similarity of Eq. (5.27) and Eq. (5.11).

5.2.2 Heating of the vibrational motion

An ion trap cannot be perfectly isolated from the surroundings and the vibration of the ions will be subject to heating due to the interaction with the environment. Relaxation due to the interaction between the vibration and a thermal reservoir may be described by the master equation for the density matrix

$$\frac{d}{dt}\rho^{tot} = -i\big[H, \rho^{tot}\big] + \mathcal{L}(\rho^{tot}), \tag{5.28}$$

where $\mathcal{L}(\rho^{tot})$ is of the Lindblad form

$$\mathcal{L}(\rho^{tot}) = -\frac{1}{2}\sum_m \big(C_m^\dagger C_m \rho^{tot} + \rho^{tot} C_m^\dagger C_m\big) + \sum_m C_m \rho^{tot} C_m^\dagger \tag{5.29}$$

with relaxation operators $C_1 = \sqrt{\Gamma(1+n_{th})}a$ and $C_2 = \sqrt{\Gamma n_{th}}a^\dagger$, where Γ characterizes the strength of the interaction, and n_{th} is the mean vibrational

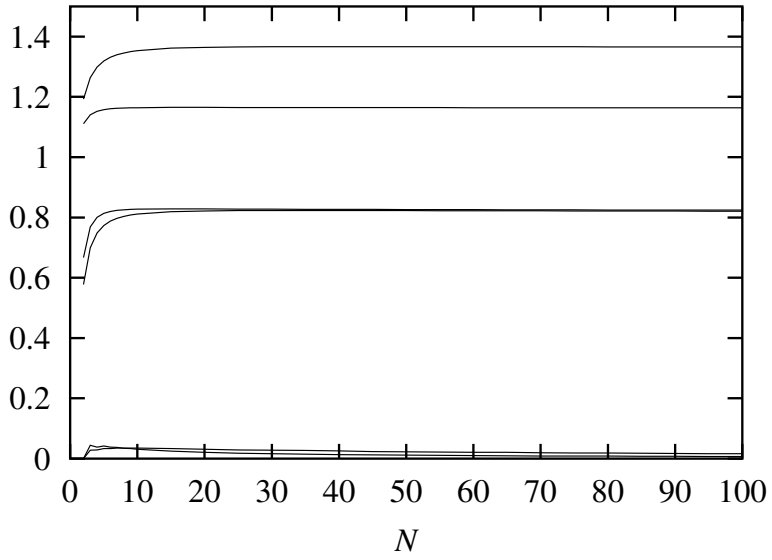

Figure 5.3: Evaluation of the sums $\sigma_1 ... \sigma_6$ for different number of ions N. Starting from above at $N \approx 5$ the curves represent σ_4, σ_3, σ_1, σ_2, σ_6, and σ_5.

number in thermal equilibrium. C_1 and C_2 were also used to describe heating in the numerical simulations in chapter 4.

We calculate the effect of heating assuming that the ions remain in the Lamb-Dicke limit. Changing to the interaction picture with respect to the Hamiltonian (4.11), the time evolution of ρ^{tot} is entirely due to the heating, *i.e.* the Lindblad terms, which are transformed using the propagator (4.12)

$$\begin{aligned} \tilde{C_1} =& U^\dagger C_1 U = \sqrt{\Gamma(1+n_{th})}\left(a + J_y \frac{G(t) - iF(t)}{\sqrt{2}}\right) \\ \tilde{C_2} =& U^\dagger C_2 U = \sqrt{\Gamma n_{th}}\left(a^\dagger + J_y \frac{G(t) + iF(t)}{\sqrt{2}}\right). \end{aligned} \tag{5.30}$$

The density matrix is most conveniently expressed in the basis of J_y eigenstates, and by tracing over the vibrational states we find the time derivative of the internal state density matrix in the interaction picture

$$\frac{d}{dt}\rho_{M_y,M_y'} = -(M_y - M_y')^2 \Gamma(1+2n_{th}) \frac{G(t)^2 + F(t)^2}{4} \rho_{M_y,M_y'}. \tag{5.31}$$

This equation is readily integrated, and at times $\tau = K 2\pi/(\nu - \delta)$ we get

$$\rho_{M_y,M_y'}(\tau) = \rho_{M_y,M_y'}(0) \mathrm{e}^{-(M_y - M_y')^2 \frac{\Gamma(1+2n_{th})}{4K}\tau}. \tag{5.32}$$

The initial state is expanded on the J_y eigenstates as in Eq. (5.8) and the population of the initial state (which is ideally constant in the interaction picture) equals

$$F = \frac{1}{2^{2N}} \sum_{j=0}^{N} \sum_{k=0}^{N} \begin{pmatrix} N \\ j \end{pmatrix} \begin{pmatrix} N \\ k \end{pmatrix} \mathrm{e}^{-(j-k)^2 \frac{\Gamma(1+2n_{th})}{4K}\tau}. \tag{5.33}$$

For two ions this expressions can be readily evaluated

$$F = \frac{3}{8} + \frac{1}{2}\mathrm{e}^{-\frac{\Gamma(1+2n_{th})}{4K}\tau} + \frac{1}{8}\mathrm{e}^{-4\frac{\Gamma(1+2n_{th})}{4K}\tau}. \tag{5.34}$$

In the limit of many ions ($N >> 1$) and short times ($\frac{\Gamma(1+2n_{th})}{4K}\tau << 1$) we may again approximate the expression in Eq. (5.33) by assuming that j and k are continuous variables and replacing the binomial coefficients by Gaussian distributions with the same width. In this limit the fidelity becomes

$$F = \frac{1}{\sqrt{1 + N\frac{\Gamma(1+2n_{th})}{4K}\tau}}. \tag{5.35}$$

For 2 ions the deviation between (5.34) and (5.35) is less than 0.02 for all values of F larger than 0.5.

In the above expressions we have assumed the Lamb-Dicke approximation. This corresponds to a situation where the heating is counteracted for example by laser cooling on some ions reserved for this purpose. If the ions are not cooled, the heating will proceed towards high vibrational numbers with a heating rate Γn_{th} and the heating will eventually take the ions out of the Lamb-Dicke limit. With strong fields ($K \sim 1$) the reduction in the fidelity described by Eq. (5.35) will ruin the entangled state before the heating has made a significant change in the vibrational state ($\Gamma n_{th}\tau \gtrsim 1$). For weak fields ($K >> 1$) however, the situation is different. With weak fields one may produce an entangled state even though the time required to entangle the ions is much longer than the decoherence time of the vibrational motion which is used to communicate between the ions, *i.e.*, if $K > N\Gamma n_{th}\tau$ the effect of heating is small even though the change in the average vibrational number $\Gamma n_{th}\tau$ is larger than unity. Since the effective Rabi-frequency has a small dependence on the vibrational quantum number n as described in Eq. (5.5), the heating will have an indirect effect on the internal state preparation. This can be modelled by changing the probabilities in Eqs. (5.7-5.10) into time dependent functions $P_n(t)$ reflecting the change in the vibrational motion occurring during the internal state preparation.

Summarizing this chapter, we have investigated various deviations from the ideal behaviour considered in chapter 4. With the expressions derived here, an

experimentalist can insert the parameters of of a given experiment and estimate the fidelity that one can achieve with these parameters. The final expressions for the decrease in fidelity are summarized in table 5.1.

Table 5.1: Reduction in the fidelity of entangled states of N ions $\frac{1}{\sqrt{2}}(|gg...g\rangle - i|ee...e\rangle)$ created by interaction with a bichromatic field (4.10) $H_{\rm int} = 2\Omega J_x \cos\delta t - \sqrt{2}\eta\Omega J_y[x(\cos(\nu-\delta)t + \cos(\nu+\delta)t) + p(\sin(\nu-\delta)t + \sin(\nu+\delta)t)]$ obeying $\frac{\eta\Omega}{\nu-\delta} = \frac{1}{2\sqrt{K}}$, $K = 1, 2, 3, ...$ for a duration $\tau = 2\pi K/(\nu-\delta)$. The fidelity of the preparation is reduced by various causes, listed in the table.

Cause of deviation	Direct off-resonant coupling; J_x term in (4.10)	Deviations from Lamb-Dicke $\langle n\|e^{i\eta(a+a^\dagger)}\|n+1\rangle \neq i\eta\sqrt{n+1}$	Spectator vibrational modes: (i) Direct coupling to other modes	Spectator vibrational modes: (ii) Debye-Waller	Heating of the vibration towards vibrational number n_{th} with rate Γn_{th}
$1-F$	$\frac{N\Omega^2}{2\delta^2}$	$\eta^4\frac{\pi^2 N(N-1)}{8}\mathrm{Var}(n_1)$	$N\frac{\eta^2\Omega^2}{\nu^2}0.8(\bar{n}_1+1)$	$\eta^4\frac{\pi^2 N(N-1)}{8}\times(0.2\bar{n}_1^2+0.4\bar{n}_1)$	$N\frac{\Gamma(1+2n_{th})\tau}{8K}$
Eq.	(5.4)	(5.11)	(5.26)	(5.27) minus (5.11)	(5.35)

Chapter 6

Multi-bit gates

As discussed in chapter 2, the CONTROL-NOT can be combined with single particle operations to produce any unitary operation acting on all the bits [24], and with the CONTROL-NOT described in chapter 4 one can use our bichromatic scheme to implement any quantum algorithm. This method in general involves several one and two particle gates to produce multi-bit gates. Experimentally each gate corresponds to turning on a given Hamiltonian for a certain duration, and therefore each gate adds an experimental complication and/or possibility of error. In this chapter we pursue a different strategy for implementing multi-bit gates. We will show that one may extend the trick in Eq. (4.9) to produce higher order gates directly. For this purpose, we shall start from a slightly more general version of Eq. (4.9) where each of the J_z operators in H_1 and H_2 are replaced by two commuting operators $\hat{A}$ and $\hat{B}$

$$\exp(i\xi_1 x\hat{A})\exp(i\xi_2 p\hat{B})\exp(-i\xi_1 x\hat{A})\exp(-i\xi p\hat{B}) = \exp(-i\xi_1\xi_2\hat{A}\hat{B}). \quad (6.1)$$

By coupling different internal state operators to x and p we can use this relation to construct gates acting only on the internal states of the the bits. We may, for instance, obtain a CONTROL-NOT operation by using $\hat{A} = (\sigma_{z1}+1)/2$, $\hat{B} = \sigma_{x2}$, and $\xi_1\xi_2 = \pi/2$, *cf.*, the discussion of Eq. (4.18). By replacing $\hat{A}$ and $\hat{B}$ with other single particle operators we can construct a large family of two-bit gates. The $\hat{A}$'s and $\hat{B}$'s which are easy to make in practice are sums of individual particle operators, since the sums are obtained by simply illuminating more ions with the lasers. When $\hat{A}$ and $\hat{B}$ only have terms which are linear in the individual particle operators, the right hand side of Eq. (6.1) is the exponential of an expression which is quadratic in these operators, and we cannot directly apply this procedure to make multi-bit gates which involves exponentials of the product of three or more operators. Below we show how to extend the trick (6.1) to any number of operators.

6.1 CONTROL^{n_c}-NOT

In this section we shall construct the CONTROL^{n_c}-NOT gate, which is a generalization of the CONTROL-NOT gate. In the CONTROL^{n_c}-NOT gate the n_c+1st qubit is flipped if the first n_c all are in the state $|1\rangle$. This gate is frequently used, *e.g.*, in error correcting codes [98, 99]. To construct a CONTROL^{n_c}-NOT gate we need a projection operator which projects onto the space where all the n_c control bits are in the $|1\rangle$ state. Such a projection operator can be written as a product of single particle projection operators $\prod_{l=1}^{n_c}(\sigma_{zl}+1)/2$, and the CONTROL^{n_c}-NOT operation may be expressed as

$$U_{\mathrm{C}^{n_c}\mathrm{NOT}} = \exp\left(-i\pi/2\prod_{l=1}^{n_c}\frac{(\sigma_{zl}+1)}{2}\sigma_{xn_c+1}\right). \tag{6.2}$$

From this expression it is seen that we cannot use (6.1) because (6.2) involves the product of n_c+1 Pauli operators.

To extend our previous results to CONTROL^{n_c}-NOT and other multi-bit gates, we change the interaction (4.11) slightly and consider a situation described by

$$H(t) = v(t)\hat{A}x + w(t)\hat{B}p + r(t)\hat{C}n, \tag{6.3}$$

where $\hat{A}$, $\hat{B}$ and $\hat{C}$ are commuting operators acting on the internal states of the ions, n is the number operator for the harmonic oscillator, and v, w, and r are arbitrary functions of time. Compared with the previous interaction (4.11), we have added a term $r(t)\hat{C}n$. In the ion trap such a term may be obtained be adding a laser which is slightly detuned from one of the sidebands of a transition. If the Rabi frequency of the light is sufficiently small ($\Omega << \nu-\delta$) the only effect is to cause a shift of the energy levels. Like in Eq. (4.4) the energy shifts involve terms which are proportional to n and the laser light adds an interaction described by the operator $\Omega^2\eta^2/(\nu-\delta)/4\ \sigma_{zk}n$, where k is the number of the ion which is illuminated by the laser.

With the Hamiltonian (6.3) the time dependent Schrödinger equation for the propagator $idU(t)/dt = H(t)U(t)$ has the solution

$$U = \mathrm{e}^{-i\hat{S}(t)}\mathrm{e}^{-in\hat{R}(t)}\mathrm{e}^{-ix\hat{V}(t)}\mathrm{e}^{-ip\hat{W}(t)}, \tag{6.4}$$

with

$$\begin{aligned}
\hat{R}(t) &= \hat{C}\int_0^t r(t')dt' \\
\hat{V}(t) &= \int_0^t \hat{A}v(t')\cos(\hat{R}(t')) - \hat{B}w(t')\sin(\hat{R}(t'))dt' \\
\hat{W}(t) &= \int_0^t \hat{B}w(t')\cos(\hat{R}(t')) + \hat{A}v(t')\sin(\hat{R}(t'))dt' \\
\hat{S}(t) &= -\int_0^t \hat{V}(t')[\hat{B}w(t')\cos(\hat{R}(t')) + \hat{A}v(t')\sin(\hat{R}(t'))]dt'.
\end{aligned} \tag{6.5}$$

It is straightforward to check the solution by taking the time derivative of U and using the Baker-Hausdorff relation to simplify the result. In the xp-phase space the net action of this propagator is to perform translations $(x,p) \rightarrow (x+\hat{W}(t), p-\hat{V}(t))$ followed by a rotation by an angle $\hat{R}(t)$ around the origin. Since the functions $\hat{V}$, $\hat{W}$, and $\hat{R}$ involve the internal state operators $\hat{A}$, $\hat{B}$, and $\hat{C}$ the translation and rotation are entangled with the internal states of the bits. Generalizing the previous requirement that the functions F and G in Eq. (4.13) should vanish at time τ, we now require that $\hat{V}$, $\hat{W}$, and $\hat{R}$ vanish after a certain time τ. At this time the harmonic oscillator is returned to its initial state, and we are left with an internal state evolution operator $\exp(-i\hat{S}(\tau))$, where $\hat{S}(\tau)$ is the area enclosed by the trajectory in the phase space. Note, that the expression for $\hat{S}(\tau)$ does not involve operators referring to the harmonic oscillator, so that the gate is insensitive to the initial state of the oscillator. This gate can be applied with the oscillator in an unknown state, *e.g.*, in a thermal state.

As a first concrete example of our procedure consider three bits which are subject to the time independent Hamiltonian

$$H = \chi\left(\frac{\sigma_{z1}+\sigma_{z2}+1}{4\sqrt{K}}x - \sigma_{x3}\left(n+\frac{1}{32K}\right)\right), \tag{6.6}$$

where K is an integer. After a duration $\tau = K2\pi/\chi$ the propagator (6.4) reduces to $\exp(-i\pi[(\sigma_{z1}+\sigma_{z2}+1)^2-1]\sigma_{x3}/16) = \exp(-i\pi(\sigma_{z1}+1)(\sigma_{z2}+1)\sigma_{x3}/8)$, which is exactly the CONTROL^2-NOT gate also known as the Toffoli gate. (We have used the fact that for a single particle Pauli operator σ, $\sin(\theta\sigma) = \sin(\theta)\sigma$). In the ion trap quantum computer the gate can be achieved by applying a single pulse of suitably directed and detuned fields to the ions.

The three particle Toffoli-gate, can be constructed so easily because the constant term in $\sigma_{z1}+\sigma_{z2}+1$ can be chosen so that this operator squared yields the desired combination of internal state operators apart from a single particle rotation. This technique is not directly applicable for more than three particles, and we have not been able to devise a similar simple construction

with only a single Hamiltonian in this situation. Instead we shall produce gates by sequentially applying three different Hamiltonians.

The problem with the CONTROL^{n_c}-NOT operation (6.2) is that it involves the product of several individual particle operators, whereas the operators that are easy to make in practice are *sums* of such operators like $\hat{J}_z - J = \sum_{l=1}^{n_c} \frac{(\sigma_{zl}-1)}{2}$. To turn the sum into a product, we observe that if and only if all n_c control qubits are in the $|1\rangle$ state, not only is the product $\prod_{l=1}^{n_c} \frac{(\sigma_{zl}+1)}{2}$ equal to unity, also $\hat{J}_z - J$ vanishes. We now use the Fourier transform $\sum_{k=1}^{m} \cos(2\pi \frac{k}{m} N) = m\delta(N \bmod m)$ which can also be applied to operators so that:

$$\prod_{l}^{n_c} \frac{(\sigma_{zl}+1)}{2} = \frac{1}{n_c+1} \sum_{k=1}^{n_c+1} \cos\left(\frac{2\pi k}{n_c+1}(\hat{J}_z - J)\right). \tag{6.7}$$

The CONTROL^{n_c}-NOT gate is thus the product of $n_c + 1$ terms $\exp(\frac{i\pi}{2(n_c+1)} \cos(\frac{2\pi k}{n_c+1}(\hat{J}_z - J))\sigma_{xn_c+1})$ $(k = 1, 2, ..., n_c + 1)$.

To implement a unitary operator of the form $\exp(-i\mu\hat{A}\cos(\theta\hat{C}))$, where $\hat{A}$ and $\hat{C}$ are internal state operators, we make explicit use of the fact that we have an internal state operator appearing inside a trigonometric function in the expression for $\hat{S}$ (6.5). Geometrically, we follow the construction of the parallelogram in Fig. 6.1 (b): First, we apply a Hamiltonian proportional to $\hat{A}p$ which performs a translation along the x-axis. Then a Hamiltonian $H \sim \hat{C}n$ makes a rotation of the phase space by an angle $\theta\hat{C}$: $\exp(i\theta\hat{C}n)x\exp(-i\theta\hat{C}n) = \cos(\theta\hat{C})x + \sin(\theta\hat{C})p$, and we perform a translation along the p-axis with $\hat{B}$ equal to the identity, etc. The enclosed area is proportional to $\hat{A}\cos(\theta\hat{C})$ and the propagator has the desired form $\exp(-i\mu\hat{A}\cos(\theta\hat{C}))$. By varying the strength and duration of the pulses one can control the parameters θ and μ, and using $\hat{A} = \sigma_{x,n_c+1}$ and $\hat{C} = \hat{J}_z - J$ the parallelogram results in the time evolution operator $\exp(-i\mu\cos(\theta(\hat{J}_z - J))\sigma_{x,n_c+1})$.

By using the operator identity (6.7) we can devise a CONTROL^{n_c}-NOT gate by following the outline of $n_c + 1$ such parallelograms, one after the other. By rotating each parallelogram, so that the first linear displacement is precisely the opposite of the last displacement of the previous parallelogram, we can save half of the translations. See Fig. 6.1 (b).

6.2 Grover search

In chapter 2 we discussed Grovers search algorithm [29] that identifies the single value x_0 which fulfills $f(x_0) = 1$ for a function $f(x)$ provided, *e.g.*, by an oracle (all other arguments lead to vanishing values of the function). If x is an integer on the range between 0 and $N - 1 = 2^n - 1$, the search algorithm is able to find x_0 after on the order of $\sqrt{N}$ evaluations of the function. In the following we show how our proposal can be used to implement the search algorithm.

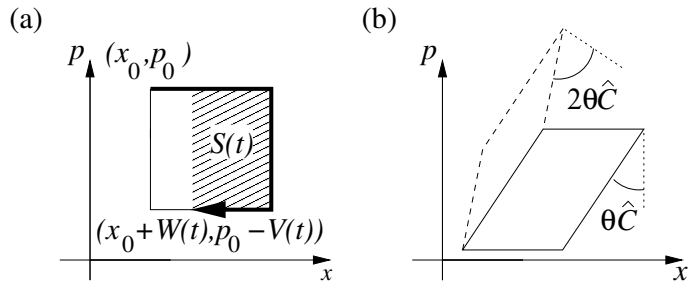

Figure 6.1: Translations in xp-phase space of the oscillator during gate operation: (a) In the evolution described by Eq. (6.1), the oscillator is displaced by the amount $\xi_2\hat{B}$ along the x-axis, then by $-\xi_1\hat{A}$ along the p-axis, etc., and when it eventually ends up in the initial state, a geometric (and internal state dependent) phase factor given by the enclosed area $\xi_1\xi_2\hat{A}\hat{B}$ multiplies the state vector of the system. (b) By application of an interaction proportional to $\hat{C}n$, the displacement along the p-direction in part (a) of the figure can be rotated into another direction given by the angle $\theta\hat{C}$, and the area enclosed by the solid line becomes $\xi_1\xi_2\hat{A}\hat{B}\cos(\theta\hat{C})$. To perform a Grover search or CONTROL^{n_c}-NOT operation we need to enclose several parallelograms with angles which are multipla of $\hat{C}\theta$. An effective way to achieve this is to place all subsequent parallelograms so that they share one side with the previous one, as shown with the dashed curve for the second parallelogram. With this construction, the multi-bit operation can be achieved by traversing only the outline of the combined figure.

The quantum algorithm first prepares an initial trial state vector populating all basis states with equal probability and then evaluates the function $f(x)$. To implement a full Grover search the function $f(x)$ has to be a non-trivial function which is implemented by the quantum computer, but for demonstrational purposes, the function $f(x)$ can be encoded by letting the state of the register undergo a transformation where the amplitude of the x_0 component changes sign and all other amplitudes are left unchanged. This step can be implemented by writing x_0 in binary form, $b_0b_1b_2...b_{n-1}$, and applying the unitary operator

$$U_f = \exp\left(i\pi \prod_{l=0}^{n-1}\left(\frac{\sigma_{zl}+2b_l-1}{2}\right)\right). \tag{6.8}$$

Below we show how this time evolution may be implemented with our procedure. Note that the corresponding effective Hamiltonian vanishes when applied to any state where the qubit value (eigenvalue of σ_{zl}) does not coincide with $2b_l-1$, *i.e.*, the state must be the exact representation of x_0 to acquire the sign change.

The crucial step in Grover's algorithm is the 'inversion about the mean', where the amplitude with the sign changed will grow in comparison with the other amplitudes. In the $n-$qubit computer with $N=2^n$ possible inputs, the

inversion about the mean is achieved by an operator $U_G = \frac{2}{N}M - I$, where I is the $N \times N$ identity matrix and where M is the $N \times N$ matrix with unit elements in all positions, see Eq. (2.7).

A straightforward calculation shows that the M matrix fulfill $(sM)^k = s^k N^{k-1} M$, and hence we have the exponential

$$\exp(sM) = I + \sum_{k=1}^{\infty} \frac{(sM)^k}{k!} = I + \frac{1}{N}(e^{sN} - 1)M. \tag{6.9}$$

Thus, by choosing $sN = i\pi$, we get $\exp(sM) = I - \frac{2}{N}M$, which apart from an irrelevant global phase yields precisely the inversion about the mean.

In the standard binary basis, the matrix M couples all states to any other state, and it can be written as the tensor product $\Pi_{l=0}^{n-1}(\sigma_{xl} + 1)$, where the single qubit operators $\sigma_{xl} + 1$ are 2×2 matrices with unit elements in all positions. The inversion about the mean is therefore produced directly by the action of the following multi-particle operator

$$U_G = \exp\left(i\pi \prod_{l=0}^{n-1} \left(\frac{\sigma_{xl} + 1}{2}\right)\right), \tag{6.10}$$

where we have used $N = 2^n$.

Both U_f and U_G can be implemented efficiently using (6.7). To implement the function (6.8), it is easiest to first invert all the bits, which have the value zero in x_0, so that U_f on that state should encode only unit bit values, *i.e.*, U_f is precisely the exponential of the projection operator in the left hand side of Eq. (6.7). Following the outline of the parallelogram in Fig. 6.1 (b) with $\hat{A}$ and $\hat{B}$ equal to the identity and $\hat{C} = \sum_{l=0}^{n-1} \frac{(\sigma_{zl}-1)}{2}$ we obtain the exponential of one of the terms in the sum on the right hand side, and by combining $n + 1$ such terms one can construct the full sum. After application of this simple U_f, the qubits encoding the value zero should be flipped back again. All qubits should then have their σ_x components rotated into the z-direction, to use again the operation in (6.7) to implement U_G, which is the same operator, defined for the x-components of the spins. The whole algorithm only requires individual access for the single qubit spin flips which encode x_0 and for the final readout. An easy demonstration experiment where $x_0 = 1111...1$ can thus be performed without individual access at all (one only needs to verify that the number of excited qubits at the end equals the total number of qubits).

It is known how to make C^2-NOT and C^3-NOT gates by means of one- and two-bit gates, but it is difficult to make a theoretical comparison of these implementations with our proposal, since we build up the desired one-, two-, and multi-bit interactions continuously in time. From a practical perspective, however, our scheme should be really advantageous. The essential operation in the Grover search (6.10) is implemented without access to the individual

qubits and, *e.g.*, in the ion trap it is much easier to implement the Hamiltonian $H = \sum_l (\sigma_{zl} - 1)n$ than just a single term $H = (\sigma_{zl} - 1)n$ in that sum. In addition, it is an experimental advantage to apply as few control Hamiltonians as possible, since imprecision in timing accumulates if many operations are needed.

A feature of our proposal worth emphasizing is that all operations are expressed as unitary gates acting on the qubit degrees of freedom. The oscillator is certainly important, and only at the end of the gates, do the qubits actually decouple from the oscillator. One consequence is that the initial state of the oscillator does not have to be specified. It can be in the ground state, an excited state, or even in an incoherent mixture of states, possibly entangled with environmental degrees of freedom, as long as this entanglement does not evolve during gate operation.

Part III

Neutral atoms and spin squeezing

Chapter 7

Introduction to neutral atoms and spin squeezing

Despite the experimental achievements with trapped ions it is still uncertain in which direction quantum computation will evolve in the future, and one should be open to other approaches. Neutral atoms is such an alternative approach, and in the following chapters we present our work in this direction [4, 7, 9, 11, 15]. Rather than studying the possibility of creating a full scale general purpose quantum computer which is extremely challenging experimentally, our work has mainly addressed the issue of what one might achieve with simpler experimental means, *i.e.*, the RISQ approach discussed in chapter 2. It is our hope that the knowledge which is gained by studying the entanglement created in such simpler experiments, will be useful in the future development of a quantum computer.

In chapter 8 we consider atoms trapped in an optical lattice and shows that even if we do not have experimental access to the individual atoms in the lattice, we may still use this premature quantum computer to solve non-trivial physics problems. Furthermore the interaction between the atoms can be used to create some very interesting entangled states called spin squeezed states. In chapter 9 we consider a two component Bose-Einstein condensate and demonstrate that the collisional interaction between the atoms can be used to create entanglement. The collisional interaction is naturally present in all experiments with Bose-Einstein condensates, and in our proposal substantial entanglement is created by shining a single microwave pulse onto the condensate. Finally, in chapter 10 we explore the connection between spin squeezing and entanglement.

Typically, the main challenge in constructing a quantum computer or entangling atoms is the engineering of a controlled interaction between the atoms.

The interaction between two neutral atoms is significantly different from the interaction between two ions because of the Coulomb interaction of the ions. Since the underlying interactions are different one cannot apply the ion trap proposals to neutral atoms and in section 7.1 we briefly describe the interaction which is used in the neutral atom proposals.

A motivation for studying entanglement in neutral atoms comes from the fact that the current time standards and the definition of the second are based on neutral atoms. Spin squeezed states are entangled states which could be used to improve the sensitivity of atomic clocks and most of our work on neutral atoms has been concerned with proposals for generating such states. In section 7.2 we give an introduction to spin squeezing.

7.1 Neutral atoms

One of the main problems with the trapped ions considered in part II is the heating of the vibrational motion. With neutral atoms this problem is reduced considerably because the interaction with stray external field is much weaker when the particles have no net charge, and the motion of neutral atoms is therefore better shielded from the surroundings than the motion of ions. However, the strong coupling of the vibrational motion due to the charge of the ions is essential for the functioning of the ion trap schemes. Without the Coulomb interaction all vibrational modes in the ion trap are degenerate and the processes involving different vibrational modes interfere destructively so that $\tilde{\Omega}$ in Eq. (4.3) vanishes.

The force between two neutral atoms is much weaker and has a much shorter range than the force between two ions. For this reason the strong coupling of vibrational modes has no counterpart for trapped neutral atoms and new schemes have to be developed. Our work mainly considers atoms which are interacting through collisional interactions. This was first proposed as a means for quantum computation in Ref. [100]. We shall consider a cold atomic gas where the velocity of the atoms is so low that the De Broglie wavelength is much larger than the range of the atom-atom interaction. In this limit the interaction between atoms in internal states a and b may be described by an effective zero-range potential [101]

$$V_{ab}(\mathbf{r}, \mathbf{r}') = U_{ab}\delta(\mathbf{r} - \mathbf{r}'). \tag{7.1}$$

The strength of the potential U_{ab} can be found from the scattering length a_{ab}: $U_{ab} = 4\pi\hbar^2 a_{ab}/M$, where M is the atomic mass. A necessary condition for this approximation to be valid is that the atomic gas is sufficiently dilute so that the separation between the atoms is much larger than the scattering length $na_{ab}^3 << 1$, where n is the atomic density. Since the first observation of Bose-Einstein condensation in trapped atomic gases in 1995 [102, 103], the

interaction (7.1) has been successfully used to describe the properties of these gases.

In the proposals presented in chapters 8 and 9 the ideal situations is that the collisional interaction is so weak that we can neglect its influence on the spatial wavefunction of the atoms and treat the interaction as a perturbation to the energy levels. To understand how the collisional interaction can be used to create entanglement, we consider the interaction between two particles in the internal states $|e\rangle$ and $|g\rangle$ with spatial wavefunction $\psi_e(\mathbf{r},t)$ and $\psi_g(\mathbf{r},t)$, where $\mathbf{r}$ is the spatial coordinates and t is the time. If the atoms interact for a time T the perturbation of the energy levels by the interaction (7.1) will introduce a phase shift

$$\phi_{eg} = \int_0^T dt \int d^3\mathbf{r}\, U_{eg} |\psi_e(\mathbf{r},t)|^2 |\psi_g(\mathbf{r},t)|^2. \tag{7.2}$$

To create entanglement we assume that both atoms are initially prepared in a superposition of $|e\rangle$ and $|g\rangle$ and that the atoms are brought together so that they interact. If the phase shift ϕ_{eg} in (7.2) is different from the phase shift of the other components ϕ_{gg}, ϕ_{ee}, and ϕ_{ge}, one generally cannot split the state into a product of two single particle states and the atoms are entangled.

To make the phase shifts differ, two different strategies can be used. In chapter 8 we use the method proposed in [100, 104, 105] and split the spatial wavefunction into two separate wavepackets dependent on the internal state. With this procedure one can move the wavepackets so that for instance only the 'e-wavepacket' of the first atom overlaps with the 'g-wavepacket' of the second atom, and ϕ_{eg} is thus the only phase shift which is non-zero. In chapter 9 we assume that all spatial wavefunctions are identical and that the difference in the phase shifts is caused by a dependence of the scattering length on the internal state.

The collisional interaction is not the only possible method to construct a quantum computer with neutral atoms; other methods have been proposed: In Ref. [106] it is proposed to use laser induced dipole-dipole interaction. By a slight modification of this proposal it also fits into the framework considered in chapter 8. Another possibility is to use the strong dipole interaction between Rydberg atoms [107, 108]. One can also use the interaction of atoms with the quantized field either in a cavity [109, 110] or in free space [111, 112].

7.2 Spin squeezing

Our neutral atom work has mainly been focused on the generation of spin squeezed states. To introduce spin squeezing we shall first consider a simple thought experiment: Suppose we have a collection of N atoms which are all prepared in the state $(|e\rangle + |g\rangle)/\sqrt{2}$, and suppose that we perform a measurement which projects onto the internal state $|e\rangle$ and $|g\rangle$ and that we count the

number of atoms in the state $|e\rangle$. Since every atom has the probability 1/2 of being in the $|e\rangle$ state we expect to find an average of $N/2$ atoms in this state. In a concrete experimental realization it is unlikely that we will find exactly $N/2$ atoms because the atoms are independent particles, and the number of atoms in $|e\rangle$ will fluctuate binomially with a variance of $N/4$. The aim of spin squeezing is to entangle the atoms in such a way that this variance is reduced.

To describe spin squeezing it is convenient to change to the spin representation of the internal states. Each atoms is considered as a spin 1/2 particle and the internal states $|e\rangle$ and $|g\rangle$ are the eigenstates of the j_z operator with eigenvalues 1/2 and $-1/2$ respectively. Spin squeezing is a collective property of all the atoms, and the total spin operators which represent these collective properties are obtained by summing over the angular momentum operators for the individual particles $J_\xi = \sum_k j_{\xi,k}$ ($\xi = x,\ y,\ z$). These operators obey the standard angular momentum commutation relation $[J_y, J_z] = iJ_x$ which leads to Heisenberg's uncertainty relation

$$\Delta J_y \cdot \Delta J_z \geq |\langle J_x \rangle|/2. \tag{7.3}$$

In the example given in the begining of this section, the atoms were all prepared in the state $(|e\rangle + |g\rangle)/\sqrt{2}$. This state is an eigenstate of $\vec{J}^{\,2}$ and J_x with eigenvalues $N/2\cdot(N/2+1)$ and $N/2$, corresponding to an effective spin $J = N/2$ polarized along the x-axis. The measurement of the number of atoms in the state $|e\rangle$ corresponds to a measurement of $J_z + N/2$, and the variance of the measurement is given by $(\Delta J_z)^2$. If we take the equality sign in (7.3) and use $\Delta J_z = \Delta J_y$ we find exactly that $(\Delta J_z)^2 = N/4$, as we found be considering a binomial distribution, and the spin representation is just a convenient method to express the counting statistics.

Without violating Heisenberg's uncertainty relation, it is possible to redistribute the uncertainty unevenly between J_y and J_z, so that a measurement of either J_y or J_z become more precise than the standard quantum limit $\sqrt{|\langle J_x \rangle|/2}$. States with this property are called spin squeezed states in analogy with the squeezed states of a harmonic oscillator.

The states and the amount of spin squeezing produced by applying Hamiltonians J_x^2 and $J_x^2 - J_y^2$ to an initial $|J_z = J\rangle$ state have been studied [113], and the squeezed states which satisfy the equality sign in (7.3), the so-called minimum-uncertainty-product states, have been identified [114–116]. A number of experimental proposals for atomic spin squeezing have appeared involving interaction of atoms with squeezed light [116, 117], quantum non demolition measurement of atomic spin states[118], interaction between Rydberg atoms [119], and atomic collisional interactions (see chapters 8 and 9). Recently, the first experimental realizations of spin squeezing have been achieved [120–122].

In Ramsey type spectroscopy on a collection of two-level atoms, a signal proportional to the length of the mean collective spin is recorded and the noise

is given by the uncertainty of one of the orthogonal components $J_\perp$. Wineland *et al.* have shown [123] that the frequency variance in spectroscopy on N two-level atoms contains the factor

$$\xi^2 = \frac{N(\Delta J_\perp)^2}{\langle \vec{J} \rangle^2}, \tag{7.4}$$

which is reduced by spin squeezing. In this way, spin squeezing becomes an important ingredient in high precision spectroscopy and in atomic clocks, which are presently limited precisely by the fundamental spin noise [124]. By preparing the atoms in a spin squeezed state before they are injected into an atomic clock, the variance of the clock is improved by a factor ξ^2. Furthermore, spin squeezing is an important ingredient in quantum information. As we show below, a squeezed state with $\xi^2 < 1$ is an entangled state, and the quantum entanglement leads to possibilities, *e.g.* for atomic teleportation [111].

Squeezing and entanglement

In this subsection we shall prove that any collection of two level atoms in a squeezed state with $\xi^2 < 1$ is an entangled state. An N-particle density matrix ρ is defined [125, 126] to be separable (non-entangled) if it can be decomposed into

$$\rho = \sum_k P_k \rho_k^{(1)} \otimes \rho_k^{(2)} \otimes ... \otimes \rho_k^{(N)}, \tag{7.5}$$

where the coefficients P_k are positive real numbers fulfilling $\sum_k P_k = 1$, and $\rho_k^{(i)}$ is a density matrix for the ith particle. The variance of J_z may be described as $(\Delta J_z)^2 = \frac{N}{4} - \sum_k P_k \sum_i \langle j_z^{(i)} \rangle_k^2 + \sum_k P_k \langle J_z \rangle_k^2 - \langle J_z \rangle^2$, and using Cauchy-Schwarz's inequality and $\langle j_x^{(i)} \rangle_k^2 + \langle j_y^{(i)} \rangle_k^2 + \langle j_z^{(i)} \rangle_k^2 \leq 1/4$ we find three inequalities for separable states $\sum_k P_k \langle J_z \rangle_k^2 \geq \langle J_z \rangle^2$, $-\sum_k P_k \sum_i \langle j_z^{(i)} \rangle_k^2 \geq -\frac{N}{4} + \sum_k P_k \sum_i \langle j_x^{(i)} \rangle_k^2 + \langle j_y^{(i)} \rangle_k^2$, and $\langle J_x \rangle^2 \leq N \sum_k P_k \sum_i \langle j_x^{(i)} \rangle_k^2$. From these inequalities we immediately find that any separable state obeys

$$\frac{N(\Delta J_z)^2}{\langle J_x \rangle^2 + \langle J_y \rangle^2} \geq 1. \tag{7.6}$$

If we orientate the coordinate system so that the mean spin is in the xy-plane and look for the noise in the z-direction, this expression can be written as $\xi^2 \geq 1$ and we conclude that any state with $\xi^2 < 1$ is non-separable and hence entangled.

Squeezing from general spin-spin interactions

In this thesis spin squeezing is discussed in connection with neutral atoms. The concept of squeezing is, however, not restricted to neutral atoms. These two

topics are only discussed together because our spin squeezing proposals deals with neutral atoms and because spin squeezed states of neutral atoms have practical applications in atomic clocks. In a different implementation, spin squeezing may not be of so much interest in its own right, but the detection of spin squeezing could provide an important diagnostic tool in the early stages of the development of a quantum computer. Specifically, if the experimental setup is not able to control and detect the states of the individual qubits, spin squeezing provides a means of producing and verifying entanglement by only controlling and detecting the qubits collectively. To construct a quantum computer it is essential to have an interaction between the qubits, and in the following we shall show that spin squeezing is naturally produced by a very large class of interactions.

Consider a collection of spin 1/2 particles which only interacts through pairwise interactions. The most general Hamiltonian describing this situation is given by

$$H = \sum_{k \neq l} \vec{j}_k{}^{\mathbb{T}} \cdot \underline{\underline{m}}^{kl} \cdot \vec{j}_l, \tag{7.7}$$

where $^{\mathbb{T}}$ denotes the transpose $\vec{j}_k{}^{\mathbb{T}} = (j_{x,k}, j_{y,k}, j_{z,k})$, and where $\underline{\underline{m}}^{kl}$ are real 3 by 3 matrices. We assume that the particles are initially prepared in a state where all spins are pointing in a given direction and we compute the time evolution of the noise in a component perpendicular to the direction of the mean spin. A convenient representation of this situation is by a collective spin state $\hat{R}(\alpha, \beta, \gamma)|JJ\rangle$, where $\hat{R}$ is a rotation operator given by the three Euler angles α, β, and γ, and where $|JM\rangle$ denotes an eigenstate of $\vec{J}^{\,2}$ and J_z with eigenvalues $J(J+1)$ and M. The noise in a direction perpendicular to the mean spin can be found by calculating the square of the rotated J_x operator $J_\perp = \hat{R} J_x \hat{R}^\dagger$.

With the general Hamiltonian (7.7) it is not possible to calculate the full time evolution of the noise. It is however straightforward to determine the short time evolution by Ehrenfest's theorem

$$\frac{d}{dt}(\Delta J_\perp)^2 = i\langle JJ|[\tilde{H}, J_x^2]|JJ\rangle, \tag{7.8}$$

where we have introduced the transformed Hamiltonian $\tilde{H} = \hat{R}^\dagger H \hat{R}$ and we have used $\langle J_\perp \rangle$=0. By using $\hat{R}^\dagger \vec{J} \hat{R} = \underline{\underline{R}} \cdot \vec{J}$, where $\underline{\underline{R}}$ is the 3 by 3 matrix representation of the rotation in coordinate space, we may express the transformed Hamiltonian as $\tilde{H} = \sum_{k \neq l} \vec{j}_k{}^{\mathbb{T}} \cdot \underline{\underline{\tilde{m}}}^{kl} \cdot \vec{j}_l$, where $\underline{\underline{\tilde{m}}}^{kl} = \underline{\underline{R}}^{\mathbb{T}} \cdot \underline{\underline{m}}^{kl} \cdot \underline{\underline{R}}$. By

calculating the commutator and evaluating the expectation value we find

$$\frac{d}{dt}(\Delta J_\perp)^2 = \frac{1}{2}(0,1,0)\cdot\underline{\underline{\tilde{M}}}\cdot\begin{pmatrix}1\\0\\0\end{pmatrix}. \tag{7.9}$$

In this expression we have introduced a matrix $\underline{\underline{M}} = \sum_{k\neq l}\underline{\underline{m}}^{k,l}$, and transformed it with the rotation matrix $\underline{\underline{\tilde{M}}} = \underline{\underline{R}}^{\mathbb{T}}\cdot\underline{\underline{M}}\cdot\underline{\underline{R}}$.

In Eq. (7.7) the terms involving the kth and lth particles are $\vec{j}_k{}^{\mathbb{T}}\cdot\underline{\underline{m}}^{kl}\cdot\vec{j}_l$ and $\vec{j}_l{}^{\mathbb{T}}\cdot\underline{\underline{m}}^{lk}\cdot\vec{j}_k$. The sum of these terms can also be written as $1/2(\vec{j}_k{}^{\mathbb{T}}\cdot(\underline{\underline{m}}^{kl}+\underline{\underline{m}}^{lk\ \mathbb{T}})\cdot\vec{j}_l + \vec{j}_l{}^{\mathbb{T}}\cdot(\underline{\underline{m}}^{lk}+\underline{\underline{m}}^{kl\ \mathbb{T}})\cdot\vec{j}_k)$. From this expression we see that without loss of generality we can assume the matrix $\underline{\underline{M}}$ to be symmetric and hence diagonalizable and in a convenient coordinate system we have

$$\underline{\underline{M}} = \begin{pmatrix}M_x & 0 & 0\\ 0 & M_y & 0\\ 0 & 0 & M_z\end{pmatrix}. \tag{7.10}$$

By calculating $\underline{\underline{\tilde{M}}}$ using the form (7.10) for the matrix $\underline{\underline{M}}$ and the well known rotation matrices $\underline{\underline{R}}$, we can find the time derivative of the noise perpendicular to the mean spin for any orientation of the spin by using Eq. (7.9). Since we start out in a state with $\xi^2 = 1$ and since $d/dt\langle\vec{J}\,\rangle^2 = 0$ at $t = 0$, the interaction produces spin squeezing if we can find any set of Euler angles α, β, and γ which gives a negative derivative in Eq. (7.9). The optimal orientation of the spin is found by minimizing the derivative (7.9) with respect to the angles α, β, and γ. We find that the extrema of Eq. (7.9) are always with the mean spin along one of the eigenvectors of $\underline{\underline{M}}$. If the spin is polarized along the z-axis the change in the noise is maximal for the perpendicular components $J_{\pm\pi/4} = 1/\sqrt{2}(J_x \pm J_y)$ and we find

$$\frac{d}{dt}(\Delta J_{\pm\pi/4})^2 = \pm\frac{1}{4}(M_y - M_x). \tag{7.11}$$

Similar expressions are found if the spin is oriented along the x or y-axes.

Note that no assumptions about the values of the coupling matrices are made, they may vary randomly for any pair (k,l) of spins. Only the sum needs to be specified to determine the short time spin squeezing. If the interaction between the qubits in the quantum computer is of the type (7.7), Eq. (7.11) shows that spin squeezing can be produced by preparing all the qubits in the same internal state and letting the system evolve with the pairwise interaction

for a short time (provided M is not proportional to the identity). Since the initial state is the same for all qubits, this state can be prepared by applying the same interaction to all qubits, for instance a broad optical pumping beam, and to verify the entanglement only two quantities like $\langle J_x \rangle$ and $(\Delta J_{\pm\pi/4})^2$ have to be measured. The mean and variance of a particular spin component can be measured by first rotating it into the z direction using resonant fields, and then counting the number of atoms in the state $|e\rangle$. By repeating the preparation and detection a few times, the mean and variance can be constructed, and we emphasize that the entire procedure can be accomplished without resolving the individual qubit experimentally. Such a measurement of spin squeezing in a premature quantum computer could provide a test of the functioning of the interaction among the qubits.

Chapter 8

Optical lattices

A possible implementation of quantum computation with neutral atoms is in optical lattices. Optical lattices are produced in regions where several laser beams are overlapping. If two counter propagating laser beams are overlapping, they produce a standing wave just like the field in a cavity. The resultant field consists of planes perpendicular to the laser beams with constructive interference and planes where the lasers interfere destructively. Depending on the detuning of the lasers the field can be either attractive (red detuning) or repulsive (blue detuning), so that atoms may be trapped in the planes with either constructive or destructive interference. If such pairs of counter propagating lasers are present along three perpendicular directions, a cubic interference pattern is created, and the atoms may be trapped in potential wells at the lattice sites of a cubic lattice. Other lattice structures may be produced by different arrangements of the lasers.

In Refs. [100, 106] two different methods to perform a coherent evolution of the joint state of pairs of atoms in optical lattices were proposed. Both methods involve displacements of two identical optical lattices with respect to each other. Each lattice traps one of the two internal states $|g\rangle$ and $|e\rangle$ of the atoms. Initially, the atoms are in the same internal state $|g\rangle$ and the two lattices are on top of each other. The atoms are assumed to be cooled to the vibrational ground state in the lattice and with a resonant pulse the atoms may be prepared in any superposition of the two internal states. The lattice containing the $|e\rangle$ component of the wavefunction is now displaced so that if an atom (at the lattice site k) is in $|e\rangle$, it is transferred to the vicinity of the neighbouring atom (at the lattice site $k+1$) if this is in $|g\rangle$, causing an interaction between the two atoms, see Fig. 8.1. The procedures described here follow the proposal in Ref. [100], where the atoms interact through controlled collisions. Also the optically induced dipole-dipole interactions proposed in [106] may be adjusted to fit into this framework. After the interaction, the

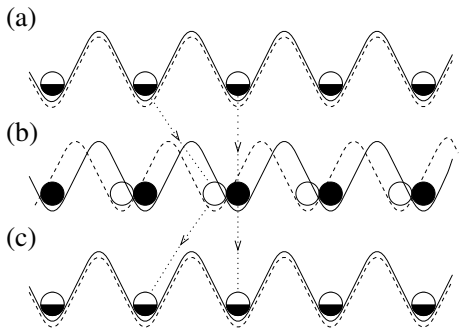

Figure 8.1: (a) Two overlapping lattices trapping the two internal states $|g\rangle$ (black circle) and $|e\rangle$ (white circle). By resonant laser pulses the atoms can be prepared in any superposition of the two internal states. **(b)** The lattices are displaced so that if an atom is in the $|e\rangle$ state, it is moved close to the neighbouring atom if this is in $|g\rangle$, causing an interaction between the two atoms. **(c)** The lattices are returned to their initial position and the atoms may be subject to single qubit rotations.

lattices are returned to their initial position and the internal states of each atom may again be subject to single particle rotations. The total effect of the displacement and the interaction with the neighbour can be tailored to yield a certain phase shift ϕ on the $|e\rangle_k|g\rangle_{k+1}$ component of the wavefunction, *cf.* Eq. (7.2),

$$\begin{aligned} |g\rangle_k|g\rangle_{k+1} &\rightarrow |g\rangle_k|g\rangle_{k+1} & |g\rangle_k|e\rangle_{k+1} &\rightarrow |g\rangle_k|e\rangle_{k+1} \\ |e\rangle_k|g\rangle_{k+1} &\rightarrow \mathrm{e}^{i\phi}|e\rangle_k|g\rangle_{k+1} & |e\rangle_k|e\rangle_{k+1} &\rightarrow |e\rangle_k|e\rangle_{k+1}, \end{aligned} \tag{8.1}$$

where $|a\rangle_k$ ($a = g$ or e) refers to the state of the atom at the kth lattice site. In [100, 106] it is suggested to build a general purpose quantum computer in an optical lattice. The necessary ingredients for a general computer are the two-atom gate in (8.1) and single qubit control, which is possible by directing a laser beam onto each atom. We have focused on what might be achieved with lesser experimental requirement [4]. Specifically, we show below that even without allowing access to the individual atoms, the lattice may still be used to perform a highly non-trivial computational task: simulation of a ferro-magnet.

8.1 Simulation of a ferro-magnet

We have previously used the fact that a two level atom could be represented as a spin 1/2 system. Here we shall use the opposite relation, that our two level atoms may describe spin 1/2 particles with the two states $|g\rangle_k$ and $|e\rangle_k$

representing $|jm\rangle_k = |1/2, -1/2\rangle_k$ and $|1/2, 1/2\rangle_k$. With this representation, the phase-shifted component of the wavefunction in Eq. (8.1) may be isolated by applying the operator $(j_{z,k} + 1/2)(j_{z,k+1} - 1/2)$, and the total evolution composed of the lattice translations and the interaction induced phase shift may be described by the unitary operator e^{-iHt} with Hamiltonian $H = \chi(j_{z,k} + 1/2)(j_{z,k+1} - 1/2)$ and time $t = \phi/\chi$. In a filled lattice the evolution is described by the Hamiltonian $H = \chi \sum_k (j_{z,k} + 1/2)(j_{z,k+1} - 1/2)$, and if we are only interested in the bulk behaviour of the atoms we may apply periodic boundary conditions, so that the Hamiltonian reduces to

$$H_{zz} = \chi \sum_{<k,l>} j_{z,k} j_{z,l}, \tag{8.2}$$

where the sum is over nearest neighbours. By appropriately displacing the lattice we may extend the sum to nearest neighbours in two and three dimensions. H_{zz} coincides with the celebrated Ising-model Hamiltonian [127, 128] introduced to describe ferro-magnetism. Hence, by elementary lattice displacements we perform a quantum simulation of a ferro-magnet. This Hamiltonian and its applications to entanglement and quantum computation has also been studied in Refs. [129, 130].

A more general Hamiltonian of the type

$$H_f = \sum_{<k,l>} \chi j_{z,k} j_{z,l} + \eta j_{x,k} j_{x,l} + \lambda j_{y,k} j_{y,l} \tag{8.3}$$

may be engineered by using multiple resonant pulses and displacements of the lattices. A resonant $\pi/2$-pulse acting simultaneously on all atoms rotates the j_z-operators into j_x-operators, $\mathrm{e}^{ij_{y,k}\pi/2} j_{z,k} \mathrm{e}^{-ij_{y,k}\pi/2} = j_{x,k}$. Hence, by applying $\pi/2$-pulses, in conjunction with the displacement sequence, we turn H_{zz} into H_{xx}, the second term in Eq. (8.3). Similarly we may produce H_{yy}, the third term in Eq. (8.3), and by adjusting the duration of the interaction with the neighbours we may adjust the coefficients χ, η and λ to any values. We cannot, however, produce H_f by simply applying H_{zz} for the desired time t, followed by H_{xx} and H_{yy}, because the different Hamiltonians do not commute. Instead we apply a physical implementation of a well-known numerical scheme: The split operator technique. If we choose short time steps, *i.e.*, small phase shifts ϕ in Eq. (8.1), the error will only be of order ϕ^2, and by repeated application of H_{zz}, H_{xx} and H_{yy}, we may stroboscopicly approximate H_f.

For a few atoms the system may be simulated numerically on a classical computer. In Fig. 8.2 we show the propagation of a spin wave in a one-dimensional string of 15 atoms which are initially in the $|1/2, -1/2\rangle$ state. The central atom is flipped at $t = 0$ and a spin wave propagates to the left and right. The figure shows the evolution of $\langle j_{z,k} \rangle$ for all atoms, obtained by repeatedly applying the

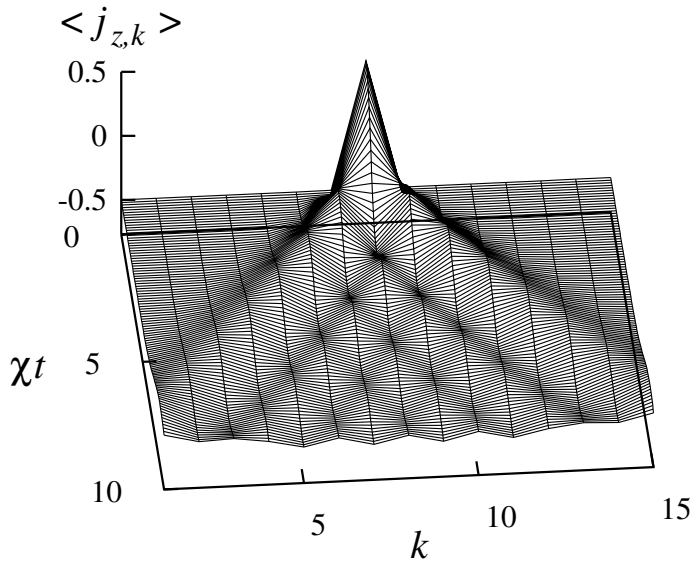

Figure 8.2: Propagation of a spin wave in a one dimensional string. The central atom is flipped at $t = 0$, and repeated application of H_{zz}, H_{xx} and H_{yy} results in a wave propagating to the left and right. The figure shows the evolution of $\langle j_{z,k} \rangle$ for all atoms (k).

Hamiltonians H_{zz}, H_{xx} and H_{yy} with $\chi = \eta = \lambda$ and periodic boundary conditions. Small time steps $dt = 0.1\chi^{-1}$ result in a stroboscopic approximation almost indistinguishable from the results of a direct numerical integration of H_f.

A host of magnetic phenomena may be simulated on our optical lattice: Solitons, topological excitations, two magnon bound states, etc. By pumping a fraction of the atoms into the $|1/2, 1/2\rangle$ state, we may also perform microcanonical ensemble calculations [128] for non-vanishing temperature. Other procedures for introducing a non-vanishing temperature are described in Ref. [34].

8.2 Spin squeezing

We now turn to the generation of spin squeezed states using the same techniques as discussed above. Ref. [113] shows that squeezing can be obtained from the non-linear couplings $H = \chi J_x^2$ and $H = \chi(J_x^2 - J_y^2)$. The product of two collective spin operators involve terms $j_{x,k} j_{x,l}$ for all atoms k and l, and this coupling may be produced by displacing the lattices several times so that the $|1/2, 1/2\rangle$ component of each atom visits every lattice site and inter-

acts with all other atoms. In a large lattice such multiple displacements are not desirable. We shall show, however, that substantial spin-squeezing occurs through interaction with only a few nearby atoms, *i.e.*, for Hamiltonians

$$H = \sum_{k,l} \chi_{k,l} j_{x,k} j_{x,l} \tag{8.4}$$

and

$$H = \sum_{k,l} \chi_{k,l} (j_{x,k} j_{x,l} - j_{y,k} j_{y,l}), \tag{8.5}$$

where the coupling constants $\chi_{k,l}$ between atoms k and l vanish except for a small selection of displacements of the lattices.

Expectation values of relevant angular momentum operators and the variance of the spin operator $J_\theta = \cos(\theta) J_x + \sin(\theta) J_y$, which is perpendicular to the mean spin, may be calculated analytically for an initially uncorrelated state with all atoms in the $|1/2, 1/2\rangle$ state, propagated by the simple coupling (8.4). If each atom visits one neighbour $\chi_{k,l} = \chi \delta_{k+1,l}$, we get the time dependent variance of the spin component $J_{\pi/4} = \frac{1}{\sqrt{2}}(J_x + J_y)$

$$(\Delta J_{\pi/4})^2 = \frac{N}{4} \left[1 + \frac{1}{4} \sin^2(\chi t) - \sin(\chi t) \right]. \tag{8.6}$$

The mean spin vector is in the positive z direction and has the expectation value

$$\langle J_z \rangle = \frac{N}{2} \cos^2(\chi t). \tag{8.7}$$

For small values of χt, $\Delta J_{\pi/4}$ decreases linearly with χt, *cf.* Eq. (7.11), whereas $|\langle J_z \rangle|$ only decreases proportional to $(\chi t)^2$ and the spin is squeezed.

In Fig. 8.3 we show numerical results for 15 atoms in a one-dimensional lattice with periodic boundary conditions. Fig. 8.3 (a) shows the evolution of $(\Delta J_\theta)^2$ when we apply the coupling (8.4) and visit 1, 2, and 3 neighbours. The squeezing angle $\theta = \pi/4$ is optimal for short times $\chi t << 1$. For longer times the optimal angle deviates from $\pi/4$, and we plot the variance $(\Delta J_\theta)^2$ minimized with respect to the angle θ. We assume the same phase shift for all interactions, *i.e.*, all non-vanishing $\chi_{k,l}$ are identical.

To quantify the produced squeezing we use the parameter ξ^2 introduced in Eq. (7.4), which describe the possible noise reduction in an atomic clock and which indicate that a state is entangled if $\xi^2 < 1$. In Fig. 8.3 (b) we show the minimum value of ξ^2 obtained with the couplings (8.4) and (8.5) as functions of the number of neighbours visited. Fig. 8.3 (b) shows that the coupling (8.5) produces better squeezing than (8.4). The coupling (8.4), however, is more attractive from an experimental viewpoint. Firstly, all $j_{x,k}$ operators commute and we do not have to apply several displacements with infinitesimal durations

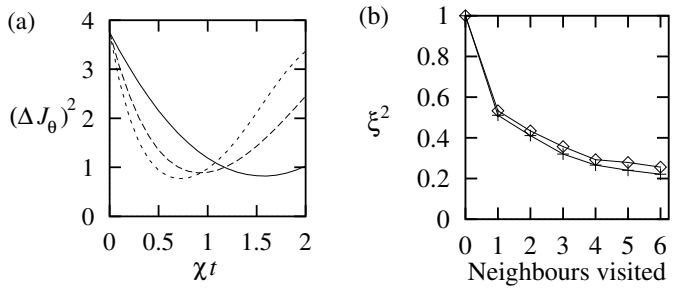

Figure 8.3: Squeezing in a one-dimensional lattice with 15 atoms. **(a)** Evolution of $(\Delta J_\theta)^2$ with the coupling (8.4) and interaction with 1, 2, and 3 neighbours (full, dashed, and short dashed line, respectively). **(b)** The optimal value of the squeezing parameter ξ^2 obtained with the coupling (8.4) ($\diamond$) and (8.5) (+). Lines are shown as guide to the eye.

to produce the desired Hamiltonian. We may simply displace the atoms so that they interact with one neighbour to produce the desired phase shift ϕ, and then go on to interact with another neighbour. Secondly, if the $j_{x,k}j_{x,l}$ coupling involves a phase shift ϕ, the operator $-j_{y,k}j_{y,l}$ requires the opposite phase shift $-\phi$. This may be produced by a long interaction time producing a phase $2\pi - \phi$, or a change of the interaction among the atoms, *i.e.*, a change of the sign of the scattering length in the implementation of Ref. [100]. Neither of these two options are desirable.

Like the analytic expression for ξ^2 obtained from (8.6) and (8.7), the results shown in Fig. 8.3 (b) are independent of the total number of atoms as long as this exceeds the 'number of neighbours visited'. When all lattice sites are visited we approach the results obtained in Ref. [113], *i.e.*, a variance scaling as $N^{1/3}$ and a constant for the couplings (8.4) and (8.5).

So far we have assumed that the lattice contains one atom at each lattice site and that all atoms are cooled to the vibrational ground state. The present experimental status is that atoms can be cooled to the vibrational ground-state, but with a filling factor below unity [131]. A mean filling factor of unity is reported in [132], but when at most a single atom is permitted at each lattice site a mean occupation of 0.44 is achieved. It has been suggested that a single atom per lattice site may be achieved by filling the lattice from a Bose-Einstein condensate [133].

To describe a partially filled lattice it is convenient to introduce stochastic variables h_k, describing whether the kth lattice site is filled $h_k = 1$ or empty $h_k = 0$. The interaction may be described by the Hamiltonian $H = \sum_{k,l} \chi_{k,l} h_k (j_{z,k} + 1/2) h_l (j_{z,l} - 1/2)$, where the sum is over all lattice sites k and l. If we, rather than just displacing the atoms in one direction, also displace the lattice in the opposite direction, so that $\chi_{k,l}$ is symmetric in k and l,

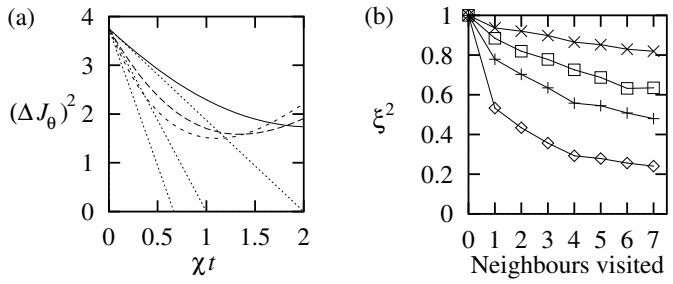

Figure 8.4: Spin squeezing in a partially filled one dimensional lattice containing 15 atoms. **(a)** Evolution of $(\Delta J_\theta)^2$ in a lattice with a filling factor $p = 50\%$ and displacements to 1, 2, and 3 neighbouring sites (full, dashed, and short dashed curve respectively). Dotted lines represent the predictions from Eq. (8.9). **(b)** Minimum attainable squeezing parameter ξ^2 for filling factors p=100% ($\diamond$), 50% (+), 25% ($\Box$), and 10% ($\times$) as functions of the number of sites visited.

we may produce the Hamiltonian

$$H = \sum_{k,l} \chi_{k,l} h_k j_{x,k} h_l j_{x,l}. \tag{8.8}$$

This Hamiltonian models ferro-magnetism in random structures, and it might shed light on morphology properties, and *e.g.*, percolation [134]. Here we shall restrict our analysis to spin-squeezing aspects, since these are both of practical interest, and they represent an ideal experimental signature of the microscopic interaction.

In Fig. 8.4 we show the result of a simulation of squeezing in a partially filled one dimensional lattice. Each lattice site contains an atom with a probability p, and the size of the lattice is adjusted so that it contains 15 atoms. In Fig. 8.4 (a) we show the decrease in the variance of J_θ, averaged over 20 realizations and minimized with respect to θ. Dotted lines indicate the predictions from the time derivatives at $t = 0$

$$\begin{aligned} \frac{d}{dt}(\Delta J_{\pi/4})^2 &= -\frac{1}{4}\sum_{k,l} \chi_{k,l} \langle h_k h_l \rangle \\ \frac{d}{dt}\langle J_z \rangle &= 0, \end{aligned} \tag{8.9}$$

where $\langle h_k h_l \rangle$ denotes the ensemble average over the distribution of atoms in the lattice, *i.e.*, the two atom correlation function. In Fig. 8.4 (b) we show the minimum value of ξ^2 for different filling factors p as a function of the number of neighbours visited. The calculations confirm that even in dilute lattices, considerable squeezing may be achieved by visiting a few neighbours.

Analytical calculations of the amount of spin squeezing produced with a partial filling are presented in Ref. [15].

In conclusion we have suggested a method to simulate condensed matter physics in an optical lattice, and we have shown how the dynamics may be employed to produce spin-squeezing. We emphasize the moderate experimental requirement for our scheme. With the two internal states represented as hyperfine structure states in alkaline atoms, all spin rotations may be performed by Raman or RF-pulses acting on all atoms simultaneously, and lattice displacements may be performed by simply rotating the polarization of the lasers [106]. With the parameters in [100], the duration of the sequence in Fig. 8.1 can be as low as a few micro-seconds. Following our suggestion, spin-squeezing may be produced in dilute optical lattices and implementation is possible with current technology.

Chapter 9

Spin squeezing from a Bose-Einstein condensate

In the previous chapter spin-squeezing was obtained by letting each atom interact with a few nearby atoms. As shown in Fig. 8.3 (b) the amount of squeezing is increased when we let each atom interact with a larger number of atoms. Ideally each atom should interact with all other atoms but with optical lattices this is not practical because it would require a very large number of lattice displacements. In this chapter we present a different proposal which allows a very large number of atoms to interact and produces a much stronger squeezing.

In this chapter we shall study atoms in a atomic Bose–Einstein condensate [101–103]. Bose–Einstein condensation occurs when a collection of bosonic atoms are cooled to very low temperatures. Below a certain transition temperatures there is a phase transition to a state where a macroscopic number of atoms are in the lowest energy quantum state. At very low temperatures almost every atom is in the same quantum state with a motional wavefunction ψ_0. Since the first experimental observations of Bose–Einstein condensation in dilute atomic vapours [102, 103], the experimental data has shown a strong influence of a collisional interaction between the atoms. This interaction has been very successfully described by the potential in Eq. (7.1). In the following we shall show that this collisional interaction can be used to entangle the atoms in the condensate. Since all atoms share the same motional wavefunction, each atom interacts equally with all other atoms and this enables the generation of much stronger squeezing than obtained in the previous chapter.

We consider a two component weakly interacting Bose-Einstein condensate [135, 136] and we assume that the interactions do not change the internal state of the atoms. If the two internal states are denoted by a and b, this situation

is described by the second quantized Hamiltonian

$$H = \sum_{j=a,b} \int d^3r \hat{\Psi}_j^\dagger(\mathbf{r}) H_{0,j} \hat{\Psi}_j(\mathbf{r}) + \frac{1}{2} \sum_{j=a,b} U_{jj} \int d^3r \hat{\Psi}_j^\dagger(\mathbf{r}) \hat{\Psi}_j^\dagger(\mathbf{r}) \hat{\Psi}_j(\mathbf{r}) \hat{\Psi}_j(\mathbf{r}) + U_{ab} \int d^3r \hat{\Psi}_a^\dagger(\mathbf{r}) \hat{\Psi}_b^\dagger(\mathbf{r}) \hat{\Psi}_a(\mathbf{r}) \hat{\Psi}_b(\mathbf{r}), \tag{9.1}$$

where $H_{0,j}$ is the one particle Hamiltonian for atoms in state j including the kinetic energy and the external trapping potential $V_j(\mathbf{r})$, $\hat{\Psi}_j(\mathbf{r})$ is the field operator for atoms in the state j, $U_{jk} = 4\pi\hbar^2 a_{jk}/M$ is the strength of the interaction between particles of type j and k, parameterized by the scattering length a_{jk}, and M is the atomic mass, *cf.* Eq. (7.1).

Assume that we start with a Bose–Einstein condensate in the internal state $|a\rangle$ at very low temperature ($T \simeq 0$), so that all the N atoms are in a single particle (motional) state $|\psi_0\rangle$. A fast $\pi/2$ pulse, *e.g.* a microwave pulse, between the states $|a\rangle$ and $|b\rangle$ prepares the atoms in the state $|\psi_0\rangle^N(|a\rangle + |b\rangle)^N/2^{N/2}$, which is an eigenstate of the J_x operator with eigenvalue $N/2$, and we study the noise reduction in the orthogonal component $J_\theta = \cos(\theta)J_z + \sin(\theta)J_y$. To show that the subsequent time evolution produces squeezing we use the same technique as we used in chapter 7, and we find the time derivative of ξ_θ^2 at $t = 0$ by using Ehrenfest's theorem

$$\frac{d}{dt}\xi_\theta^2 = \sin(2\theta)\frac{(N-1)(U_{aa} + U_{bb} - 2U_{ab})}{2\hbar} \int d^3r |\psi_0|^4. \tag{9.2}$$

This equation immediately shows that spin squeezing will be produced for certain angles θ if $U_{aa} + U_{bb} \neq 2U_{ab}$ as it is in the Na experiments [136].

To quantify the amount of squeezing which may be obtained, we assume identical trapping potentials $V_a(\mathbf{r}) = V_b(\mathbf{r})$ and identical coupling constants for the interaction between atoms in the same internal state $a_{aa} = a_{bb} > a_{ab}$. Physically, this could correspond to the $|F = 1, M_F = \pm 1\rangle$ hyperfine states of Na trapped in an optical dipole trap. Due to the symmetry of these states their scattering lengths and trapping potentials will be identical; moreover, due to angular momentum conservation there are no spin exchanging collisions between these states as required by our model. This is exactly the experimental setup used in Ref. [136]. In this experiment it is shown that these states have an antiferro-magnetic interaction $a_{ab} < a_{aa}$ which according to (9.2) enables the production of squeezed states. To avoid spin changing collisions that populate the state $|M_F = 0\rangle$[137] one has to slightly modify such an experimental set–up. If the $F = 1$ manifold is coupled to the $F = 2$ with a far off-resonant blue detuned π-polarized microwave field, the $|F = 1, M_F = 0\rangle$ state is raised in energy with respect to the $|F = 1, M_F = \pm 1\rangle$ states, because the Clebsch-Gordan coefficient for the $|F = 1, M_F = 0\rangle \rightarrow |F = 2, M_F = 0\rangle$ transition is

larger than the coefficients for the $|F=1, M_F=\pm 1\rangle \rightarrow |F=2, M_F=\pm 1\rangle$ transitions, and spin exchanging collisions become energetically forbidden. If for instance one chooses a detuning $\delta = (2\pi)25$ MHz and a resonant Rabi frequency for the $1 \rightarrow 1$ transition of $\Omega = (2\pi)2$ MHz, the energy separation is $\Delta E = 640$nK. With a typical chemical potential $\mu \approx 220$ nK[137], this energy separation is much higher than the available energy in the collisions and the $|F=1, M=0\rangle$ state is completely decoupled. In Ref. [137] a much smaller energy difference is shown to exclude spin exchanging collision and we therefore expect that much weaker fields will suffice.

The assumption $a_{aa} = a_{bb}$ has several advantages. Firstly, it reduces the effect of fluctuations in the total particle number. If $a_{aa} \neq a_{bb}$ the mean spin performs an N-dependent rotation around the z-axis, and fluctuations in the number of particles introduces an uncertainty in the direction of the spin which effectively reduces the average value and introduces noise into the system. With $a_{aa} = a_{bb}$ the mean spin remains in the x-direction independent of the number of atoms in the trap. Secondly, this condition ensures a large spatial overlap of different components of the wavefunction. After the $\pi/2$ pulse the spatial wavefunction is no longer in the equilibrium state. Due to the atomic repulsions (which are now different than before because the atoms are in different internal states), the spatial distribution of the atomic cloud will start oscillating. Furthermore, since the state of the system is now distributed over a range of number of particles in the $|a\rangle$ state (N_a), and since this number enters into the time evolution, the N_a dependent wavefunctions ψ_a and ψ_b are different for particles in the states $|a\rangle$ and $|b\rangle$. With $a_{aa} = a_{bb}$, ψ_a and ψ_b are identical if N_a equals the average number $N/2$. In the limit of large N, the width of the distribution on different N_a's is much smaller than N_a and all the spatial wavefunctions are approximately identical $\psi_a(N_a, t) \approx \psi_b(N_a, t) \approx \psi_0(t)$. This relation is only true if $a_{aa} > a_{ab}$ where small deviations from the average wavefunction perform small oscillations. In the opposite case the deviations grow exponentially [138] resulting in a reduction of the overlap of the a and the b wavefunctions and a reduced squeezing. The advantages mentioned above could also be achieved with $a_{aa} \neq a_{bb}$ by using the breath–together solutions proposed in Ref. [138].

Before analyzing quantitatively the complete system, we estimate the amount of spin squeezing we can reach with our proposal by using a simple model. Assuming that both $|a\rangle$ and $|b\rangle$ atoms can be described by the wavefunction ψ_0 which is constant and independent of the number N_a, the spin dependent part of the Hamiltonian (9.1) may be written as $H_{\rm spin} = \chi J_z^2$, where χ depends on the scattering lengths and the wavefunction ψ_0. The spin squeezing produced by this Hamiltonian can be calculated exactly [113]. In the limit of large N, the minimum obtainable squeezing parameter is $\xi_\theta^2 = \frac{1}{2}\left(\frac{3}{N}\right)^{2/3}$, which indicates that our proposal might produce a reduction of ξ_θ^2 by a factor

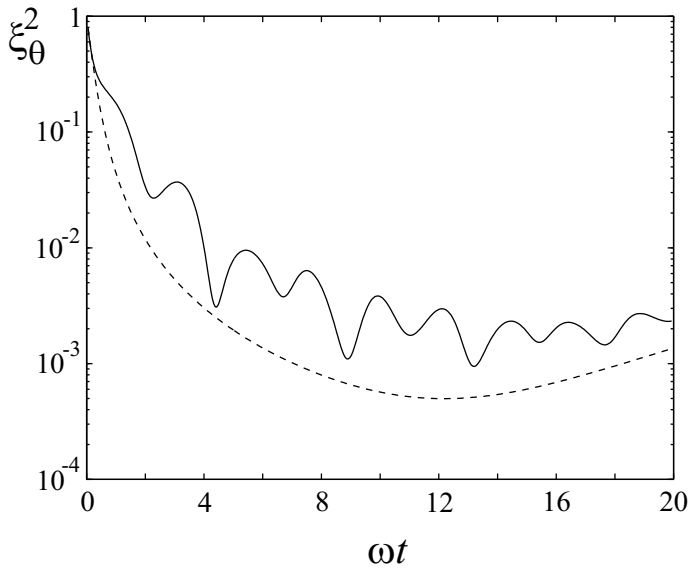

Figure 9.1: Reduction in the squeezing parameter ξ^2_θ. A fast $\pi/2$ pulse between two internal states is applied to all atoms in the condensate. The subsequent free time evolution results in a strong squeezing of the total spin. The angle θ is chosen such that ξ^2_θ is minimal. The solid line is the results of a numerical integration (see text). For numerical convenience we have assumed a spherically symmetric potential $V(r) = m\omega^2 r^2/2$. The parameters are $a_{aa}/d_0 = 6 \cdot 10^{-3}$, $a_{bb} = 2a_{ab} = a_{aa}$, and $N = 10^5$. The dashed curve shows the squeezing obtained from the Hamiltonian $H_{\rm spin} = \chi J_z^2$. The parameter χ is chosen such that the reduction of J_x obtained from the solution in Ref. [113] is consistent with the results of Ref. [138].

of $\sim N^{2/3}$ which would be more than three orders of magnitude with 10^5 atoms in the condensate.

In contrast to the simplified Hamiltonian $H_{\rm spin}$ the real Hamiltonian (9.1) will also entangle the internal and motional states of the atoms which is a source of decoherence for the spin squeezing. To quantify this effect we have performed a direct numerical integration following the procedure developed in Ref. [138]. We split the whole Hilbert space into orthogonal subspaces containing a fixed number of particles N_a and $N_b = N - N_a$ in each of the internal states, respectively. In each subspace we make a Hartree-Fock variational ansatz in terms of three-dimensional spatial wavefunctions $\psi_a(N_a, t)$ and $\psi_b(N_b, t)$, which are evolved according to the time dependent coupled Gross-Pitaevskii equations. This is an approximation to the full problem which is valid in the limit of low temperatures and short times, where the population of the Bogoliubov modes is small. Particularly it is a good approximation in our case with $a_{ab} < a_{aa}$,

a_{bb} where there are no demixing instabilities. With this procedure, the decoherence induced by the entanglement with the motional state is effectively taken into account. Together with the prediction from the simple Hamiltonian $H_{\rm spin}$ the result of the simulation is shown in Fig. 9.1. The two curves are roughly in agreement confirming that the system is able to approximate the results of the Hamiltonian $H_{\rm spin}$. The numerical solution shows fluctuations due to the oscillations of the spatial wavefunction. The large dips at $\omega t \approx 4$, 9, 13, and 18 are the points where the atomic cloud reach the initial width. At these instants the overlap of the wavefunctions is maximal and the two curves are very close (up to a factor of two). The small dips at ωt =2, 7, 11, and 16 corresponds to the points of maximum compression. With the realistic parameters used in the figure, our simulation suggests that squeezing of three orders of magnitude is possible. Also, note the time scale in the figure. The maximally squeezed state is reached after approximately two oscillation periods in the trap. For a fixed ratio of the scattering lengths a_{ab}/a_{aa}, the optimal time scales as $(a_{aa}/d_0)^{-2/5}N^{-1/15}$, where $d_0 = \sqrt{\hbar/(m\omega)}$ is the width of the ground state of the harmonic potential.

The analysis so far has left out a number of possible imperfections. Specifically, we have assumed that all scattering length are real so that no atoms are lost from the trap and we have not considered the role of thermal particles. To estimate the effect particle losses we have performed a Monte Carlo simulation [90] of the evolution of squeezing from the Hamiltonian $H_{\rm spin}$. The particle loss is phenomenologically taken into account by introducing a loss rate Γ which is identical for atoms in the $|a\rangle$ and the $|b\rangle$ state. In Fig. 9.2 we show the obtainable squeezing in the presence of loss. Approximately 10 % of the atoms are lost at the time $\chi t \approx 6 \cdot 10^{-4}$ where the squeezing is maximally without loss. With the parameters of Fig. 9.1 this time corresponds to roughly two trapping periods. Such a large loss is an exaggeration of the loss compared to current experiments and the simulation indicate that even under these conditions, squeezing of nearly two orders of magnitude may be obtained. On the other hand, the effects of thermal particles can be suppressed at sufficiently low temperatures but due to the robustness with respect to particle loses shown in Fig. 9.2, we expect to obtain high squeezing even at some finite temperatures. A number of imperfections, *e.g.* Bogoliubov modes, were also left out in the numerical treatment, but an exact stochastic simulation of the system has confirmed that the condensate is capable of producing strong squeezing [105].

We believe that this proposal is a simple and robust method to produce entangled states of a large number of atoms with present technology. The proposal offers a very strong noise reduction, and it is directly applicable to existing experimental set–ups. The Hamiltonian $H_{\rm spin}$ is of the same form as the one that was shown to produce multi–particle entangled states in chapter 4, and in future experiments with negligible particle loss even for very long

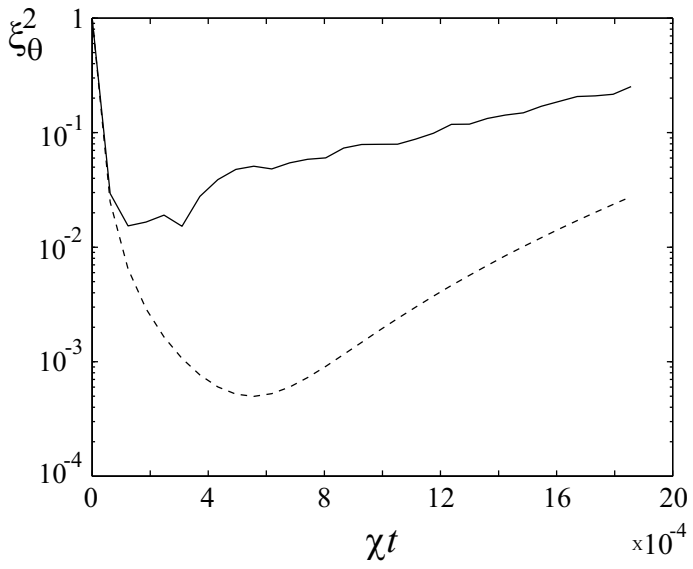

Figure 9.2: Quantum Monte Carlo simulation of squeezing in the presence of loss. The full line shows squeezing obtained from the Hamiltonian $H_{\rm spin}$ with particle loss described by a constant loss rate $\Gamma = 200\chi$. The dashed curve shows squeezing without particle loss.

interaction times, the procedures discussed in this chapter could also be used to produce maximally entangled states of any number of atoms.

Chapter 10

Spin squeezing and entanglement

In Eq. (7.4) we introduced the quantity[1] $\xi^2 = N(\Delta J_x)^2/\langle J_z\rangle^2$ that describe the reduction in the frequency variance of an atomic clock which can be obtained by using atoms in a spin squeezed state. In the derivation of this reduction it is assumed that no other sources of noise are present. The states which minimize ξ^2 are obtained in the limit $\langle J_z\rangle, \Delta J_x \to 0$, where any other source of noise will, however, deteriorate the spectroscopic resolution. In practice, the ideal states for spectroscopy are therefore states which minimize the noise ΔJ_x for a given not too small value of $\langle J_z\rangle$. Unlike the rest of this thesis we shall not restrict ourself to two-level atoms in this chapter, and in section 10.1 we identify the minimum of ΔJ_x as a function of $\langle J_z\rangle$ for system with spin J, *i.e.*, we optimize the signal to noise ratio by identifying the states with minimum quantum noise for a given value of the signal. For photons a similar analysis has been performed in Ref. [139]. Having identified the minimum of ΔJ_x, we use this information to derive an experimental criterion for entanglement in section 10.2. A measurement of two collective operators for a collection of atoms produces a sufficient criterion for entanglement which can even quantify the 'depth' of entanglement, *i.e.*, the minimum number of particles forming multi-particle entangled states in the sample.

[1] In this chapter we align the mean spin along the z-axis and look for noise in the x component of the spin.

10.1 Maximal squeezing

To get a lower limit on ΔJ_x as a function of $\langle J_z \rangle$, one can use the inequality $\langle J_x^2 \rangle + \langle J_y^2 \rangle + \langle J_z \rangle^2 \leq J(J+1)$ which together with Heisenberg's uncertainty relation (7.3) yields the limit

$$(\Delta J_x)^2 \geq \frac{1}{2}\Big[J(J+1) - \langle J_z \rangle^2 - \sqrt{(J(J+1) - \langle J_z \rangle^2)^2 - \langle J_z \rangle^2}\Big]. \qquad (10.1)$$

This does not present a tight minimum for $\mathrm{Var}(J_x)$, but for large J and $\langle J_z \rangle \approx J$ it is close to the actual minimum found by the numerical approaches discussed below. For low values of $\langle J_z \rangle$ it differs by a factor of two. The precise analysis of the minimum becomes quite different for integer spins and for half-integer spins, and we shall deal with them separately:

For integer spins our calculations show that the state which minimizes $\mathrm{Var}(J_x)$ for a given $\langle J_z \rangle$ has vanishing $\langle J_x \rangle$ and $\langle J_y \rangle$, so that it is also a minimum of $\langle J_x^2 \rangle$. Accordingly, these states can be found by minimizing $\mu \langle J_z \rangle + \langle J_x^2 \rangle$, where μ is a Lagrange multiplier, ensuring the value of $\langle J_z \rangle$. For J-values up to several hundred, it is straightforward to numerically determine the minimum, by determining the smallest eigenvalue of the operator $\mu J_z + J_x^2$ for a wide range of values of μ. By determining $\langle J_z \rangle$ and $\langle J_x^2 \rangle$ in the corresponding eigenstates one finds exactly the minimum value of $\mathrm{Var}(J_x)$=$\langle J_x^2 \rangle$ for the particular value of $\langle J_z \rangle$. The results for different values of J are shown in Fig. 10.1. For $J = 1$ it is possible to diagonalize $\mu J_z + J_x^2$ analytically, and we get $\mathrm{Var}(J_x)_{min} = (1 - \sqrt{1 - \langle J_z \rangle^2})/2$.

For half-integer spins, it is not true that the state minimizing $\langle J_x^2 \rangle$ also minimizes $\mathrm{Var}(J_x)$ at a given value of $\langle J_z \rangle$. The reason is that for half-integer spins, the operator J_x^2 has eigenvalues $\frac{1}{4}$, $\frac{9}{4}$, ..., and its expectation value will thus always exceed $\frac{1}{4}$. The variance of J_x, however, can come arbitrarily close to zero if the system approaches a J_x eigenstate. Consider for instance a $J = \frac{1}{2}$ particle, where all (pure) states can be obtained as a simple rotation of the spin up state. In this case the components perpendicular to the mean spin are never squeezed; their variances are both $\frac{1}{4}$. But if we compute the variance of J_x and the mean value of J_z, one finds that they obey the relation, $\mathrm{Var}(J_x)_{min} = \langle J_z \rangle^2$ (this result can also be found by setting $N = 1$ in Eq. (7.6)), where both sides approach zero when the state approaches either of the two $J_x = \pm\frac{1}{2}$ eigenstates. In that case, of course, the mean spin also has a component along the x direction. The state is spin squeezed in the sense of the relation (7.3), but not in the sense where one deals explicitly with a spin component perpendicular to the mean spin vector.

For large half-integer J it is more difficult to find the most squeezed states. The reason is that the problem cannot be formulated as a linear quantum mechanics problem like the diagonalization of an operator containing a Lagrange multiplier term, which we used for integer spins. To compute a variance, we

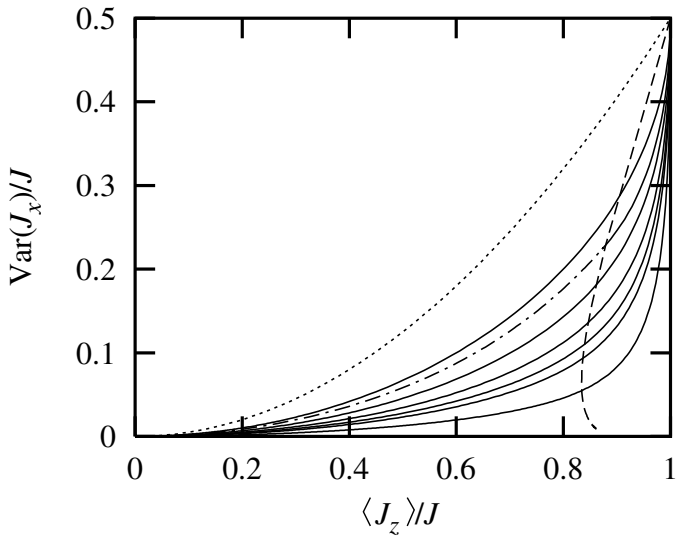

Figure 10.1: Maximal squeezing for different values of J. The curves starting at the origin represent the minimum obtainable variance as a function of the mean spin. Starting from above, the curves represent $J = 1/2, 1, 3/2, 2, 3, 4, 5, 10$. The dotted curve for $J = 1/2$ is the limit identified in chapter 7. The full curves are obtained by diagonalization of the operator $\mu J_z + J_x^2$. The dashed curve represents the position of a bifurcation in the solution for half-integer spins. To the right of this curve the diagonalization may be applied. To the left of the curve the minimum is found by a variational calculation (dash-dotted curve for $J = 3/2$).

have to determine the square of a mean value which is an expression to fourth order in the wavefunction amplitudes. It is easy, however, to implement a Monte Carlo variational calculation which minimizes $\mu\langle J_z\rangle + \mathrm{Var}(J_x)$, by randomly modifying the amplitudes of a state vector as long as the variational functional is reduced. Like above, the Lagrange multiplier term is used to adjust the mean value of J_z, so that for each value of μ the identified state vector minimizes $\mathrm{Var}(J_x)$ for the given value of $\langle J_z\rangle$. When applied to larger half-integer values of J, this method shows that large values of $\langle J_z\rangle$ are accompanied by vanishing mean values of J_x and J_y, and the solution thus coincides with the one found by the diagonalization method. But, for a critical value of $\langle J_z\rangle$, the solution bifurcates, and two states with opposite non vanishing mean values of J_x have the smallest variance. See Fig. 10.2. These states approach the two $J_x = \pm\frac{1}{2}$ eigenstates in the limit of small $\langle J_z\rangle$. Due to the noise in the simulation, the Monte-Carlo method is not efficient for a precise determination of the critical point of the bifurcation for large values of J. Before the bifurcation the state is the eigenstate corresponding to the lowest eigenvalue

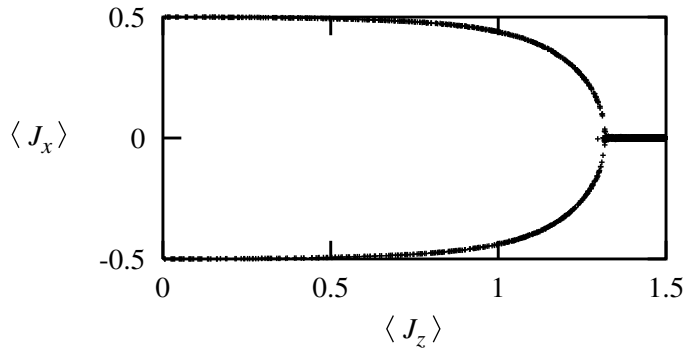

Figure 10.2: Bifurcation in the solution for $J = 3/2$. The points represent the mean value of the spin in the maximally squeezed states. The points are obtained by a Monte Carlo variational calculation which minimizes $\mu\langle J_z\rangle + \mathrm{Var}(J_x)$. Above $\langle J_z\rangle \approx 1.32$ there is a unique solution with $\langle J_x\rangle = 0$. Below $\langle J_z\rangle \approx 1.32$ the solution bifurcates, and $\langle J_x\rangle$ approaches $\pm 1/2$.

of the operator $\mu J_z + J_x^2$, and after the bifurcation the state is a superposition of the different eigenvectors with amplitudes on states with higher eigenvalues. We can therefore determine the position of the bifurcation from the properties of the eigenvectors, and for different values of $J < 100$, we find that the bifurcation happens in the interval

$$0.83 < \frac{\langle J_z\rangle}{J} < 0.88, \tag{10.2}$$

except for the special case $J = 1/2$ where $\langle J_z\rangle = J$ at the bifurcation. If we do not break the $\pm J_x$ symmetry, the variance from this point flattens out to the value $\frac{1}{4}$, but in either of the states with the broken symmetry, the variance decreases towards zero when smaller values of $\langle J_z\rangle$ and non-vanishing values of $\langle J_x\rangle$ are considered. The position of the bifurcation is plotted in Fig. 10.1. To the right of the dashed line the minimum may be found by diagonalization. To the left of the curve the variational approach has to be applied for half-integer spins.

It is the non-linearity of the problem that leads to the bifurcation and symmetry breaking of the solution. Classical approximations to many body quantum problems often show such bifurcations associated with phase transitions in the problem, *e.g.* lasing. It is interesting that a similar phenomenon appears here, in the study of a single quantum system in a (very) low-dimensional Hilbert space. We emphazise that we are not discussing an extension of quantum theory to include non-linear terms, we are simply identifying the quantum states that minimize a variance, and this is a non-linear problem.

Since we have identified the maximally squeezed states as eigenstates of the operator $\mu J_z + J_x^2$ we can devise a method to produce them even without having explicit expressions for these eigenstates. This method only works for integer spin, and for half-integer spin which are squeezed to values of the mean spin exceeding the value at the bifurcation (10.2). The system is first prepared in the $|J_z = J\rangle$ eigenstate, and one switches on a Hamiltonian $H(t) = \omega J_z + \chi(t) J_x^2$, where $\chi(t)$ increases very slowly from the value zero and where $\omega < 0$. If the state of the spin follows this Hamiltonian adiabatically, it evolves through the minimum energy eigenstates of the instantaneous $H(t)$, which is precisely the family of states identified by the above diagonalization procedure. The adiabatic process may be difficult to perform in physical systems of interest, and for practical purposes it is relevant to consider, *e.g.*, the Hamiltonian $H = \chi J_x^2$ which was proposed in Ref. [113] and which we used in the chapter 9. In the regime with large $|\langle J_z \rangle|$, the squeezing resulting from this Hamiltonian is actually close to the optimum. The Hamiltonian $H = J_x^2 - J_y^2$, also discussed in Ref. [113], leads to similar squeezing for large $|\langle J_z \rangle|$, and it follows the optimum for a larger range of parameters.

10.2 Entanglement

We have identified the minimum variance of J_x given the value of $\langle J_z \rangle$. Any measurement of these two quantities can be plotted as a point in Fig. 10.1, and this point must lie on or above the curve for the relevant J. We note that the curves depend on J, and in the chosen units, large spins can be more squeezed than small spins. This implies that the collective spin variables $\vec{\mathcal{J}} = \sum_i \vec{J}_i$ for several spin J particles can be more squeezed than the individual spins themselves. We will now show that this requires the state of the spins to be an entangled state. We have already shown, that for spin 1/2 particles, reduction of the parameter ξ below unity for the collective spin implies entanglement of the spins. We now generalize this property to arbitrary spins.

A separable (non-entangled) state of N spin J particles is defined as a in Eq. (7.5). The variance of $\mathcal{J}_x$ in such a state obeys the inequality

$$\begin{aligned} \mathrm{Var}(\mathcal{J}_x) &\geq \sum_k p_k \sum_{i=1}^{N} (\Delta J_x^2)_i^{(k)} \\ &\geq \sum_k p_k \sum_{i=1}^{N} J F_J(\langle J_z \rangle_i^{(k)}/J), \end{aligned} \tag{10.3}$$

where the function $F_J(\cdot)$ is the minimum variance of J_x divided by J for a particle with spin J, *i.e.* the curves plotted in Fig. 10.1, and where $\langle J_z \rangle_i^{(k)}$ is the mean value of J_z of the ith particle in the kth realization in the sum (7.5).

As it appears from Fig. 10.1, all the curves $F_J(\cdot)$ are convex. We can prove this property for integer spins, and for half integer spins in the range of large $|\langle J_z\rangle|$, by considering the production of the states by adiabatic passage from the $|J_z = J\rangle$ eigenstate. The positive factor in front of the J_x^2 component in the Hamiltonian $\omega J_z + \chi(t)J_x^2$ is gradually increased, and the rate of change of $\langle J_x^2\rangle$ and of $\langle J_z\rangle$ at any given time are given by Ehrenfest's theorem:

$$\begin{aligned} \frac{d}{dt}\langle J_x^2\rangle &= -i\langle[J_x^2, \omega J_z]\rangle \\ \frac{d}{dt}\langle J_z\rangle &= -i\langle[J_z, \chi(t)J_x^2]\rangle. \end{aligned} \tag{10.4}$$

The mean values on the right hand side should be evaluated in the maximally spin squeezed state and they are not known explicitly. But, we observe that they contain the same operator, and the ratio between the two rates of changes is therefore simply $-\omega/\chi(t)$. This implies that along the family of maximally squeezed states, the relative change of $\langle J_x^2\rangle$ and $\langle J_z\rangle$, *i.e.*, the slope of the curve $F_J(\cdot)$, is monotonically decreasing when we we go from right to left in Fig. 10.1 (since $\chi(t)$ is an increasing function of time and $\omega < 0$). It follows that the second derivative of the function $F_J(\cdot)$ is positive and the function is convex.

From the convexity follows that the functions $F_J(\cdot)$ obey Jensen's inequality, which states that any linear combination of $F_J(a_i)$'s with positive coefficients is larger than or equal to the function F_J evaluated on the linear combination of the arguments. It therefore follows that in any separable state

$$\begin{aligned} \mathrm{Var}(\mathcal{J}_x) &\geq \sum_k p_k NJF_J\left(\frac{1}{NJ}\sum_{i=1}^{N}\langle J_z\rangle_i^{(k)}\right) \\ &\geq NJF_J\left(\sum_k p_k \frac{1}{NJ}\sum_{i=1}^{N}\langle J_z\rangle_i^{(k)}\right) = NJF_J\left(\frac{\langle\mathcal{J}_z\rangle}{NJ}\right). \end{aligned} \tag{10.5}$$

This relation is the main result of this chapter. In an experiment with a collection of N spin J particles, it is possible to measure $\mathcal{J}_z$ and $\mathcal{J}_x$, and to determine their mean value and variance. If the data-point $(\langle\mathcal{J}_z\rangle/NJ,\ \mathrm{Var}(\mathcal{J}_x)/NJ)$ lies below the relevant curve in Fig. 10.1, the systems are not in a separable state, and they are experimentally proven to be entangled.

The extent to which the measured data point falls below the curve in the plot is a measure of the degree of entanglement. A quantitative measure of entanglement in a multi-particle system is the number of elements that must at least have gone together in entangled states. We define a k particle entangled state to be a state of N particles which *cannot* be decomposed into a convex sum of products of density matrices with all density matrices involving less than k particles: at least one of the terms is a k particle entangled density matrix. If, for example, N spin $\frac{1}{2}$ particles form $N/2$ entangled pairs, the degree of

macroscopic spin squeezing of the system is limited by the inequality (10.5) with $J = 1$ and N replaced by $N/2$. If the measured macroscopic $\langle \mathcal{J}_z \rangle$ and $\mathrm{Var}(\mathcal{J}_x)$ also lie below the corresponding $J = 1$ curve, the measurement unambiguously implies that the systems are entangled in larger than binary ensembles. The size of these ensembles is a measure of the 'depth' of entanglement, which can be determined experimentally. This criterion is similar to the one used in [44] where the fidelity of production of a maximally entangled N-particle states is used as a proof of N-particle entanglement.

As a final point we demonstrate how our procedure can be applied to identify substantial multi-particle entanglement in some of the entanglement schemes which has been presented in the thesis. In chapter 9 it was predicted that appreciable spin squeezing of atoms can be obtained in a two-component Bose-Einstein condensate. In the calculation, a reduction of $\mathrm{Var}(\mathcal{J}_x)$ by a factor of 1000 is found for a reduction of $\langle \mathcal{J}_z \rangle$ of only 1% with 10^5 atoms in the condensate. Using Eq. (10.1) these numbers imply a depth of entanglement of $\sim 4 \cdot 10^4$. In chapter 4 it was shown that it is possible to implement a Hamiltonian J_y^2 by applying bichromatic light to all ions in an ion trap, and it was shown that this Hamiltonian can be used to create a maximally entangled state of all the ions. If the decoherence in the trap is such that one cannot produce a maximally entangled state, a different strategy could be to apply the light for a short time so that squeezing is produced. For small times the squeezing obtained from the Hamiltonian J_y^2 is close to the optimal curves in Fig. 10.1, and our theory identifies a depth of entanglement close to the total number of ions in the trap. In this way one could produce and verify the production of an entangled state of many ions.

In this chapter we have considered squeezing and entanglement related to the collective operators $\mathcal{J}_z$ and $\mathcal{J}_x$. We emphazise that the collective spin components of multi-particle atomic system are readily available by standard spectroscopic methods, which require no access to the individual components. Given the large interest in spin squeezing, a criterion of entanglement based on this property is an important tool. Recall, however, that systems may well be entangled without being spin squeezed: The spin squeezing measurement provides a sufficient criterion for the depth of entanglement, not a necessary one.

Part IV

Conclusion

Chapter 11

Conclusion

Quantum computation is a field with several promising perspectives. At the present stage, however, the experiments are lacking far behind the theoretical dreams, and there is a need for proposals which may close the gap between experiments and theory. We have tried to contribute to the reduction of this gap by suggesting some simple experimental procedures for producing entanglement and small scale quantum processors which can be realized with current technology. It is our hope that by implementing some of the proposals presented in this thesis, we will learn more about the requirements and possibilities for quantum information processing and that this knowledge will aid in the development of a large quantum computer. Furthermore, the entangled states which are produced by our proposals have an interest in their own right because they can be used to increase the sensitivity of atomic clocks.

In the ion trap quantum computer we have suggested a novel method to implement gates between the ions. Our gate is designed with the specific purpose of reducing the effect of heating of the vibrational motion. The heating is one of the major obstacles to quantum computation in this system, but with our gate the effect of heating is reduced considerably. At the same time our gate has the remarkable property that it is able to prepare multi-particle entangled states without experimental access to the individual ions. By illuminating all ions in the trap with a single beam of bichromatic light, the ions can be driven into a maximally entangled state and this considerably reduces the experimental requirements for the preparation of such states. Using our proposal the experimental ion trapping group at NIST has been able to produce maximally entangled four-particle states [44]. This is the largest number of particles which has been entangled in any experiments so far, and this is a major achievement of our work.

We have performed a detailed analysis of the effect of some of the most important experimental imperfections on the functioning of our gate. With the

formulas that we have derived, an experimentalist can insert a set of parameters describing a given experimental configuration and estimate the attainable fidelity of a maximally entangled state of any number of ions. It is our hope that these calculation of decoherence mechanisms will be a useful guide in the design of future ion trap experiments.

Our bichromatic light produces two qubits gates which is sufficient for the construction of a quantum computer in the ion trap. In a practical realization it may, however, not be the ideal strategy to implement the entire algorithm by using a large number of two particle gates. We have developed a method which makes more active use of the vibrational motion to implement higher order gates between the bits. Also this proposal is ideally suited for situations with limited experimental access to the individual qubits. By only addressing the qubits collectively it is possible to implement the inversion about the mean which plays a central role in Grovers search algorithm.

We have demonstrated that it is possible to simulate interesting quantum many-body systems, such as ferro-magnetism, with neutral atoms trapped in an optical lattice. As the number of particles grow, these systems become impossible to simulate on a classical computer and the optical lattice simulator allows us to extract information which we cannot obtain without quantum computation. This specific purpose quantum computer is much simpler to construct than a general purpose quantum computer in the optical lattice.

The major part of our work with neutral atoms has been devoted to the study of spin squeezed states. Spin squeezed states are entangled states which can potentially be used to increase the precision of atomic clocks. We have proposed two different experimental proposals for the preparation of these states by using atoms in optical lattices and Bose–Einstein condensates. Both proposals uses the collisional interaction to entangle the atoms but each of the two proposals has is it own advantage. In optical lattices it is possible to obtain much higher trapping frequencies than in the current experiments with condensates. The higher trapping frequencies in the lattices confines the spatial wavefunction to a smaller spatial region, and since the atoms are more confined the collisional interaction is much stronger, *cf.* Eq. (7.2). The stronger interaction permits a much shorter interaction time which is a huge advantage if decoherence mechanisms are present. On the other hand the quality of the squeezing is much better in the condensate proposal. Compare for instance Fig. 8.3 (b) with the results obtained for the condensate. In the figure it is shown that the squeezing increases as each atom interacts with a larger number of neighbouring atoms. In the condensate the atoms share the same spatial wavefunction so that every atoms interacts with all other atoms in the sample, and the condensate proposal corresponds to the limit where $5 \cdot 10^4$ neighbours are visited in Fig. 8.3 (b). For this reason the squeezing is orders of magnitude better in the condensate proposal.

We have developed a method to analyse the entanglement in a spin squeezed state. Our method relies on the measurement of only two experimental quantities: the mean spin and the fluctuations in a component perpendicular to it. By measuring these two quantities an experimentalist can not only conclude that the state is entangled but also estimate the depth of entanglement. The depth of entanglement is the minimum number of particles which must have been entangled in the state in order to reproduce the experimental results. With this method and our proposals for generating spin squeezing it should be possible to produce and verify entanglement of a large number of particles.

Much of our work studies the possibility of partially implementing experimental proposals for quantum computation. We have demonstrated that several interesting states and effects may be produced without the ability the control and detect the individual qubits in the computer. Such RISQ (reduced instruction set quantum) devices should be simpler to construct in practice than a general purpose quantum computer and could provide information about the functioning of the underlying interactions in a premature quantum computer. On top of this RISQ devices could also provide useful technological spin-offs, *e.g.* improved atomic clocks.

Finally, we wish to emphasize that even if a final quantum computer is not implemented they way we propose here, our work has presented novel ideas for constructing gates and these ideas may be useful in other experimental setup. The procedure developed for the ion trap involves qubits which are coupled to a harmonic oscillator. This situation is quite general and already a number of theoretical papers have appeared which operates along the same lines as our proposal [60, 82, 96, 140–142]. One of these schemes has even been implemented experimentally [143].

Appendix A

Summary

A.1 English summary

Entanglement is a quantum mechanical property which enables separated quantum systems to exhibit instantaneous non-local correlations even if the systems are very far from each other. A quantum computer is a computer which is fundamentally different from the classical computers we know today. A quantum computer exploits entanglement to solve problems which are impossible to solve on a classical computer. The enhanced computational power of a quantum computer arises from a difference in quantum and classical logic. Whereas a classical computer operates on classical bits which are *either* 0 *or* 1, a quantum computer uses the ability of a quantum system to be in a superposition or mixture of two states, so that the quantum bit (the qubit) is in *both* 0 *and* 1 at same time. The quantum computer has several promising applications both in physics and commercially, but unfortunately it is a very difficult task to entangle particles and construct a quantum computer in practice, because various sources of noise disturb the quantum mechanical effect. We have tried to solve this problem and the thesis presents a number of different experimental proposals for the construction of a quantum computer and producing multi-particle entanglement in practice.

In the first half of the thesis we propose an implementation of quantum computation and multi-particle entanglement where the qubits are encoded in the internal states of trapped ions. We have developed a method to exploit the electrical Coulomb interaction of the ions to communicate between different ions in a trap by illuminating them with bichromatic light. Our proposal has the experimental advantage that it is insensitive to the vibrational motion of the ions in the trap which is one of the major sources of noise in other ion trap proposals. To construct a quantum computer it is essential to be able to control

and detect the individual qubits and in the ion trap quantum computer this is achieved by focusing a laser beam onto each ion in the trap. In practice this is hard to implement experimentally, but our ion trap proposal has the additional attractive feature that it is capable of producing entanglement even without addressing the qubits individually. The thesis suggests a method to produce a maximally entangled state of all ions in the trap by illuminating the ions with a single beam of bichromatic light. By using our approach the ion trapping group at the National Institute of Standards and Technology in Boulder, USA has been able to produce a maximally entangled state of four ions. This is the largest number of particles which has been entangled in any experiment so far. In addition to the proposal, the thesis also presents a detailed analysis of possible imperfections in an experimental implementation of the scheme and a possible generalization of the proposal so that one can implement more sophisticated interactions among the ions.

In the second half of the thesis we consider neutral atoms and suggest various methods to entangle them by using the collisions between the atoms. By moving two different optical lattices with respect to each other, the atoms in the lattices collide with the neighbouring atoms and we demonstrate that with relatively simple experimental means, one can use the optical lattices to simulate many-body quantum physics problems like ferro-magnetism. If the number of particles in the simulation is large such a simulation is impossible to perform on a classical computer. In the optical lattice this quantum simulator is much easier to construct than a full quantum computer and the realization of this proposal would provide a powerful computational tool to physicists.

In the optical lattices it is also possible to use the same procedures to create some very interesting spin squeezed states. In spin squeezed states the atoms are entangled in such a way that the noise in some physical observable is reduced below the noise for a similar unentangled state. An example of such a noise reduction could be an experiment where you have a very large number of atoms and where each atom has the same probability of being in two internal states. If one counts the total number of atoms in the internal states, half of the atoms will be in each of the states on average, but if the atoms are uncorrelated there will statistical fluctuations in the exact number. By entangling the atoms in a spin squeezed state, the noise in the counting statistics can be reduced considerably and this have potential application in atomic clocks. In atomic clocks which are the most precise clocks that one can construct today, the precision is limited by the counting statistics described here, and by entangling the atoms in a spin squeezed state it is possible to improve the precision of the clocks.

We also present a method to construct spin squeezed states using atoms in a Bose-Einstein condensate. A Bose-Einstein condensate is a special quantum mechanical phase where all atoms occupy exactly the same quantum mechanical

state and we propose to create entangled spin squeezed states by illuminating the entire condensate with a single microwave-pulse. After the microwave-pulse the system evolves freely and the collisions in the gas creates the desired entangled state. Each of the two proposals for generating spin squeezed states has its own advantage. In the optical lattice proposal the time required to create an entangled state is very short which is an advantage if the environment is affecting the atoms, but in the condensate proposal which take longer time, the quality of the squeezing is much higher.

The spin squeezed states are entangled states and the thesis contains a method to quantify the entanglement in an experimental realization of spin squeezing. With this method the measurement of only two quantities is sufficient to characterize the depth of entanglement in an experiment with several particles. With this method and our proposals for generating spin squeezing it should be possible to produce and verify entanglement of a very large number of particles.

A.2 Danish translation

Entanglement er en kvantemekanisk egenskab, som tillader adskilte kvantesystemer at udvise øjeblikkelige ikke-lokale korrelationer selv hvis systemerne er meget langt fra hinanden. En kvantecomputer er en computer, der er fundamentalt forskellig fra de klassiske computere vi kender i dag. En kvantecomputer udnytter entanglement til at løse opgaver som er umulige at løse på en klassisk computer. Kvantecomputerens større beregningskraft stammer fra en forskel i klassisk og kvantemekanisk logik. Hvor en klassisk computer bruger bits som *enten* er 0 *eller* 1, bruger kvantecomputeren kvantesystemers evne til at være i en superposition eller blanding af to tilstande, så kvantebiten (qubiten) er *både* 0 *og* 1 på samme tid. Kvantecomputeren har mange lovende anvendelsesmuligheder både i fysik og kommercielt, men desværre er det en meget svær opgave at entangle partikler og bygge en kvantecomputer i praksis, fordi forskellig former for støj forstyrrer den kvantemekaniske effekt. Vi har forsøgt at løse dette problem, og afhandlingen indeholder en række forskellige forslag til hvordan man bygger en kvantecomputer og laver mange-partikel entanglement i praksis.

I den første halvdel af afhandlingen foreslår vi at bygge en kvantecomputer og lave mange-partikel entanglement ved at indkode qubitsene i de indre tilstande i fangede ioner. Vi har udviklet en metode som udnytter ionernes elektriske Coulomb vekselvirkning til at kommunikere mellem qubitsene ved at belyse dem med to-farvet lys. Vores forslag har den eksperimentelle fordel at det er upåvirket af ionernes vibrationsbevægelse i fælden, hvilket er en af de største støjkilder i andre ionfælde forslag. For at bygge en kvantecomputer er det nødvendigt at man er i stand til at kontrollere og detektere de individuelle

qubits, og i ionfælden opnår man dette ved at fokusere en laser på hver enkelt ion i fælden. I praksis er det meget svært at gøre dette eksperimentelt, og vores forslag har den yderligere fordel, at det er i stand til at lave entanglement uden at adressere de individuelle qubits. Afhandlingen foreslår en måde at producere en maksimalt entanglet tilstand af alle ionerne i fælden ved at belyse ionerne med en enkelt stråle to-farvet lys. Ved at bruge vores forslag er det lykkedes ionfælde gruppen på National Institute of Standards and Technology i Boulder, USA at lave maksimalt entanglede tilstande af fire ioner. Dette er det største antal partikler der er blevet entanglet i noget eksperiment indtil videre. Udover forslaget indeholder afhandlingen en detaljeret analyse af mulige fejlkilder i en eksperimentel udførsel af forslaget og en mulig generalisering af forslaget så man kan lave mere avancerede vekselvirkninger mellem ionerne.

I den anden halvdel af afhandlingen betragter vi neutrale atomer og foreslår forskellige måder at entangle dem ved at bruge kollisioner mellem atomerne. Ved at flytte to forskellige optiske gitre i forhold til hinanden kolliderer atomerne i gitrene med nabo atomerne, og vi viser at med ret simple eksperimentelle teknikker er det muligt at simulere mange-legeme kvantefysiske problemer som f.eks. ferro-magnetisme. Hvis antallet af partikler i simulationen er meget stort er det umuligt at udføre sådan en simulation på en klassisk computer. I de optiske gitre er det meget lettere at lave denne kvantesimulator end en fuld kvantecomputer, og ved at realisere dette forslag vil fysikerne få et meget kraftfuldt beregningsmæssigt redskab.

I de optiske gitre er det også muligt at bruge de samme teknikker til at lave nogle meget interessante spin squeezede tilstande. I spin squeezede tilstande er atomerne entanglede på en sådan måde at støjen i en fysisk observabel er mindre end støjen i en tilsvarende uentanglet tilstand. Et eksempel på sådan en støjreduktion kunne være et eksperiment hvor man har et stort antal atomer, og hvor hvert atom har den samme sandsynlighed for at være i to indre tilstande. Hvis man tæller antallet af atomer i hver af de to indre tilstande, vil halvdelen af atomerne være i hver af tilstandene i gennemsnit, men hvis atomerne er ukorrelerede vil der være statistiske fluktuationer i det præcise antal. Ved at entangle atomerne i en spin squeezet tilstand kan støjen på tællestatistikken reduceres betydeligt, og dette har mulige anvendelser i atomare ure. I atomare ure, der er de mest de mest præcise ure som man kan lave i dag, begrænses præcisionen af den tællestatistik vi har beskrevet her, og ved at entangle atomerne i en spin squeezet tilstand er det muligt at forbedre urenes præcisionen.

Vi beskriver også en metode til at lave spin squeezede tilstande ud fra atomer i et Bose-Einstein kondensat. Et Bose-Einstein kondensat er en speciel kvantemekanisk fase, hvor alle atomerne er i præcis den samme kvantemekaniske tiltand, og vi foreslår at lave spin squeezede tilstande ved at belyse alle atomerne med en enkelt mikrobølge-puls. Efter mikrobølge-pulsen udvikler systemet sig frit, og kollisionerne i gassen laver den ønskede entanglede tilstand. De to

spin squeezing forslag har hver deres egen fordel. I forslaget med optiske gitre bliver den entanglede tilstand lavet meget hurtigt, hvilket er en fordel hvis omgivelserne påvirker atomer, men i kondensat forslaget, som er langsomt, er kvaliteten af squeezingen langt højere.

De spin squeezede tilstande er entanglede tilstande og afhandlingen indeholder en metode til at kvantificere denne entanglement i et eksperiment med spin squeezing. Med denne metode er en måling af bare to størrelser nok til at karakterisere dybden af entanglement i et eksperiment med mange partikler. Med denne metode og vores forslag til at lave spin squeezing skulle det være muligt at producere og bekræfte entanglement af et meget stort antal partikler.

Bibliography

[1] A. Sørensen and K. Mølmer, Phys. Rev. A **58**, 2745 (1998).

[2] A. Sørensen and K. Mølmer, Phys. Rev. Lett. **82**, 1971 (1999).

[3] K. Mølmer and A. Sørensen, Phys. Rev. Lett. **82**, 1835 (1999).

[4] A. Sørensen and K. Mølmer, Phys. Rev. Lett. **83**, 2274 (1999).

[5] A. Sørensen and K. Mølmer, Phys. Rev. A **62**, 022311 (2000).

[6] A. Sørensen and K. Mølmer, Fortschr. Phys. **48**, 811 (2000).

[7] L.-M. Duan, A. Sørensen, J. I. Cirac, and P. Zoller, Phys. Rev. Lett. **85**, 3991 (2000).

[8] K. Mølmer and A. Sørensen, J. Modn. Optics **47**, 2515 (2000).

[9] A. Sørensen, L.-M. Duan, J. I. Cirac, and P. Zoller, Nature **409**, 63 (2001).

[10] X. Wang, A. Sørensen, and K. Mølmer, Phys. Rev. Lett. **86**, 3907 (2001).

[11] A. S. Sørensen and K. Mølmer, Phys. Rev. Lett. **86**, 4431 (2001).

[12] A. Sørensen and K. Mølmer, in *Mysteries, Puzzles, and Paradoxes in Quantum Mechanics*, edited by R. Bonifacio (AIP, New York, 1999), p. 251.

[13] A. Sørensen and K. Mølmer, in *EMCSR 2000*, edited by R. Trappl (Austrian Society for Cybernetic Studies, Vienna, 2000), p. 159.

[14] K. Mølmer and A. Sørensen, *Multi-particle entanglement in quantum computers*, submitted to Journal of Superconducticity.

[15] X. Wang, A. S. Sørensen, and K. Mølmer,
E-print: http://xxx.lanl.gov/abs/quant-ph/0106065
to appeat in Phys. Rev. A.

[16] J. J. Sakurai, *Modern Quantum Mechanics* (Addison-Wesley, Reading, Ma, 1994).

[17] A. Aspect, J. Dalibard, and G. Roger, Phys. Rev. Lett. **49**, 1804 (1982).

[18] I. L. Chuang, L. M. K. Vandersypen, X. Zhou, D. W. Leung, and S. Lloyd, Nature **393**, 143 (1998).

[19] I. L. Chuang, N. Gershenfeld, and M. Kubinec, Phys. Rev. Lett. **80**, 3408 (1998).

[20] J. A. Jones, M. Mosca, and R. H. Hansen, Nature **393**, 344 (1998).

[21] J. A. Jones, Fortschr. Phys. **48**, 909 (2000).

[22] A. Steane, Rept. Prog. Phys. **61**, 117 (1998).

[23] Special issue on quantum information [Phys. World **11**, 33-57 (1998)].

[24] A. Barenco, C. H. Bennett, R. Cleve, D. P. DiVincenzo, N. Margolus, P. Shor, T. Sleator, J. A. Smolin, and H. Weinfurter, Phys. Rev. A **52**, 3457 (1995).

[25] S. Lloyd, Phys. Rev. Lett. **75**, 346 (1995).

[26] D. Deutsch, A. Barenco, and A. Ekert, Proc. R. Soc. London. A **449**, 669 (1995).

[27] J. L. Dodd, M. A. Nielsen, M. J. Bremner, and R. T. Thew, E-print: http://xxx.lanl.gov/abs/quant-ph/0106064.

[28] P. Shor, in *Proceedings of the 35th Annual Symposium on Foundations of Computer Science*, edited by S. Goldwasser (IEEE Computer Society, Los Alamos, CA, 1994), p. 124.

[29] L. K. Grover, Phys. Rev. Lett. **79**, 325 (1997).

[30] C. H. Bennett and G. Brassard, in *Proc. of IEEE Int. Conf on Computers, Systems and Signal Processing, Bangalore, India* (IEEE, New York, 1984), p. 175.

[31] C. H. Bennett, Phys. Rev. Lett. **68**, 3121 (1992).

[32] D. Mayers and A. Yao, E-print: http://xxx.lanl.gov/abs/quant-ph/9802025.

[33] R. P. Feynman, Int. J. Theor. Phys. **21**, 467 (1982).

[34] S. Lloyd, Science **273**, 1072 (1996).

[35] A. Einstein, B. Podolsky, and N. Rosen, Phys. Rev. **47**, 777 (1935).

[36] D. M. Greenberger, M. A. Horne, and A. Zeilinger, Physics Today **46**, 22 August 1993.

[37] D. M. Greenberger, M. A. Horne, A. Shimony, and A. Zeilinger, Am. J. Phys. **58**, 1131 (1990).

[38] J.-W. Pan, D. Bouwmeester, M. Daniell, H. Weinfurter, and A. Zeilinger, Nature **403**, 515 (2000).

[39] E. Schrödinger, Naturwissenschaften **23**, 807 (1935); translation in J. A. Wheeler and W. H. Zurek, *Quantum Theory and Measurement* (Princeton Univ. Press, Princeton, NJ, 1983).

[40] C. Monroe, D. M. Meekhof, B. E. King, and D. J. Wineland, Science **272**, 1131, (1996).

[41] M. Brune, E. Hagley, J. Dreyer, X. Maître, A. Maali, C. Wunderlich, J. M. Raimond, and S. Haroche, Phys. Rev. Lett. **77**, 4887 (1996).

[42] M. Arndt, O. Nairz, J. Vos-Andreae, C. Keller, G. van der Zouw, and A. Zeilinger, Nature **401**, 680 (1999).

[43] J. R. Friedman, V. Patel, W. Chen, S. K. Tolpugo, and J. E. Lukens, Nature **406**, 43 (2000).

[44] C. A. Sackett, D. Kielpinski, B. E. King, C. Langer, V. Meyer, C. J. Myatt, M. Rowe, Q. A. Turchette, W. M. Itano, D. J. Wineland, and C. Monroe, Nature **404**, 256 (2000).

[45] W. K. Wootters and W. H. Zurek, Nature **299**, 802 (1982).

[46] A. M. Steane, Phys. Rev. Lett. **77**, 793 (1996).

[47] A. R. Calderbank and P. Shor, Phys. Rev. A **54** 1098 (1996).

[48] S. J. van Enk, J. I. Cirac and P. Zoller, Phys. Rev. Lett. **78**, 4293 (1997).

[49] Special issue on experimental proposal for quantum computation [Fortschr. Phys. **48**, 765-1140 (1998)].

[50] P. G. Kwiat, K. Mattle, H. Weinfurter, A. Zeilinger, A. V. Sergienko, and Y. Shih, Phys. Rev. Lett. **75**, 4337 (1995).

[51] Z. Y. Ou, S. F. Pereira, H. J. Kimble, and K. C. Pen, Phys. Rev. Lett. **68**, 3663 (1992).

[52] C. H. Bennett, G. Brassard, C. Crépeau, R. Jozsa, A. Peres, and W. K. Wootters, Phys. Rev. Lett. **70**, 1895 (1993).

[53] D. Bouwmeester, J.-W. Pan, K. Mattle, M. Eibl, H. Weinfurter, and A. Zeilinger, Nature **390**, 575 (1997).

[54] A. Furusawa, J. L. Sørensen, S. L. Braunstein, C. A. Fuchs, H. J. Kimble, and E. S. Polzik, Science **282**, 706 (1998).

[55] D. Boschi, S. Brance, F. De Martini, L. Hardy, and S. Popescu, Phys. Rev. Lett. **80**, 1121 (1998).

[56] S. Lloyd and S. L. Braunstein, Phys. Rev. Lett. **82**, 1784 (1999).

[57] E. Knill, R. Laflamme, and G. J. Milburn, Nature **409**, 46 (2001).

[58] B. E. Kane, Nature **393**, 133 (1998).

[59] D. Loss and D. P. DiVincenzo, Phys. Rev. A **57**, 120 (1998).

[60] A. Imamoglu, D. D. Awschalom, G. Burkard, D. P. DiVincenzo, D. Loss, M. Sherwin, and A. Small, Phys. Rev. Lett. **83**, 4204 (1999).

[61] Y. Makhlin, G. Schön, and A. Shnirman, Nature **398**, 305 (1999).

[62] Y. Nakamura, Y. A. Pashkin, and J. S. Tsai, Nature **398**, 786 (1999).

[63] N. H. Bonadeo, J. Erland, D. Gammon, D. Park, D. S. Katzer, and D. G. Steel, Science **282**, 1473 (1998).

[64] H.-J. Briegel, W. Dür, J. I. Cirac, and P. Zoller, Phys. Rev. Lett. **81**, 5932 (1998).

[65] D. Kielpinski, V. Meyer, M. A. Rowe, C. A. Sackett, W. M. Itano, C. Monroe, and D. J. Wineland, Science **291**, 1013 (2001).

[66] M. A. Rowe, D. Kielpinski, V. Meyer, C. A. Sackett, W. M. Itano, C. Monroe, and D. J. Wineland, Nature **409**, 791 (2001).

[67] D. J. Wineland, C. Monroe, W. M. Itano, D. Leibfried, B. E. King, and D. M. Meekhof, J. Res. Natl. Inst. Stand. Tech. **103**, 259 (1998).

[68] M. Drewsen, C. Brodersen, L. Hornekær, J. S. Hangst, and J. P. Schiffer, Phys. Rev. Lett. **81**, 2878 (1998).

[69] L. Hornekær, N. Kjærgaard, A. M. Thommesen, and M. Drewsen, Phys. Rev. Lett. **86**, 1998 (2001).

[70] D. F. V. James, Appl. Phys. B **66**, 181 (1998).

[71] J. I. Cirac and P. Zoller, Phys. Rev. Lett. **74**, 4091 (1995).

[72] D. M. Meekhof, C. Monroe, B. E. King, W. M. Itano, and D. J. Wineland, Phys. Rev. Lett. **76**, 1796 (1996).

[73] W. Nagourney, J. Sandberg, and H. Dehmelt, Phys. Rev. Lett. **56**, 2797 (1986).

[74] B. E. King, C. S. Wood, C. J. Myatt, Q. A. Turchette, D. Leibfried, W. M. Itano, C. Monroe, and D. J. Wineland, Phys. Rev. Lett. **81**, 1525 (1998).

[75] H. Rohde, S. T. Gulde, C. F. Roos, P. A. Barton, D. Leibfried, J. Eschner, F. Schmidt-Kaler, and R. Blatt, J. Opt. B **3**, 34 (2001).

[76] D. Leibfried, Phys. Rev. A **60**, 3335 (1999).

[77] Q. A. Turchette, C. S. Wood, B. E. King, C. J. Myatt, D. Liebfried, W. M. Itano, C. Monroe, and D. J. Wineland, Phys. Rev. Lett. **81**, 3631 (1998).

[78] J. F. Poyatos, J. I. Cirac, and P. Zoller, Phys. Rev. Lett. **81**, 1322 (1998).

[79] S. Schneider, D. F. V. James, and G. J. Milburn, J. Mod. Opt. **47**, 499 (2000).

[80] G. J. Milburn, E-print: http://xxx.lanl.gov/abs/quant-ph/9908037.

[81] D. Jonathan, M. B. Plenio, and P. Knight, Phys. Rev. A **62**, 042307 (2000).

[82] D. Johathan and M. B. Plenio,
E-print: http://xxx.lanl.gov/abs/quant-ph/0103140.

[83] F. Mintert and C. Wunderlich,
E-print: http://xxx.lanl.gov/abs/quant-ph/0104041.

[84] D. G. Enzer, M. M. Schauer, J. J. Gomez, M. S. Gulley, M. H. Holzscheiter, P. G. Kwiat, S. K. Lamoreaux, C. G. Peterson, V. D. Sandberg, D. Tupa, A. G. White, R. J. Hughes, and D. James, Phys. Rev. Lett. **85**, 2466 (2000).

[85] R. G. DeVoe, Phys. Rev. A **58**, 910 (1998).

[86] J. I. Cirac, P. Zoller, H. J. Kimble, and H. Mabuchi, Phys. Rev. Lett. **78**, 3221 (1997).

[87] J. I. Cirac and P. Zoller, Nature **404**, 579 (2000).

[88] T. Calarco, J. I. Cirac, and P. Zoller, Phys. Rev. A **63**, 062304 (2001).

[89] L. Allan and J. M. Eberly, *Optical resonance and two-level atoms* Ch. 9 (Dover, New York, 1987).

[90] K. Mølmer, Y. Castin, and J. Dalibard, J. Opt. Soc. Am. B **10**, 524 (1993).

[91] J. J. Bollinger, W. M. Itano, D. J. Wineland, and D. J. Heinzen, Phys. Rev. A **54**, 4649 (1996).

[92] S. F. Huelga, C. Macchiavello, T. Pellizzari, A. K. Ekkert, M. B. Plenio, and J. I. Cirac, Phys. Rev. Lett. **79**, 3865 (1997).

[93] D. M. Brink and G. R. Satchler, *Angular Momentum* (Clarendon Press, Oxford, 1962).

[94] B. Yurke and D. Stoler, Phys. Rev. Lett. **57**, 13 (1986).

[95] B. E. King, private communications.

[96] E. Solano, R. L. de Matos Filho, and N. Zagury, Phys. Rev. A **59**, 2539 (1999).

[97] R. L. de Matos Filho and W. Vogel, Phys. Rev. Lett. **76**, 4520 (1996).

[98] A. M. Steane, Nature **399**, 124 (1999).

[99] R. Laflamme, C. Miquel, J. P. Paz, and W. H. Zurek, Phys. Rev. Lett. **77**, 198 (1996).

[100] D. Jaksch, H.-J. Briegel, J. I. Cirac, C. W. Gardiner, and P. Zoller, Phys. Rev. Lett. **82**, 1975 (1999).

[101] A. S. Parkins and D. F. Walls, Physics Reports **303**, 1 (1998).

[102] M. H. Anderson, J. R. Ensher, M. R. Matthews, C. E. Wieman, and E. A. Cornell, Science **269**, 198 (1995).

[103] K. B. Davis, M.-O. Mewes, M. R. Andrews, N. J. van Druten, D. S. Durfee, D. M. Kurn, and W. Ketterle, Phys. Rev. Lett. **75**, 3969 (1995).

[104] T. Calarco, E. A. Hinds, D. Jaksch, J. Schmiedmayer, J. I. Cirac, and P. Zoller, Phys. Rev. A **61**, 022304 (2000).

[105] U. V. Poulsen and K. Mølmer,
E-print: http://xxx.lanl.gov/abs/quant-ph/0103138.

[106] G. K. Brennen, C. M. Caves, P. S. Jessen, and I. H. Deutsch, Phys. Rev. Lett. **82**, 1060 (1999).

[107] D. Jaksch, J. I. Cirac, P. Zoller, S. L. Rolston, R. Côté, and M. D. Lukin, Phys. Rev. Lett. **85**, 2208 (2000).

[108] M. D. Lukin, M. Fleischhauer, R. Côté, L.-M. Duan, D. Jaksch, J. I. Cirac, and P. Zoller, E-print: http://xxx.lanl.gov/abs/quant-ph/0011028.

[109] P. Domokos, J. M. Raimond, M. Brune, and S. Haroche, Phys. Rev. A **52**, 3554 (1995).

[110] A. Rauschenbeutel, G. Nogues, S. Osnaghi, P. Bertet, M. Brune, J.-M. Raimond, and S. Haroche, Science **288**, 2024 (2000).

[111] L.-M. Duan, J. I. Cirac, P. Zoller, and E. S. Polzik, Phys. Rev. Lett. **85**, 5643 (2000).

[112] L.-M. Duan, M. D. Lukin, J. I. Cirac, and P. Zoller, E-print: http://xxx.lanl.gov/abs/quant-ph/0105105.

[113] M. Kitagawa and M. Ueda, Phys. Rev. A **47**, 5138 (1993).

[114] M. A. Rashid, J. Math. Phys. **19**, 1391 (1978).

[115] K. Wódkiewicz and J. H. Eberly, J. Opt. Soc. Am. B **2**, 458 (1985).

[116] G. S. Agarwal and R. R. Puri, Phys. Rev. A **41**, 3782 (1990).

[117] A. Kuzmich, K. Mølmer, and E. S. Polzik, Phys. Rev. Lett. **80**, 3487 (1998).

[118] A. Kuzmich, N. P. Bigelow, and L. Mandel, Europhys. Lett **42**, 481 (1998).

[119] I. Bouchoule and K. Mølmer, E-print: http://xxx.lanl.gov/abs/quant-ph/0105144.

[120] J. Hald, J. L. Sørensen, C. Schori, and E. S. Polzik, Phys. Rev. Lett. **83**, 1319 (1999).

[121] A. Kuzmich, L. Mandel, and N. P. Bigelow, Phys. Rev. Lett. **85**, 1594 (2000).

[122] C. Orzel, A. K. Tuchman, M. L. Fenselau, M. Yasuda, and M. A. Kasevich, Science **291**, 2386 (2001).

[123] D. J. Wineland, J. J. Bollinger, W. M. Itano, and D. J. Heinzen, Phys. Rev. A **50**, 67 (1994).

[124] G. Santarelli, P. Laurent, P. Lemonde, A. Clairon, A. G. Mann, S. Chang, A. N. Luiten, and C. Salomon, Phys. Rev. Lett. **82**, 4619 (1999).

[125] R. Werner, Phys. Rev. A **40**, 4277 (1989).

[126] A. Peres, Phys. Rev. Lett. **77**, 1413 (1996).

[127] E. Ising, Z. Physik **31**, 253 (1925).

[128] F. Reif, *Fundamentals of statistical and thermal physics* (McGraw-Hill, Singapore 1985).

[129] H. J. Briegel and R. Raussendorf, Phys. Rev. Lett. **86**, 910 (2001).

[130] R. Raussendorf and H. J. Briegel, Phys. Rev. Lett. **86**, 5188 (2001).

[131] S. E. Hamann, D. L. Haycock, G. Klose, P. H. Pax, I. H. Deutsch, and P. S. Jessen, Phys. Rev. Lett. **80**, 4149 (1998).

[132] M. T. DePue, C. McCormick, S. L. Winoto, S. Oliver, and D. S. Weiss, Phys. Rev. Lett. **82**, 2262 (1999).

[133] D. Jaksch, C. Bruder, J. I. Cirac, C. W. Gardiner, and P. Zoller, Phys. Rev. Lett. **81**, 3108 (1998).

[134] M. Plischke and B. Bergersen, *Equilibrium statistical physics* (World Scientific, Singapore, 1994).

[135] D. S. Hall, M. R. Matthews, J. R. Ensher, C. E. Wieman, and E. A. Cornell, Phys. Rev. Lett. **81**, 1539 (1998).

[136] J. Stenger, S. Inouye, D. M. Stamper-Kurn, H.-J. Miesner, A. P. Chikkatur, and W. Ketterle, Nature **396**, 345 (1998).

[137] H.-J. Miesner, D. M. Stamper-Kurn, J. Stenger, S. Inouye, A. P. Chikkatur, and W. Ketterle, Phys. Rev. Lett. **82**, 2228 (1999).

[138] A. Sinatra and Y. Castin, Eur. Phys. J. D **8**, 319 (2000).

[139] H. P. Yuen, Phys. Lett. A **56**, 105 (1976).

[140] L.-M. Duan, J. I. Cirac, and P. Zoller, Science **292**, 1695 (2001).

[141] S.-B. Zheng and G.-C. Guo, Phys. Rev. Lett. **85**, 2392 (2000).

[142] E. Solano, C. L. Cesar, R. L. de Matos Filho, and N. Zagury, Eur. Phys. J. D **13**, 121 (2001).

[143] S. Osnaghi, P. Bertet, A. Auffeves, P. Maioli, M. Brune, J. Raimond, and S. Haroche, E-print: http://xxx.lanl.gov/abs/quant-ph/0105063.